ANALYSIS AND DESIGN OF A NOVEL RECIPROCATING COMPRESSOR UTILIZING A MINFAS-TAR MECHANISM(S)

A THESIS SUBMITTED TO
THE GRADUATE SCHOOL OF NATURAL AND APPLIED SCIENCES
OF
MIDDLE EAST TECHNICAL UNIVERSITY

BY

ABDULKADİR ERCAN

IN PARTIAL FULFILLMENT OF THE REQUIREMENTS
FOR
THE DEGREE OF MASTER OF SCIENCE
IN
MECHANICAL ENGINEERING

JANUARY 2021

Approval of the thesis:

ANALYSIS AND DESIGN OF A NOVEL RECIPROCATING COMPRESSOR UTILIZING A MINFAS-TAR MECHANISM(S)

Submitted by **ABDULKADİR ERCAN** in partial fulfillment of the requirements for the degree of **Master of Science in Mechanical Engineering, Middle East Technical University** by,

Prof. Dr. Halil Kalıpçılar
Dean, Graduate School of **Natural and Applied Sciences** _____

Prof. Dr. M. A. Sahir Arıkan
Head of the Department, **Mechanical Engineering** _____

Prof. Dr. Reşit Soylu
Supervisor, **Mechanical Engineering, METU** _____

ExaminingCommitteeMembers:

Prof. Dr. Zafer Dursunkaya
Mechanical Engineering, METU _____

Prof. Dr. Reşit Soylu
Mechanical Engineering, METU _____

Assoc. Prof. Dr. Ergin Tönük
Mechanical Engineering, METU _____

Assoc. Prof. Dr. Yiğit Yazıcıoğlu
Mechanical Engineering, METU _____

Prof. Dr. Ahmet Demir Bayka
Mechanical Engineering, Başkent University _____

Date:26.01.2021

I hereby declare that all information in this document has been obtained and presented in accordance with academic rules and ethical conduct. I also declare that, as required by these rules and conduct, I have fully cited and referenced all material and results that are not original to this work.

Name, Last name :Abdulkadir ERCAN

Signature :

ABSTRACT

ANALYSIS AND DESIGN OF A NOVEL RECIPROCATING COMPRESSOR UTILIZING A MINFAS-TAR MECHANISM(S)

Ercan, Abdulkadir
Master of Science, Mechanical Engineering
Supervisor : Prof. Dr. Reşit Soylu

January 2021, 198 pages

Similar to the slider crank mechanism that is utilized in a conventional reciprocating compressor, the MinFaS-TaR (Minimum Friction and Shaking – Translation to any Rotation) mechanism may also be used to convert a rotational motion into a translational motion. In the MinFaS-TaR mechanism, the translational and rotational motions can be related to each other in any desired manner. Furthermore, it has favourable dynamic properties.

In this study, the piston motion function, $x_p(\theta)$, or the chamber pressure function, $P_c(\theta)$, has been used as a design "function" to optimize the performance, especially energy consumption, of a compressor utilizing one, or more, MinFaS-TaR mechanisms. Here, x_p , θ and P_c denote the position of the piston of the compressor, the angular position of the crank of the compressor and the chamber pressure, respectively. In addition, the diameter of the cylinder, the diameters of the inlet and outlet valves and the motor speed of the compressor are utilized as design parameters. It is shown that using $P_c(\theta)$ as the design function is more

advantageous (than using $x_p(\theta)$ as the design function), leading to compressors in which the chamber pressure is constant during the suction and discharge phases.

In order to assess the effects of various design parameters on the performance of a reciprocating compressor, parametric studies have been performed. Furthermore, 7 case studies have been considered. For each case study, optimal MinFaS-TaR based compressors have been obtained by using the developed algorithms. The performances of these optimal MinFaS-TaR based compressors have been compared to that of the slider crank based compressors. The results indicate that the energy consumptions and the power requirements of the driving motors of MinFaS-TaR based compressors may be reduced significantly (compared to the slider crank based compressors). It should be noted that, the shaking forces and moments transmitted to the chassis are identically zero in a MinFaS-TaR based compressor.

Keywords: Reciprocating Compressors, Energy Consumption of Reciprocating Compressors, Overconstrained Mechanisms, Shaking Force and Moment Balancing

ÖZ

MİNSVS-KHD MEKANİZMASI(LARI) İÇEREN YENİLİKÇİ PİSTONLU KOMPRESÖRLERİN TASARIMI VE ANALİZİ

Ercan, Abdulkadir
Yüksek Lisans, Makina Mühendisliği
Tez Yöneticisi: Prof. Dr. Reşit Soylu

Ocak 2021, 198 sayfa

Pistonlu kompresörlerde kullanılan krank biyel mekanizmasına benzer bir şekilde, "MinSvS-KhD" (Minimum Sürtünme ve Sarsma – Kaymadan Herhangi Dönmeye) mekanizması da bir dönme hareketini bir kayma hareketine dönüştürmektedir. MinSvS-KhD mekanizması kullanılarak, dönme ve kayma hareketleri arasında istenen herhangi bir ilişki elde edilebilir. Ayrıca, MinSvS-KhD mekanizması avantajlı dinamik özelliklere de sahiptir.

Bu çalışmada, piston hareketi, $x_p(\theta)$, veya hazne basıncı, $P_c(\theta)$, bir tasarım "fonksiyonu" olarak kullanılarak, bir veya daha fazla MinSvS-KhD mekanizması içeren kompresörlerin performans en iyilemesi (özellikle kompresör enerji tüketimi açısından) yapılmıştır. Burada x_p, θ ve P_c , sırasıyla, piston pozisyonunu, krank açısını ve hazne basıncını simgelemektedir. Ayrıca, kompresör silindir çapı, giriş ve çıkış valflerinin çapları ve motor hızı da tasarım değişkenleri olarak kullanılmaktadır. Tasarım fonksiyonu olarak $P_c(\theta)$'yı kullanmanın daha avantajlı ($x_p(\theta)$ kullanmaya göre) olduğu; ve bu durumda, hazne basıncının emme ve tahliye fazlarında sabit kalmasının sağlanabildiği gösterilmiştir.

Tasarım değişkenlerinin kompresör performansı üzerindeki etkilerini görebilmek amacıyla parametrik analizler gerçekleştirilmiştir. Ayrıca, 7 adet durum çalışması da gerçekleştirilmiştir. Oluşturulan algoritmalar aracılığıyla, her bir durum çalışması için optimal MinSvS-KhD temelli kompresörler elde edilmiştir. Elde edilen bu optimal MinSvS-KhD temelli kompresörler, benzer krank biyel mekanizması temelli kompresörler ile karşılaştırılmıştır. Sonuçlar, MinSvS-KhD temelli kompresörlerin, kullanılan tahrik motorlarının enerji tüketimini ve güç ihtiyacını önemli ölçüde azaltabileceğini göstermektedir. Ayrıca, MinSvS-KhD temelli kompresörlerde ana gövdeye (şase) aktarılan sarsma kuvvet ve momentlerinin daima sıfır olduğu da göz önünde bulundurulmalıdır.

Anahtar Kelimeler: Pistonlu Kompresörler, Pistonlu Kompresörlerin Enerji Tüketimi, Aşırı Kısıtlı Mekanizmalar, Sarsma Kuvvet ve Momentlerinin Dengelenmesi

To my family

ACKNOWLEDGMENTS

I would like to express my deepest appreciation to my thesis supervisor Prof. Dr. Reşit Soylu for his invaluable contribution, support, and patience that cannot be underestimated throughout this study.

I would also like to thank İbrahim Murat Karbancıoğlu for his encouragement to start this study.

Last and foremost, I want to thank my brother Nabi Ercan for his priceless support.

TABLE OF CONTENTS

LIST OF TABLES

TABLES

LIST OF FIGURES

FIGURES

LIST OF ABBREVIATIONS

ABBREVIATIONS

A	Area (m^2)
a	Acceleration (m/s^2)
BDC	Bottom Dead Center
b_2	Length of Link-2 of MinFaS-TaR (m)
c	Damping Coefficient (Nsm^{-1})
cap	Capacity (m^3/hr)
C_{di}	Discharge Coefficient of Inlet Valve
C_{do}	Discharge Coefficient of Outlet Valve
CFD	Computational Fluid Dynamics
CMC	Cycloidal Motion Curve
c_p	Heat Capacity for Ideal Gas at Constant Pressure ($Jkg^{-1}K^{-1}$)
c_v	Heat Capacity for Ideal Gas at Constant Volume ($Jkg^{-1}K^{-1}$)
D	Diameter (m)
D_c	Cylinder Bore Diameter (m)
DP	Design Parameters
DV	Design Variables
E	Energy (J)
F	Force (N)
F	Degree of Freedom of Mechanism

f_i	i^{th} joint Degree of Freedom
h	Enthalpy (J)
H	Total Follower Rise of Cam (m)
j	Number of Joints
k	Spring Coefficient (Nm^{-1})
l	Number of Links
l	Rod Length (m)
m	Mass (kg)
MinFaS-TaR	Minimum Friction and Shaking Translation to any Rotation
MTG	Mechanical Torque Generator
obj	Objective
P	Pressure (Pa)
PDFA	Percent Deviation from Average
Pow	Power (Watt)
PPR	Percent Power Ratio
PTR	Percent Torque Ratio
$\dot{Q}$	Heat Flow Rate (W)
r	Crank Length (m)
R	Ideal Gas Constant ($Jkg^{-1}K^{-1}$)
rms	Root Mean Square
SC	Slider Crank

str	Stroke(m)
s	Displacement of Link 3 and 5 of MinFaS-TaR (m)
T	Temperature (K)
T	Period (sec)
TDC	Top Dead Center
u	Internal Energy (J)
V	Volume (m^3)
W	Work (J)
x	Displacement (m)
y	Valve Opening (m)

LIST OF SYMBOLS

SYMBOLS

v	Velocity (m/s)
β	Rotation Angle of the Cam Corresponding to the Stroke (rad)
γ	Specific Heat Ratio
η	Efficiency
θ	Crank Angle (rad)
λ	Degree of Freedom of Space
ρ	Density (kgm^{-3})
τ	Torque (Nm)
ω	Rotational Velocity of Actuator Shaft (rad/s)

SUBSCRIPTS AND SUPERSCRIPTS

a	Average
abs	Absolute
c	Chamber
cl	Clearance
fw	Flywheel
ht	Heat Transfer
i	Inlet
iner	Inertial

isen	Isentropic
iso	Isothermal
m	Motor
max	Maximum
min	Minimum
mod	Modified
neg	Negative
net	Net
o	Outlet
org	Original
p	Piston
pcl	Percent Clearance Volume
pm	Per Mass
pos	Positive
pres	Pressure
sim	Simulation
v	Valve
w	Wall

CHAPTER 1

INTRODUCTION

A mechanism is a group of links connected to each other by joints, where one of the links is fixed. Mechanisms are used to transmit, mechanically, motion, force, moment and/or energy from one location to another. When designing a mechanism, it is necessary to take into account many different criteria, some of which are listed below.

- Energy consumption
- Frictional losses
- Size
- Fluctuation of the actuator torque and power
- Shaking forces and moments transmitted to the ground
- Generated noise

In order to improve the performance of a machine, the mechanisms in a machine are designed according to the above criteria. In the literature, there are many studies that aim to optimize a specific objective.

Recently, a novel, overconstrained mechanism, with favourable kinematic and dynamic properties, has been proposed by Soylu[1]. This novel mechanism, which has been labelled as Minimum Friction and Shaking, Translation to any Rotation (MinFaS-TaR) mechanism is somewhat similar to the slider crank mechanism. In this study, reciprocating compressors which utilize the MinFaS-TaR mechanism, instead of the slider crank mechanism, will be investigated in detail. This novel design will be compared, in detail, with the conventional, slider crank based reciprocating compressors.

1.1 Overconstrained Mechanism

Mechanisms which are in permanently critical form are known as overconstrained mechanisms. These mechanisms do not obey the general degree of freedom equation (see, for instance, [2]) which is given below.

$$F = \lambda(l - j - 1) + \sum_{i=1}^{j} f_i \tag{1.1}$$

λ: Degree of freedom of space

l: Number of links (including fixed link)

j: Number of joints

f_i: ith joint degree of freedom

F : Degree of freedom of mechanism

An overconstrained mechanism has strictly more degrees of freedom than the one obtained from the general degree of freedom equation. This is because the constraints imposed by the joints of an overconstrained mechanism are not independent (since it possesses special kinematic dimensions). In other words, overconstrained mechanisms are in permanent critical form due to special dimensions.

In Figure 1.1, 2 topologically same mechanisms, Mech-1 and Mech-2, are shown. The kinematic dimensions of the 2 mechanisms, however, are different.

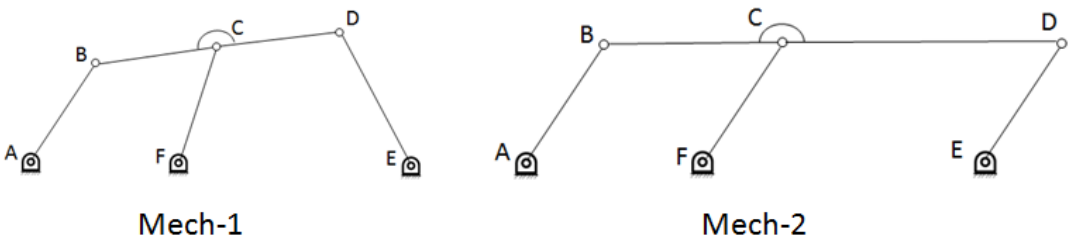

Figure 1.1. Overconstrained Mechanism

Using equation (1.1), the degree of freedom of Mech-1 and Mech-2 are both found to be zero. In other words, equation (1.1) implies that Mech-1 and Mech-2 are both structures. However, due to its special kinematic dimensions, Mech-2 has an actual degree of freedom of 1. Hence, Mech-2 is an overconstrained mechanism.

1.1.1 Reciprocating Compressors Which Utilize a MinFaS-TaR Mechanism

The slider crank mechanism that is utilized in a conventional reciprocating compressor converts a rotational motion into a translational motion (or, vice versa). The MinFaS-TaR mechanism (see Figure 1.2), which is a 1 degree of freedom overconstrained mechanism, may also be used to convert a rotational motion into a translational motion. The MinFaS-TaR mechanism has two important advantages over the slider crank mechanism.

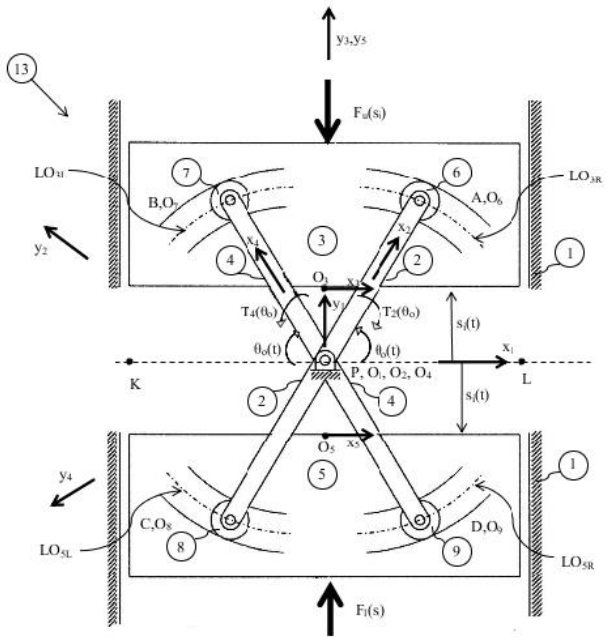

Figure 1.2. MinFaS-TaR Mechanism[1]

(i) In the MinFaS-TaR mechanism, the translational and rotational motions can be related to each other in any desired manner. Clearly, this is not possible in the slider crank mechanism.

(ii) When gravitational acceleration is neglected, the reaction forces and moments associated with each of the joints that connect the MinFaS-TaR mechanism to the ground will always be identically zero (regardless of the motion of the mechanism and regardless of the loading on the mechanism). Clearly, this is not the case in the slider crank mechanism.

Under the light of the above two advantages, it is clear that a reciprocating compressor utilizing a MinFaS-TaR mechanism will be more advantageous than a reciprocating compressor utilizing a slider crank mechanism.

In this study, in order to benefit from the first advantage, the piston motion function $x_p(\theta)$ will be used as a design "function" to optimize the performance of the compressor. Here, x_p, which is designated by $s_i(t)$ in Figure 1.2, denotes the position of each of the 2 pistons of the compressor (which are rigidly connected to links 3 and 5 in Figure 1.2). θ, which is designated by $\theta_o(t)$ in Figure 1.2, on the other hand, denotes the angular position of each of the 2 cranks of the compressor (links 2 and 4 in Figure 1.2).

Due to the second advantage, on the other hand, shaking forces which result vibrations transmitted to the chassis of the compressor will be eliminated. Furthermore, the frictional losses associated with the compressor and the wear associated with the bearings that are used to connect the compressor to the ground will also be minimized due to reduced joint reaction forces.

1.2 Reciprocating Compressor

There are various types of compressors which are used for different applications. One of the most popular types is the reciprocating compressor which is widely used in many different applications. A conventional reciprocating compressor is shown

in Figure 1.3. The slider crank mechanism is used to convert the rotational input motion, provided by the motor, into the translational motion of the piston. The compressor also includes two valves for suction and discharge purposes.

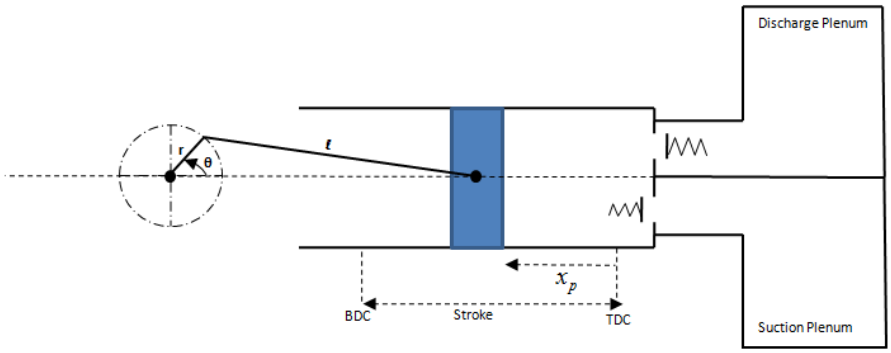

Figure 1.3. A Conventional Reciprocating Compressor

Hollingsworth et al.[4], for instance, discuss various features of reciprocating compressors in detail. They also discuss the advantages and disadvantages of reciprocating compressors compared to other types of compressors.

In order to improve the performance of reciprocating compressors, various new designs have been suggested. These new designs usually involve a modification in the valve characteristics, or in the driving mechanism.

Ooi et al. [5] proposed a new compressor design which utilizes a new mechanism that replaces the slider crank. This new design has been named as " Rotoprocating Compressor " (see Figure 1.4). The mechanism consists of a piston, with a groove cut on its inner surface, and a T-Shaft which provides a rotational input. A mathematical model of this " Rotoprocating Compressor " has been developed. In addition to the mechanical considerations, the developed model takes into account the compressor and valve dynamics and the thermodynamic processes that are involved. According to the authors, the advantages of the rotoprocating compressor are as follows.

- Improved Capacity: By using the same motor (which is used in a conventional compressor), the new mechanism can compress gasses with different capacities.
- Compactness: The new compressor design provides an inline construction for the motor and the compressor unit,
- Simple Construction: The rotaprocating compressor has fewer moving parts than the conventional one.

In the same study, the torque characteristic of the rotoprocating compressor has been compared with that of the conventional reciprocating compressor. The results indicate that the torque requirement is more than the conventional reciprocating compressor. According to the authors, the larger torque requirement is due to the frictional losses associated with the grooved profile.

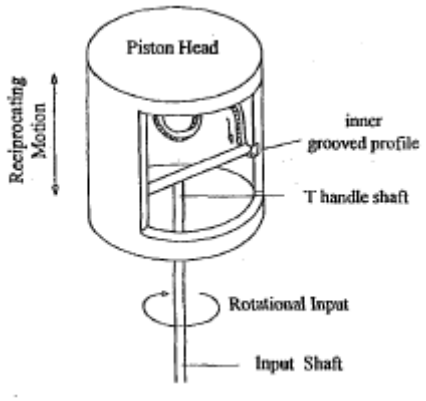

Figure 1.4. Rotoprocating Compressor [4]

In [6], which can be considered to be a continuation of [5], Ooi et al. propose different motion profiles for the inner groove of the rotaprocating compressor. Furthermore, they present some parametric case studies.

Sultan et al. [7] attempted to improve the performance of a reciprocating compressor by designing an optimum piston motion curve (other than the piston motion curve that is provided by a slider crank mechanism). In their study, they tried to answer the following two questions.

- What is the optimum piston motion curve that optimizes the performance of a reciprocating compressor?
- What will be the link dimensions of a selected mechanism which will generate the aforementioned optimum piston motion curve?

In order to demonstrate their approach, Sultan et al. used the geared five bar mechanism shown in Figure 1.5.

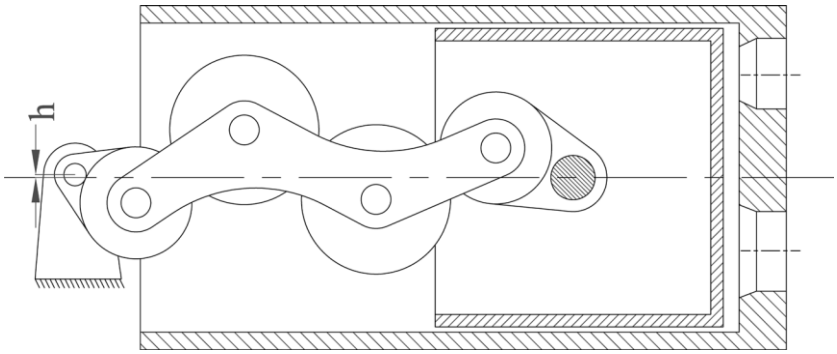

Figure 1.5. Geared Five Bar Mechanism[7]

In [7], the performance measures were taken to be volumetric efficiency, torque steadiness and cooling susceptibility. Two parameters, which are the crank angle duration for the compression process and the crank angle duration for the dwell at the end of the suction process, were selected to optimize the piston trajectory. The optimal values of the two parameters and the corresponding optimum piston motion curve are shown in Figure 1.6. Note that, in Figure 1.6, the conventional design refers to the piston motion curve provided by a slider crank mechanism.

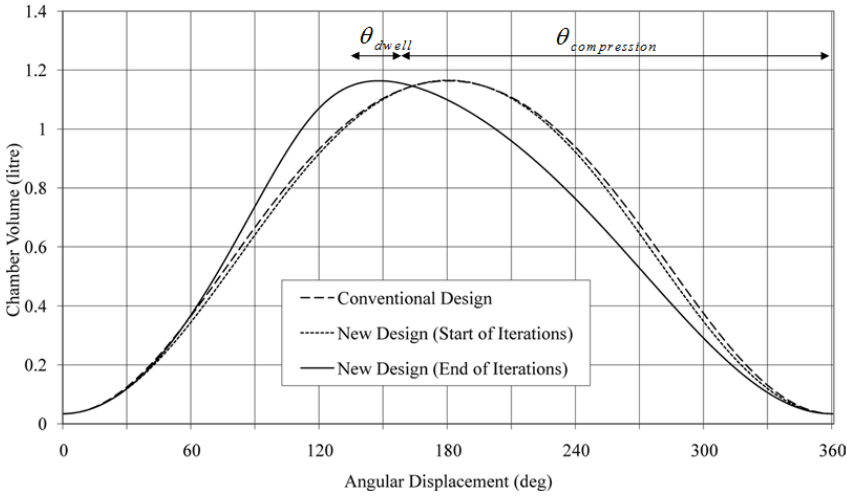

Figure 1.6. Optimum Piston Motion Curve Found by Sultan et al. [7]

Sol et al. [8] designed a new mechanism, named as "Efficient Motion Converter (EMC)", to replace the slider crank mechanism in reciprocating pumps. For this mechanism (see Figure 1.7) , force and the motion analyses have been performed. The results have been compared with an equivalent slider crank mechanism. The main advantages of this new mechanism, which have been listed in [8], are listed below.

- Due to the reduced unfavorable radial forces, a more efficient motion conversion is achieved. The forces that act on the bearings are reduced extensively, which leads to lower friction losses.
- The risk of cavitation is reduced since the EMC has significantly lower accelerations (% 15.4 lower acceleration).
- The EMC is able to withstand heavy shock load.

The disadvantages of this mechanism, on the other hand, have not been taken into account. The suggested mechanism is very complex since it has many components. The analyses that have been performed are not sufficiently detailed. At the end of the paper, the authors state that "the analysis is an initial analysis, and further analysis on strength, vibration and lubrication is required for determining the feasibility of the mechanism".

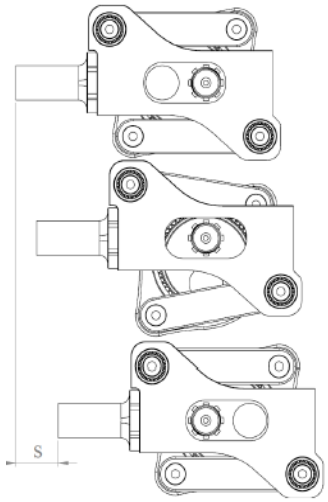

Figure 1.7. Efficient Motion Converter [8]

1.2.1 Mathematical Modelling of Reciprocating Compressors

Modelling a reciprocating compressor is a thermo-fluid problem. There are many studies related to this subject. Three dimensional computational fluid dynamics (CFD) gives the most accurate results for the analysis of a compressor. During the design process, however, CFD is employed only frequently (due to the heavy computational time requirements). Instead of CFD, the lumped parameter model (also named as the 0D model), which gives quite accurate results, is preferred. Hence, a 0D model is employed in this study. By using this model, the pressure and temperature in the cylinder, the valve motions and the pressure losses at the valves can be determined.

Stouffs et al.[9] developed a comprehensive model based on dimensionless parameters which are physically meaningful and which characterize the compressor. Later, Sultan and Kalim [7] extended this mathematical model. Tuhovcak et al.[10] also analysed a reciprocating compressor using a 0D model. In this study, conservation of energy for the cylinder, the flow through the valves, the heat losses and the pressure changes in the cylinder have been investigated. The lumped parameter approach has also been used by Liu et al.[11] and Faezaneh et

al.[12]. In their studies, they compared the results obtained from the mathematical models with available experimental data. Both of the aforementioned studies assume that flow through the valves is incompressible.

In this study, a 0D model is employed. The model takes into account the energy balance of the control volume, the piston motions, flows through the valves and the heat transfer between the walls of the cylinder and the fluid.

1.3 Scope of the Thesis

The MinFaS-TaR mechanism is a novel mechanism which can be used to convert any rotational input to a translational output motion. In this study, it is proposed to replace the slider crank mechanism that is used in reciprocating compressors with the MinFas-TaR mechanism.

The outline of the thesis is given below.

- In Chapter 2, mathematical modeling of a reciprocating compressor, via a detailed thermo-fluid model, is discussed.
- Chapter 3 is related to the performance analysis of reciprocating compressors. Firstly, various properties of a reciprocating compressor that are related to different performance aspects are discussed. Using these properties as design parameters, parametric analyses are then performed for a conventional reciprocating compressor. Next, basic cam motion curves, which may be used to model the piston motion of a reciprocating compressor regardless of the mechanism that is utilized, are discussed. Lastly, the effects of valve losses, heat transfer and piston motion profile on the performance of a reciprocating compressor are investigated.
- In Chapter 4, optimization of the piston motion curve is discussed. Two different methods are utilized for the optimization. In the first method, the piston motion function, $x_p(\theta)$, is taken to be the design function. Here, x_p

denotes the position of the piston and θ denotes the angular position of the crank. The corresponding chamber pressure function, $P_c(\theta)$, on the other hand, is obtained via simulation. In the second method, the chamber pressure function is taken to be the design function. The corresponding piston motion function, on the other hand, is obtained via simulation. If the piston motion function is selected to be the design function, it is difficult to predict the "shape" of the optimal design function. However, prediction of the optimal "shape" of the chamber pressure function is quite intuitive (the chamber pressure must be constant during the suction and discharge periods in order to minimize the valve losses). Hence, the second method is used in most of the optimizations. 7 case studies (which include single stage, multi stage and multi cylinder reciprocating compressors) are considered for the optimizations. The performance of the MinFaS-TaR based compressors are then compared with the corresponding slider crank based compressors.

- Finally, the conclusions and discussions are presented in Chapter 5.

In the thesis, the simulations are realized via SIMULINK. Some symbolic manipulations are carried out via MATHEMATICA. Finally, MATLAB is used for the optimizations.

CHAPTER 2

MODELLING OF RECIPROCATING COMPRESSORS

2.1 Introduction

Conventional reciprocating compressors mainly consist of a piston, a cylinder, a suction valve, a discharge valve, a connection rod and a crank. Schematic figure of a conventional reciprocating compressor is shown in Figure 2.1.

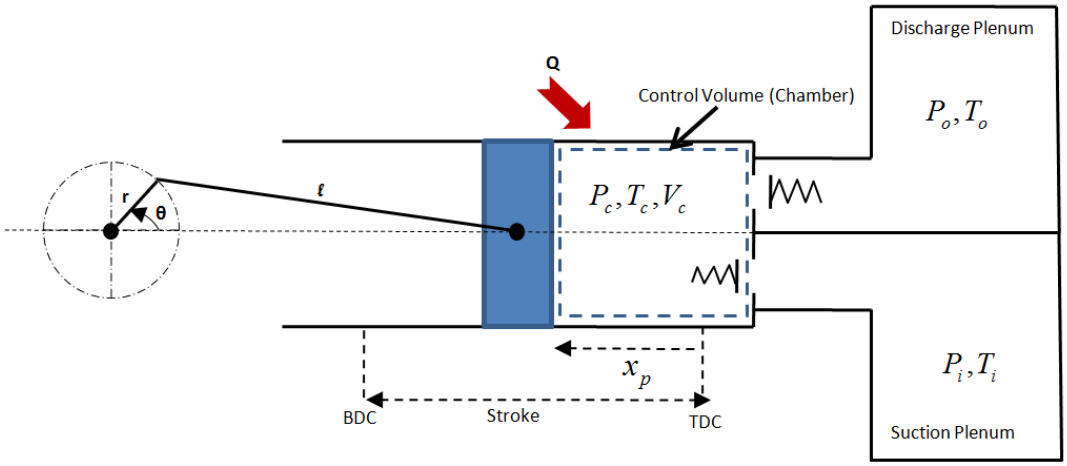

Figure 2.1.Reciprocating Compressor

In Figure 2.1, P_c, T_c and V_c indicate the pressure, the temperature and the volume of the gases in the control volume, respectively. On the other hand, P_o and T_o indicate the outlet pressure and the outlet temperature, respectively. Similarly, P_i and T_i indicate the inlet pressure and the inlet temperature, respectively. Furthermore, x_p is the piston displacement. BDC and TDC means bottom dead center and top dead center respectively.

A typical pressure versus volume graph of a reciprocating compressor is presented in Figure 2.2.

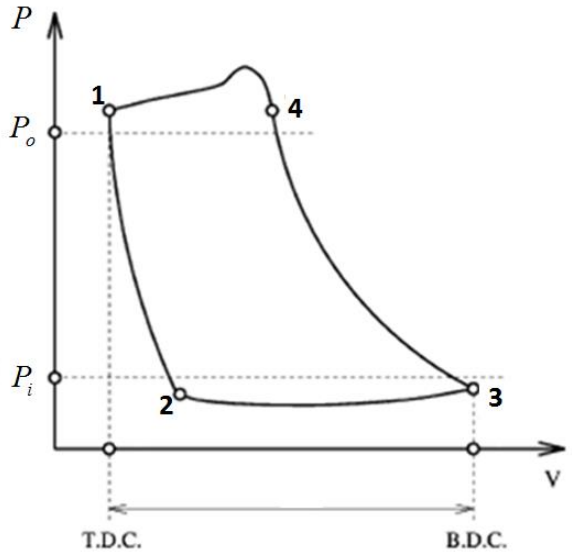

Figure 2.2. Pressure vs Volume for a Typical Reciprocating Compressor [9]

Referring to Figures 2.2 and 2.3, the four fundamental phases of a reciprocating compressor are listed below.

- (1-2) **Expansion**: The discharge phase is completed at the top dead center (TDC) and expansion starts. At this stage, the gas contained in the clearance volume expands to the inlet pressure.
- (2-3) **Suction**: It starts when the gas pressure reaches to a lower value than the inlet pressure. Due to this pressure difference, the suction valve opens and the gas flows into the cylinder.
- (3-4) **Compression**: After the piston reaches to the bottom dead center (BDC), the piston starts compressing the gas in the cylinder
- (4-1) **Discharge:** When the pressure inside the cylinder is greater than the pressure in the discharge plenum, the discharge valve opens and the gas flows from the cylinder into the discharge plenum.

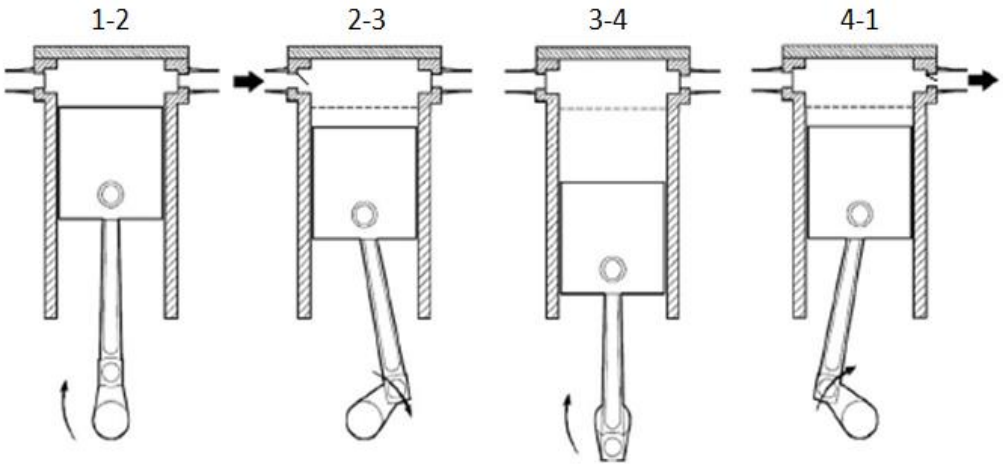

Figure 2.3.Fundamental Phases of a Reciprocating Compressor [13]

2.2 Thermo-Fluid Model of a Reciprocating Compressor

The control volume for the compressor is the volume between the piston head, the cylinder wall and the cylinder cover as shown in Figure 2.1. This control volume is labelled to be the chamber. Clearly, the control volume changes as the piston moves.

2.2.1 Piston Motion

In a conventional reciprocating compressor, the piston motion is generated by using a slider crank mechanism (which converts a rotational motion into a translational motion). The piston displacement, x_p, is given by

$$x_p(\theta) = r * \big(1 - cos(\theta)\big) + l * \left(1 - \sqrt{1 - \frac{r^2}{l^2} * sin^2(\theta)}\right) \qquad (2.1)$$

where θ is the crank angle (see Figure 2.1). Furthermore, r and l are the crank and the connecting rod lengths, respectively. The chamber volume, V_c, on the other hand, is defined via the equation

$$V_c = V_{cl} + A_p * x_p \tag{2.2}$$

where V_{cl} is the clearance volume and A_p is the area of the piston.

2.2.2 Energy

The first law of thermodynamics (in the rate of energy form), written for the control volume, is given below.

$$\dot{Q} + \sum \frac{dm_i}{dt} h_i = \dot{W} + \sum \frac{dm_o}{dt} h_o + \frac{d(m_c u)}{dt} \tag{2.3}$$

In equation (2.3), W is defined as the work done at the moving boundary in the cylinder, $\dot{Q}$ is defined as the heat transfer rate, u is the internal energy of the gas and h is the enthalpy of the gas. On the other hand, m_i, m_o and m_c are the inlet mass, the outlet mass and chamber mass, respectively. Furthermore, it is assumed that the gas in the cylinder is ideal and c_v and c_p are constant. Hence one can write down the following equations.

$$P = \rho RT \tag{2.4}$$

$$du = c_v dT \tag{2.5}$$

$$dh = c_p dT \tag{2.6}$$

$$c_p - c_v = R \tag{2.7}$$

where P, ρ and T indicates the pressure, the density and the temperature of the gas, respectively. c_p is heat capacity for ideal gas at constant pressure, c_v is heat capacity for ideal gas at constant volume and R is ideal gas constant.

Although the chamber temperature varies throughout the process, for simplicity, the values of c_v and c_p are taken to be constant at T_i. The effects of this assumption on the results will be checked in Appendix E (Note that it is checked after the end of all simulations).

Using equation (2.5), the last term in equation (2.3) can be expressed as shown below.

$$\frac{d(m_c u)}{dt} = m_c c_v \frac{dT_c}{dt} + T_c c_v \frac{dm_c}{dt} \tag{2.8}$$

The density of the gas in the chamber, ρ_c, on the other hand, can be calculated via the equation

$$\rho_c = \frac{m_c}{V_c} \tag{2.9}$$

whereas, the pressure in the chamber, P_c can be calculated via the equation

$$P_c = \rho_c R T_c \tag{2.10}$$

The rate of work done at the moving boundary is given by the equation

$$\frac{dW}{dt} = P_c \frac{dV_c}{dt} \tag{2.11}$$

Hence, using the above equations, equation (2.3) can be rearranged as follows.

$$\frac{dT_c}{dt} = \frac{1}{m_c(c_p - R)}\left(\dot{Q} + c_p \dot{m}_i T_i - P_c \dot{V}_c - c_p \dot{m}_o T_c - \left(c_p - R\right)(\dot{m}_i - \dot{m}_o)T_c\right) \tag{2.12}$$

2.2.3 Continuity

It should be recalled that the chamber between the piston and the cylinder is taken to be the control volume for the thermodynamic analysis. Conservation of mass equation for this control volume is given below.

$$\frac{dm_c}{dt} = \frac{dm_i}{dt} - \frac{dm_o}{dt} \tag{2.13}$$

2.2.4 Heat Transfer

Heat transfer between the fluid inside the chamber and the cylinder wall can be calculated by using the following convection heat transfer equation.

$$\dot{Q} = hA_{ht}(T_w - T_c) \tag{2.14}$$

where A_{ht} is the heat transfer area and T_w is the wall temperature. The heat transfer area, consists of the area of the wall, the area of the piston head and the area of the base of the cylinder. In other words,

$$A_{ht} = \frac{V_{cl}}{D_{cyl}} + \pi D_{cyl} x_p + \frac{\pi D_{cyl}^2}{2} \tag{2.15}$$

Here, D_{cyl} is the bore diameter of the cylinder. Heat transfer between the piston and the cylinder has been mostly studied for internal combustion engines. Several approximations for the heat transfer coefficient have been proposed. Two leading studies for the heat transfer correlation in a piston-cylinder assembly (in an internal combustion engine) are due to Annand [14] and Woschni [15]. Although the study by Woschni is not related to reciprocating compressors, the Woschni correlation has been frequently used to predict the heat transfer coefficient in reciprocating compressors. Hence, in this study, the Woschni correlation has been selected for

approximating the heat transfer coefficient. This correlation (see [15][16]) is presented below.

$$h = 0.0129{D_{cyl}}^{-0.2}P_c^{0.8}T_c^{-0.55}v^{0.8} \tag{2.16}$$

where,

$v = 2.28\left(v_p\right)_{avg}$ (during compression and expansion)

$v = 6.18\left(v_p\right)_{avg}$ (during suction and discharge)

Here, D_{cyl} is the bore diameter in m, P_c is the pressure in the chamber in Pa, T_c is the chamber temperature in K and $\left(v_p\right)_{avg}$ is the average velocity of the piston in m/s which is given by the equation

$$\left(v_p\right)_{avg} = \frac{\Delta x_p}{\Delta t} \tag{2.17}$$

For a reciprocating compressor employing a slider crank mechanism, $\left(v_p\right)_{avg}$ is given by the equation

$$\left(v_p\right)_{avg} = \frac{str}{T/2} \tag{2.18}$$

where str is the stroke and

$$T = \frac{2\pi}{\omega} \tag{2.19}$$

where ω indicates the motor speed. Adair et al.[17] state that the change in the wall temperature, with respect to time, is not significant. Hence, in this study, T_w is assumed to be constant.

2.2.5 Models for the Valve Motion and for the Flow Through the Valves

In this study, the suction and the discharge valves are modelled as mass spring damper systems. Hence, the inlet and the outlet valve openings, y_i and y_o (see Figure 2.4), are calculated by solving the two differential equations given by (2.20) and (2.22).

$$\frac{d^2y_i}{dt^2} = \frac{1}{m_{vi}}\left(f_{vi} - \frac{dy_i}{dt} * c_{vi} - y_i * k_{vi}\right) \tag{2.20}$$

where

$$f_{vi} = \frac{\pi D_{vi}^2}{4} * (P_i - P_c) \tag{2.21}$$

$$\frac{d^2y_o}{dt^2} = \frac{1}{m_{vo}}\left(f_{vo} - \frac{dy_o}{dt} * c_{vo} - y_o * k_{vo}\right) \tag{2.22}$$

where

$$f_{vo} = \frac{\pi D_{vo}^2}{4} * (P_c - P_o) \tag{2.23}$$

In the equations above, m_{vi} and m_{vo} indicate the mass of the inlet valve and the mass of the outlet valve, respectively. D_{vi} and D_{vo} indicate the diameter of the inlet valve and the diameter of the outlet valve, respectively. k_{vi} and k_{vo} indicate the spring coefficient of the inlet valve and the spring coefficient of the outlet valve, respectively. c_{vi} and c_{vo} indicate the damping coefficient of the inlet valve and the damping coefficient of the outlet valve, respectively.

The valves are stopped by hard stops at y=L, where L designates the opening limit of the valves. The mass spring model and the equivalent nozzle diagram of the discharge valve are shown in Figure 2.4.

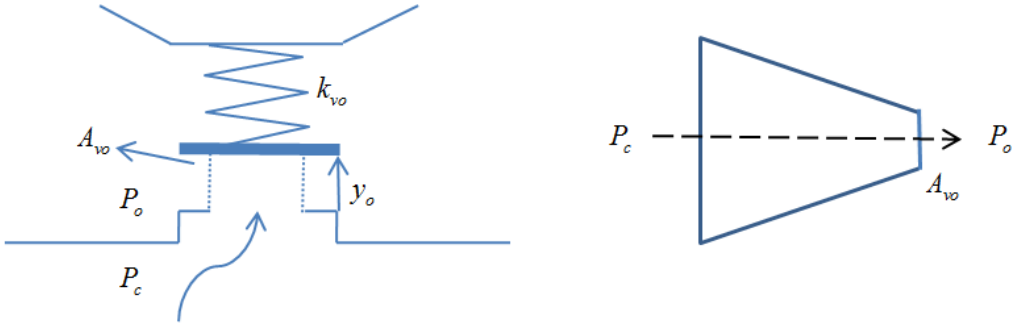

Figure 2.4. Mass Spring Model and Nozzle Diagram of the Discharge Valve

The instantaneous valve areas A_{vi} and A_{vo} are given by the expressions below.

$$A_{vi} = \pi D_{vi} y_i \tag{2.24}$$

$$A_{vo} = \pi D_{vo} y_o \tag{2.25}$$

The flow through a valve is modelled as a reversible and adiabatic flow through a convergent nozzle. In order to determine the mass flow rate through a reversible and adiabatic convergent nozzle, one proceeds as follows.

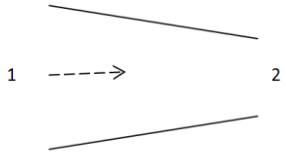

Figure 2.5. Convergent Nozzle

The energy equation for the nozzle (see Figure 2.5) is given below.

$$h_1 + \frac{V_1^2}{2} = h_2 + \frac{V_2^2}{2} \tag{2.26}$$

Assuming A_1 is large and the flow velocity V_1 is negligible, one obtains:

$$V_2 = \sqrt{2c_p(T_1 - T_2)} = \sqrt{2c_p T_1(1 - \frac{T_2}{T_1})} \tag{2.27}$$

The relations due to the isentropic flow and the ideal gas state equation are given by

$$\left(\frac{P_2}{P_1}\right)^{\frac{\gamma-1}{\gamma}} = \frac{T_2}{T_1} \tag{2.28}$$

$$T_1 = \frac{P_1}{\rho_1 R} \tag{2.29}$$

respectively. The relationship between c_p, R and γ, on the other hand, is

$$\frac{c_p}{R} = \frac{\gamma}{\gamma - 1} \tag{2.30}$$

Substituting (2.28), (2.29) and (2.30) into (2.27), one obtains

$$V_2 = \sqrt{2\frac{\gamma}{\gamma-1}\frac{P_1}{\rho_1}\left(1 - \left(\frac{P_2}{P_1}\right)^{\frac{\gamma-1}{\gamma}}\right)} \tag{2.31}$$

Hence, the mass flow rate through the nozzle is obtained to be

$$\dot{m}_2 = \rho_2 A_2 V_2 = A_2 \rho_1 \left(\frac{P_2}{P_1}\right)^{\frac{1}{\gamma}} \sqrt{2\frac{\gamma}{\gamma-1}\frac{P_1}{\rho_1}\left(1 - \left(\frac{P_2}{P_1}\right)^{\frac{\gamma-1}{\gamma}}\right)} \tag{2.32}$$

If the flow is chocked, i.e.[13],

$\frac{P_2}{P_1} \leq \left(\frac{2\gamma}{\gamma+1}\right)^{\frac{\gamma}{\gamma-1}} = 0.528,$

equation (2.32) is not applicable. In this case, the velocity of the fluid will be equal to the speed of sound, i.e.[7],

$$V_2 = \sqrt{\gamma R T_1} \tag{2.33}$$

Equations (2.26)-(2.33) have been derived for the nozzle in Figure 2.5. The notation that is used in these equations is modified according to the type valve. For the inlet valve, subscripts 1 and 2 should be changed to i and c, respectively. For the outlet valve, subscripts 1 and 2 should be changed to c and o, respectively. Hence, the mass flow rates through the suction and discharge valves are obtained as follows.

$$\frac{dm_i}{dt} = \begin{cases} C_{di} A_{vi} \rho_i \left(\frac{P_c}{P_i}\right)^{\frac{1}{\gamma}} \sqrt{2 \frac{\gamma}{\gamma - 1} \frac{P_i}{\rho_i} \left(1 - \left(\frac{P_c}{P_i}\right)^{\frac{\gamma-1}{\gamma}}\right)} & if\ P_i > P_c\ \&\ \frac{P_c}{P_i} > 0.528 \\ C_{di} A_{vi} \rho_i \sqrt{\gamma R T_i} & \frac{P_c}{P_i} \le 0.528 \\ -C_{di} A_{vi} \rho_c \left(\frac{P_i}{P_c}\right)^{\frac{1}{\gamma}} \sqrt{2 \frac{\gamma}{\gamma - 1} \frac{P_c}{\rho_c} \left(1 - \left(\frac{P_i}{P_c}\right)^{\frac{\gamma-1}{\gamma}}\right)} & if\ P_i < P_c\ \&\ \frac{P_i}{P_c} > 0.528 \\ -C_{di} A_{vi} \rho_c \sqrt{\gamma R T_c} & \frac{P_i}{P_c} \le 0.528 \end{cases} \tag{2.34}$$

$$\frac{dm_o}{dt} = \begin{cases} C_{do} A_{vo} \rho_c \left(\frac{P_o}{P_c}\right)^{\frac{1}{\gamma}} \sqrt{2 \frac{\gamma}{\gamma - 1} \frac{P_c}{\rho_c} \left(1 - \left(\frac{P_o}{P_c}\right)^{\frac{\gamma-1}{\gamma}}\right)} & if\ P_c > P_o\ \&\ \frac{P_o}{P_c} > 0.528 \\ C_{do} A_{vo} \rho_c \sqrt{\gamma R T_c} & \frac{P_o}{P_c} \le 0.528 \\ -C_{do} A_{vo} \rho_o \left(\frac{P_c}{P_o}\right)^{\frac{1}{\gamma}} \sqrt{2 \frac{\gamma}{\gamma - 1} \frac{P_o}{\rho_o} \left(1 - \left(\frac{P_c}{P_o}\right)^{\frac{\gamma-1}{\gamma}}\right)} & if\ P_c < P_o\ \&\ \frac{P_c}{P_o} > 0.528 \\ -C_{do} A_{vo} \rho_o \sqrt{\gamma R T_o} & \frac{P_c}{P_o} \le 0.528 \end{cases} \tag{2.35}$$

The temperature of the discharged gas, on the other hand, may be calculated from the isentropic relation, yielding

$$T_o = T_c \left(\frac{P_o}{P_c}\right)^{\frac{\gamma-1}{\gamma}} \tag{2.36}$$

2.2.6 Work Done and Shaft Torque

Work done by the piston on the fluid is calculated via the equation

$$W_p = -\int P_c \frac{dV_c}{dt} dt \tag{2.37}$$

By neglecting inertial effects, the instantaneous shaft torque, τ, on the other hand, is given by the equation

$$\tau = \frac{\frac{dW_p}{dt}}{\omega} = \frac{-P_c \frac{dV_c}{dt}}{\omega} \tag{2.38}$$

2.3 Numerical Solution of the Thermo-Fluid Model of a Reciprocating Compressor

In the previous sections, the reciprocating compressor has been mathematically modelled. In this model, the crank angle, $\theta(t)$, is considered to be the input. The simulation block diagram of the model is presented in Figure 2.6. The piston motion provided by $\theta(t)$ and the constant terms can be considered to be design parameters that can be selected in the beginning of the simulation.

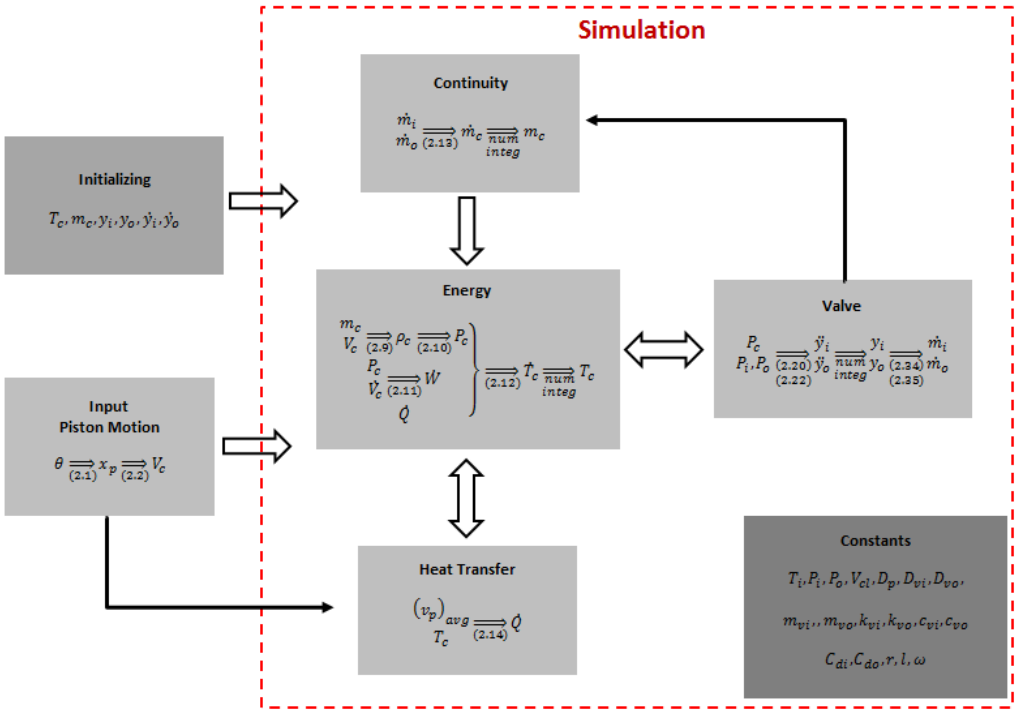

Figure 2.6. Simulation Block Diagram

There are 13 "unknown" time functions $[i.e., \dot{T}_c(t), \dot{m}_c(t), V_c(t), \rho_c(t), P_c(t), \dot{Q}(t), \ddot{y}_i(t), \ddot{y}_o(t), \dot{m}_i(t), \dot{m}_o(t), T_o(t), W_p(t), \tau(t)]$ and 13 equations (i.e., equations 2.2, 2.9, 2.10, 2.12, 2.13, 2.14, 2.20, 2.22, 2.34, 2.35, 2.36, 2.37, 2.38). Four of these equations [namely, energy equation (2.12), continuity equation (2.13) and equations of motion for the inlet and outlet valves (2.20) and (2.22)] are differential equations. These 13 equations are solved via a code developed in Simulink. Fourth order Runge-Kutta is chosen as the solver and the time step is taken to be 10^{-5} seconds.

Since the 13 equations include 2 first order and 2 second order differential equations, 6 initial conditions are required. The initial conditions for $T_c, m_c, y_i, y_o, \dot{y}_i, \dot{y}_o$ are calculated using the iterative approach that was used by Sultan[7]. This approach is based on the periodicity of the model. In other words, the values of T_c, m_c, y_i and y_o at the start of the cycle must be equal to the values of T_c, m_c, y_i and y_o at the end of the cycle. To this purpose, an error, e, is defined via the equation

$$e = \sqrt{\begin{matrix} \left(\frac{T_c(\theta) - T_c(\theta + 2\pi)}{\bar{T}_c}\right)^2 + \left(\frac{m_c(\theta) - m_c(\theta + 2\pi)}{\bar{m}_c}\right)^2 \\ + \left(\frac{y_i(\theta) - y_i(\theta + 2\pi)}{\bar{y}_i}\right)^2 + \left(\frac{y_o(\theta) - y_o(\theta + 2\pi)}{\bar{y}_o}\right)^2 \\ + \left(\frac{\dot{y}_i(\theta) - \dot{y}_i(\theta + 2\pi)}{\bar{\dot{y}}_i}\right)^2 + \left(\frac{\dot{y}_o(\theta) - \dot{y}_o(\theta + 2\pi)}{\bar{\dot{y}}_o}\right)^2 \end{matrix}} \quad (2.39)$$

where

$$\bar{T}_c = \frac{T_c(\theta) + T_c(\theta + 2\pi)}{2}, \qquad \bar{m}_c = \frac{m_c(\theta) + m_c(\theta + 2\pi)}{2}$$

$$\bar{y}_i = \frac{y_i(\theta) + y_i(\theta + 2\pi)}{2}, \quad \bar{y}_o = \frac{y_o(\theta) + y_o(\theta + 2\pi)}{2}$$

$$\bar{\dot{y}}_i = \frac{\dot{y}_i(\theta) + \dot{y}_i(\theta + 2\pi)}{2}, \quad \bar{\dot{y}}_o = \frac{\dot{y}_o(\theta) + \dot{y}_o(\theta + 2\pi)}{2}$$

The steps of the iterative approach are given below.

1. $T_c(0)$, $m_c(0)$, $y_i(0)$, $y_o(0)$, $\dot{y}_i(0)$, $\dot{y}_o(0)$ are assigned to their user predicted values.
2. Simulation program is run.
3. e is calculated from equation (2.39).
4. Set $T_c(0) = \bar{T}_c$, $m_c(0) = \bar{m}_c$, $y_i(0) = \bar{y}_i$, $y_o(0)=\bar{y}_o$, $\dot{y}_i(0) = \bar{\dot{y}}_i$, $\dot{y}_o(0) = \bar{\dot{y}}_o$
5. If e is less than a predefined value, stop iterations. If not, repeat steps 2-4 until e is less than a predefined value.

The wall temperature, on the other hand, is taken to be equal to the mean temperature (with respect to time) of the chamber. In order to determine T_w, an iterative approach is employed. The iteration starts by assuming that $T_w = T_i$; and runs until $T_{w,n+1} - T_{w,n} < 0.5\ ^\circ C$ where n designates the iteration counter.

The numerical data for the slider crank based, single cylinder reciprocating compressor taken from [7] is shown in Table 2.1. The missing data have been estimated from the figures, tables etc. in [7]. In this compressor, the working medium is air.

The compressor with the numerical data given in Table 2.1 has been simulated using the developed code in Simulink. The pressure versus chamber volume graph generated by the code is shown in Figure 2.7. Other graphs generated by the code have been presented in appendix A.

Table 2.1 Numerical Data for the Slider Crank Based, Single Cylinder Reciprocating Compressor

Property	**Value**	**Unit**
Clearance Volume, V_{cl}	$0.05*10^{-3}$	m^3
Percent Clearance Volume, V_{pcl}	4.23	%
Diameter of the Cylinder, D_{cyl}	0.120	m
Velocity of Motor Shaft, ω	800	rpm
Mass of Valve, $m_{vi} = m_{vo}$	50*1e-3	kg
Spring Coefficient of Valve, $k_{vi} = k_{vo}$	5000	N/m
Damping Coefficient of Valve, $c_{vi} = c_{vo}$	0	Ns/m
Max Opening of Valve, L	3*1e-3	m
Inlet Valve Diameter , D_{vi}	50*1e-3	m
Outlet Valve Diameter , D_{vo}	40*1e-3	m
Outlet Pressure, P_o	6*1e5	Pa
Inlet Pressure, P_i	1*1e5	Pa
Inlet Temperature, T_i	20	℃
Discharge Coefficient of Valve C_{di}, C_{do}	0.99	~
Crank Length, r	0.05	m
Rod Length, l	0.125	m

The percent clearance volume, given in Table 2.1, V_{pcl} is defined as below.

$$V_{pcl} = \frac{V_{cl}}{V_c(at\ BDC)} * 100 \tag{2.40}$$

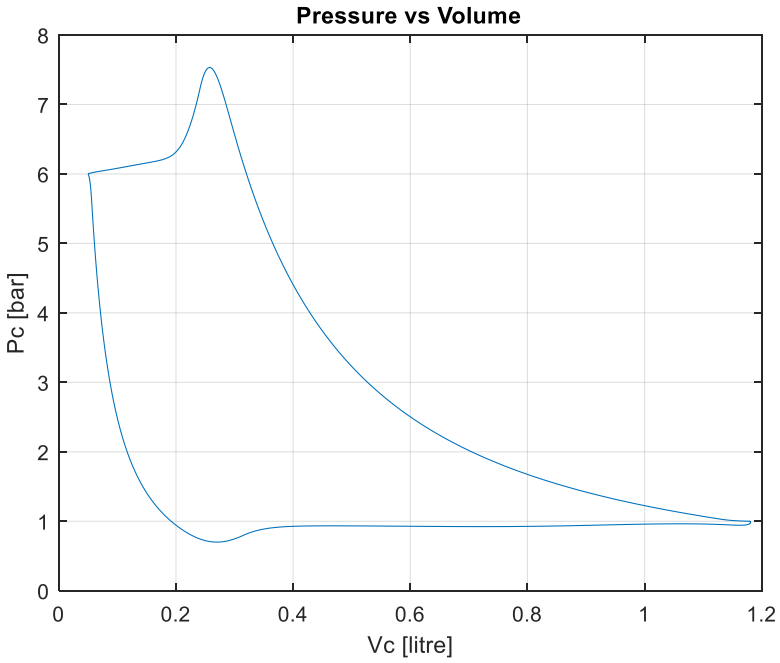

Figure 2.7. Pressure vs Chamber Volume for the Slider Crank Based, Single Cylinder Reciprocating Compressor

CHAPTER 3

PERFORMANCE ANALYSIS OF RECIPROCATING COMPRESSORS

3.1 Introduction

In this chapter, firstly, various properties of a reciprocating compressor that are related to different performance aspects are introduced. Using these properties, a parametric analysis is performed for a conventional reciprocating compressor (employing a slider crank mechanism).

Next, in order to see the effects of the piston motion on the performance of a reciprocating compressor, the motion profile of the piston is changed with typical cam motion profile curves regardless of the mechanism.

Lastly, in order to see the effects of valve losses and heat transfer on the performance, some case studies are realized.

3.2 Performance Aspects of Reciprocating Compressors

For a reciprocating compressor, some properties that are related to different performance aspects can be listed to be the volumetric efficiency, the capacity, the inertia of the flywheel, the isothermal efficiency, the work done by the motor and the output pressure energy efficiency.

3.2.1 Volumetric Efficiency

The volumetric efficiency, η_v, is a measure related to the amount of fluid (at the suction plenum conditions) that is filled into the compressor. η_v is calculated by dividing the volume of the inlet fluid to the swept volume, i.e.,

$$\eta_v = \frac{\frac{m_i R T_i}{P_i}}{V_{max} - V_{cl}} \tag{3.1}$$

where V_{max} is the volume of the chamber when the piston is at BDC.

3.2.2 Capacity

The capacity, cap, is the volume of fluid compressed per unit time. Capacity is defined via the equation

$$cap = \frac{m_i R T_i}{P_i} \omega \frac{3600}{2\pi} \tag{3.2}$$

where the units are m^3/hr

3.2.3 Inertia of Flywheel

In a mechanical device, the actuator torque, τ_{Drive} is usually constant. However, the load torque τ_{Load} , will, in general, be fluctuating. This situation is shown in Figure 3.1 for a typical machine. In this figure, θ denotes the angular position of the actuator.

The flywheel is used to absorb energy when the load torque is smaller than the actuator torque. When the load torque is greater than the actuator torque, the flywheel returns the stored energy. In the design of a reciprocating compressor, the inertia of the flywheel is a significant parameter that needs to be decided properly.

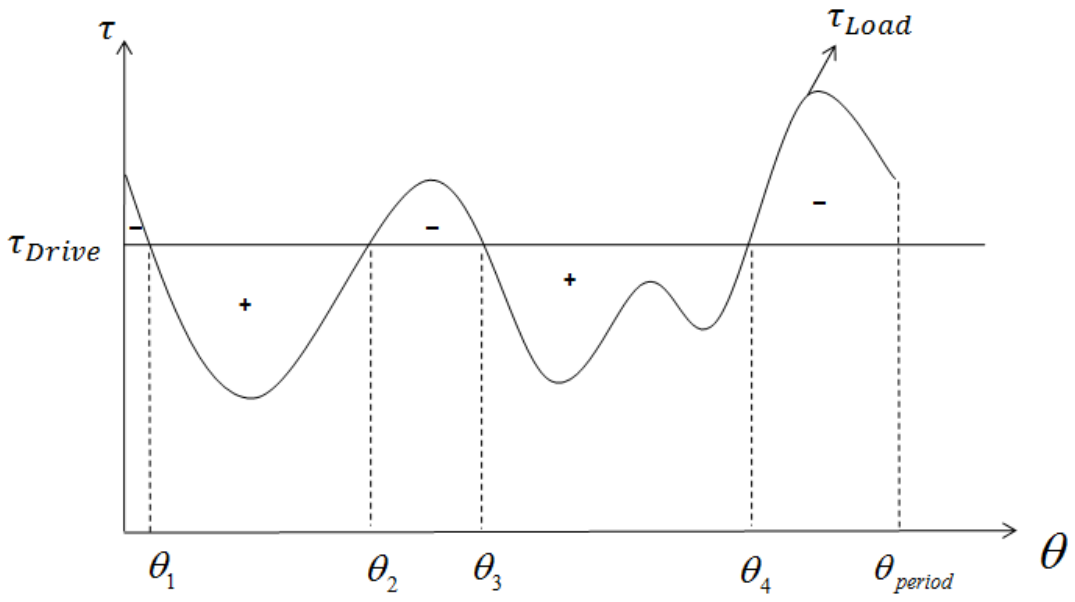

Figure 3.1. Actuator and Load Torque vs. Crank Angle of a Typical Machine

In Figure 3.1, (-) implies that the flywheel provides energy; (+) means that the flywheel absorbs energy

The energy supplied should be equal to the energy consumed. Therefore τ_{Drive} is calculated by using the equation below.

$$\int_0^{\theta_{period}} \tau_{Drive}(\theta)d\theta = \int_0^{\theta_{period}} \tau_{Load}(\theta)d\theta \tag{3.3}$$

Assuming that τ_{Drive} is constant, one obtains

$$\tau_{Drive} = \frac{1}{\theta_{period}} \int_0^{\theta_{period}} \tau_{Load}(\theta)d\theta \tag{3.4}$$

The inertia of the flywheel is defined via the equation [18]

$$I_{fw} = \frac{\Delta E_{fw}}{\delta \omega_a^2} \tag{3.5}$$

where ω_a , the average desired velocity, is given by

$$\omega_a = \frac{\omega_{max} + \omega_{min}}{2} \tag{3.6}$$

δ , the coefficient of speed fluctuation, is given by

$$\delta = \frac{\omega_{max} - \omega_{min}}{\omega_a} \tag{3.7}$$

and ΔE_{fw} denotes the energy difference (between the maximum and minimum eneries).

The maximum and the minimum energies are found from the so called energy line diagram. An example for the energy line diagram of a machine (which has the torque characteristic given in Figure 3.1) is shown in Figure 3.2.

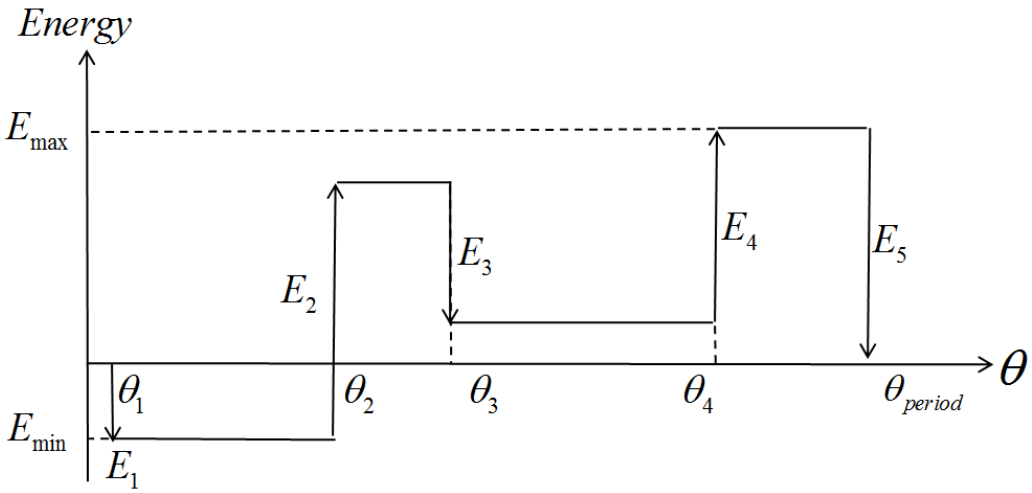

Figure 3.2. Energy Line Diagram of a Machine

In the energy line diagram, the energies $E_1, E_2, \ldots$ are calculated via the equations

$$E_1 = \int_0^{\theta_1} (\tau_{Load} - \tau_{Drive}) d\theta$$

$$E_2 = \int_{\theta_1}^{\theta_2} (\tau_{Load} - \tau_{Drive}) d\theta \qquad (3.8)$$

$$\vdots$$

The maximum energy, E_{max}, and the minimum energy, E_{min}, are determined by using the energy line diagram. The difference between the maximum and the minimum energy, the so called energy difference, is then calculated via the equation

$$\Delta E_{fw} = E_{max} - E_{min} \qquad (3.9)$$

The load torque is found by simulating the compressor. In the simulation of the compressor, $\tau_{Load}(\theta)$ is obtained by assuming that the actuator is driven at a constant speed.

3.2.4 Isothermal Efficiency

The isothermal efficiency is a widely used property that is used for comparing reciprocating compressors with each other. The minimum net work done by the compressor is realized in isothermal conditions. The assumptions for an ideal isothermal compressor are that the temperature is constant at T_i and the valves are ideal. The P-V diagram of an isothermal compressor is shown in Figure 3.3.

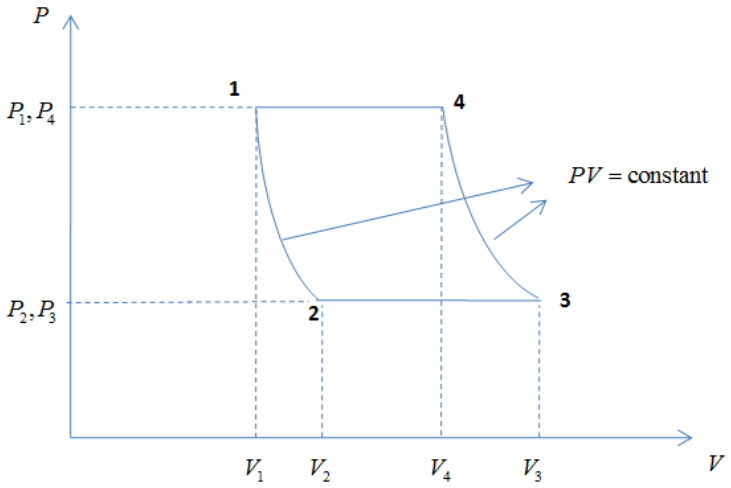

Figure 3.3. Pressure vs Volume Graph of an Isothermal Compressor

The work expressions for the processes shown in Figure 3.3.are listed below.

$$W_{1-2} = P_1 V_1 \ln\left(\frac{P_1}{P_2}\right) \tag{3.10}$$

$$W_{2-3} = P_2(V_3 - V_2) \tag{3.11}$$

$$W_{3-4} = P_3 V_3 \ln\left(\frac{P_3}{P_4}\right) \tag{3.12}$$

$$W_{4-1} = P_4(V_1 - V_4) \tag{3.13}$$

where

$$P_2 = P_3 = P_i \tag{3.14}$$

$$P_1 = P_4 = P_o \tag{3.15}$$

V_1 is the clearance volume and V_3 is the maximum volume, i.e.,

$$V_1 = V_{cl} \tag{3.16}$$

$$V_3 = V_{max} \tag{3.17}$$

V_2 and V_4 are found using the fact that the product PV is constant for processes 1-2 and 3-4. Hence, one obtains

$$P_1V_1 = P_2V_2 \Rightarrow P_oV_{cl} = P_iV_2 \Rightarrow V_2 = \frac{P_oV_{cl}}{P_i} \tag{3.18}$$

$$P_3V_3 = P_4V_4 \Rightarrow P_iV_{max} = P_oV_4 \Rightarrow V_4 = \frac{P_iV_{max}}{P_o} \tag{3.19}$$

The isothermal net work done, W^{iso}, can be calculated via the equation

$$W^{iso} = W_{1-2} + W_{2-3} + W_{3-4} + W_{4-1} \tag{3.20}$$

where

$$W_{1-2} = P_oV_{cl}\ln\left(\frac{P_o}{P_i}\right) \tag{3.21}$$

$$W_{2-3} = P_i(V_{max} - V_2) \tag{3.22}$$

$$W_{3-4} = P_iV_{max}\ln\left(\frac{P_i}{P_o}\right) \tag{3.23}$$

$$W_{4-1} = P_o(V_{cl} - V_4) \tag{3.24}$$

In order to find the net work done per unit mass, the inlet mass for a cycle can be calculated via the equation

$$m_i = \rho_i (V_3 - V_2) = \frac{P_i}{RT_i}(V_3 - V_2) \tag{3.25}$$

Therefore the isothermal net work done per mass, W_{pm}^{iso}, is found as below.

$$W_{pm}^{iso} = \frac{W^{iso}}{m_i} \tag{3.26}$$

After some manipulations, W_{pm}^{iso} can be simply expressed as shown below

$$W_{pm}^{iso} = -RT_i \ln\left(\frac{P_o}{P_i}\right) \tag{3.27}$$

The isothermal efficiency per mass, η_{pm}^{iso}, is the ratio of the isothermal net work done per mass to the actual net work done per mass (i.e., W_{pm}^{act}).

$$\eta_{pm}^{iso} = \frac{W_{pm}^{iso}}{W_{pm}^{act}} \tag{3.28}$$

3.2.5 Work Done

Depending upon the type of the electric motor, consumption of energy of the motor can be equal to the net work done, W_{net}, positive work done, W_{pos}, or absolute work done, W_{abs}, by the motor.

The motor torque is used to balance the pressure forces, the inertia forces and the frictional forces. In this study, the frictional forces are neglected. Hence, the torque and power of the motor are defined via the equations

$$\tau_m(t) = \tau_{pres}(t) + \tau_{iner}(t) \tag{3.29}$$

$$Pow_m(t) = \omega \tau_m(t) \tag{3.30}$$

Using equation (3.29) and assuming that ω is constant, equation (3.30) yields

$$Pow_m(t) = \omega \left[\tau_{pres}(t) + \tau_{iner}(t)\right] \tag{3.31}$$

The notation that is used in the above equations are given below.

$\tau_{pres}(t)$: Motor torque necessary to overcome the pressure forces

$\tau_{iner}(t)$: Motor torque necessary to overcome the inertia forces

$\tau_m(t)$: Total motor torque necessary to overcome the pressure forces and the inertia forces.

$Pow_m(t)$: Total motor power required to overcome the pressure forces and the inertia forces.

The positive power, $P_{m,pos}$, and the negative motor power, $P_{m,neg}$, can be defined as follows

$$Pow_{m,pos}(t) = \begin{cases} Pow_m(t) & if\ Pow_m(t) > 0 \\ 0 & if\ Pow_m(t) \leq 0 \end{cases} \tag{3.32}$$

$$Pow_{m,neg}(t) = \begin{cases} 0 & if\ Pow_m(t) \geq 0 \\ -Pow_m(t) & if\ Pow_m(t) < 0 \end{cases} \tag{3.33}$$

Hence, the positive work, the negative work, the absolute work and the net work done by the motor are defined via the following equations.

$$W_{pos} = \int_0^T \left[Pow_{m,pos}(t)\right] dt \tag{3.34}$$

$$W_{neg} = \int_0^T \left[Pow_{m,neg}(t)\right] dt \tag{3.35}$$

$$W_{abs} = W_{pos} + W_{neg} \tag{3.36}$$

$$W_{net} = W_{pos} - W_{neg} \tag{3.37}$$

The positive work, the absolute work and the net work done by the motor (per mass of compressed air) on the other hand, are defined via the equations

$$W_{pos}^{pm} = \frac{W_{pos}}{m_i} \tag{3.38}$$

$$W_{abs}^{pm} = \frac{W_{abs}}{m_i} \tag{3.39}$$

$$W_{net}^{pm} = \frac{W_{net}}{m_i} \tag{3.40}$$

In the slider crank based compressor, the inertias of all of the links in the slider crank mechanism (including the piston) are neglected. Hence, in the slider crank based compressor, the torque due to the inertia forces is zero. However, for the MinFaS-TaR based compressor (see MinFaS-TaR in Figure 1.2), the torque due to the inertia forces will be taken into consideration. It is assumed that the roller masses and the inertias of links 2 and 4 are neglected. The masses of links 3 and 5, on the other hand, can be adjusted such that $m_3 = m_5$. The actuator torque calculation of the MinFaS-TaR based compressor is explained in detail in section 4.1.3.

3.2.6 Output Pressure Energy Efficiency

In this thesis, a new efficiency definition, for reciprocating compressors, is introduced. This novel efficiency, which is output pressure energy per input energy

supplied by the motor, is labelled to be output pressure energy efficiency, η_{pres}. Output pressure energy, E^o_{pres}, on the other hand, is defined via the equation

$$E^o_{pres} = \int P_o \frac{dV_o}{dt} dt \tag{3.41}$$

where $\frac{dV_o}{dt}$ is the volumetric flow rate at output. If the input energy is taken to be the net work done by the motor, η_{pres} is defined via equation

$$\eta_{pres} = \frac{E^o_{pres}}{W_{net}} \tag{3.42}$$

3.2.7 Actuator Torque Characteristics

The actuator torque characteristics can be considered to be another performance aspect of a reciprocating compressor. Since the actuator torque variation affects the size of the flywheel and the life of mechanical components (since fluctuating torque causes fatigue), it should be analysed in detail. Different measures can be defined to predict the steadiness of the actuator torque. For example, the root mean square of the actuator torque, τ_{rms}, is one of the possible measures. Sultan [7] et al., on the other hand, defined the following measure for the torque steadiness.

$$\eta_\tau = 1 - \frac{\tau_{max} - \tau_{mean}}{\tau_{max} + \tau_{mean}} \tag{3.43}$$

Here, τ_{max} is the maximum value of the torque and τ_{mean} is the mean value of the torque. It should be noted that, neither τ_{rms} nor η_τ yield a prediction of ΔE which is required for the design of the flywheel as explained in Section 3.2.3 (this claim is proved, by using counter examples, in Appendix B). Hence, ΔE should be computed separately in order to see the effects of the torque variation on the size of the flywheel.

3.3 Reciprocating Compressor Employing a Slider Crank Mechanism

The simulation described in the previous chapter has been utilized to simulate the slider crank based, single cylinder reciprocating compressor discussed in [7]. The numerical data of the compressor is given in Table 2.1. The results and the performance aspects are presented in Table 3.1.

In Table 3.1, maximum (max), minimum (min), delta (difference between max value and min value), mean and root mean square (rms) of chamber pressure, chamber temperature, outlet temperature, shaft torque and heat rate are presented. Next, valve timings with respect to θ for the inlet and outlet valves are given. Definition of opening start, open, closing start and close are that at which crank angle (θ) valve starts opening, opens fully, starts closing and closes fully, respectively. Furthermore, mass in compression, mass in expansion and mass inlet mean that mass in the compression phase (phase 3-4 in Figure 2.2), mass in the expansion phase (1-2 in Figure 2.2) and mass of the inlet air, respectively.

Table 3.1 Numerical Results for the Slider Crank Based, Single Cylinder Reciprocating Compressor

Parameter	**Unit**	**Quantity**	**Value**
Chamber Pressure	[bar]	max	7,532
		min	0,7
		delta	6,832
		mean	2,248
		rms	3,008
Chamber Temperature-	[°C]	max	267,1
		min	-11,7

Table 3.1 (continued)

		delta	278,9
		mean	81,1
		rms	113,7
Outlet Temperature	[°C]	max	234,9
		min	204,8
		delta	30,1
		mean	223,2
		rms	223,4
Shaft Torque	[Nm]	max	382,4
		min	-72,9
		delta	455,3
		mean	39,2
		rms	116,6
Heat Rate	[W]	max	291,93
		min	-1856,32
		delta	2148,25
		mean	-84,07
		rms	519,14
Inlet Valve Timing (with respect to θ)	[°]	Opening Start	35,28
		Open	49,63

Table 3.1 (continued)

		Closing Start	57,07
		Close	211,06
Outlet Valve Timing (with respect to θ)	[°]	Opening Start	310,03
		Open	318,77
		Closing Start	335,66
		Close	7,3
Mass in Compression	[g]	~	1,3191
Mass in Expansion	[g]	~	0,23405
Mass Inlet	[g]	~	1,08505
Net Heat Transfer	[J]	~	-6,29
$\boldsymbol{W_{net}}$	[J]	~	246,49
$\boldsymbol{W_{net}^{pm}}$	[kJ/kg]	~	227,17
$\boldsymbol{\eta_{pm}^{iso}}$	[%]	~	66,32
$\boldsymbol{\eta_{v}}$	[%]	~	80,68
$\boldsymbol{cap}$	[m^3/hr]	~	43,8
$\boldsymbol{W_{pos}^{pm}}$	[kJ/kg]	~	342.03
$\boldsymbol{W_{abs}^{pm}}$	[kJ/kg]	~	456.77
$\boldsymbol{\eta_{pres}}$	[%]	~	60.1
$\boldsymbol{I_{fw}}$	kgm^2	~	1.536
$\boldsymbol{\Delta E_{fw}}$	[J]	~	269.44

3.4 Parametric Analysis of a Slider-Crank Based Reciprocating Compressor

The motor speed, diameters of the valves, spring coefficients of the valves, percentage of the clearance volume, stroke, piston diameter and the wall temperature are important parameters that affect the performance of a reciprocating compressor. Hence, a parametric analysis has been realized in order to analyze the effects of these parameters on the performance of the reciprocating compressor. In this parametric analysis, only one parameter has been changed while all of the remaining parameters are fixed at their nominal values.

3.4.1 Parametric Analysis for the Motor Speed

The motor speed has been taken to be 400, 800 and 1600 rpm, while all other parameters have been kept at their nominal values. The resulting P-V diagram is shown in Figure 3.4. Numerical results and the performance aspects are tabulated in Table 3.2.

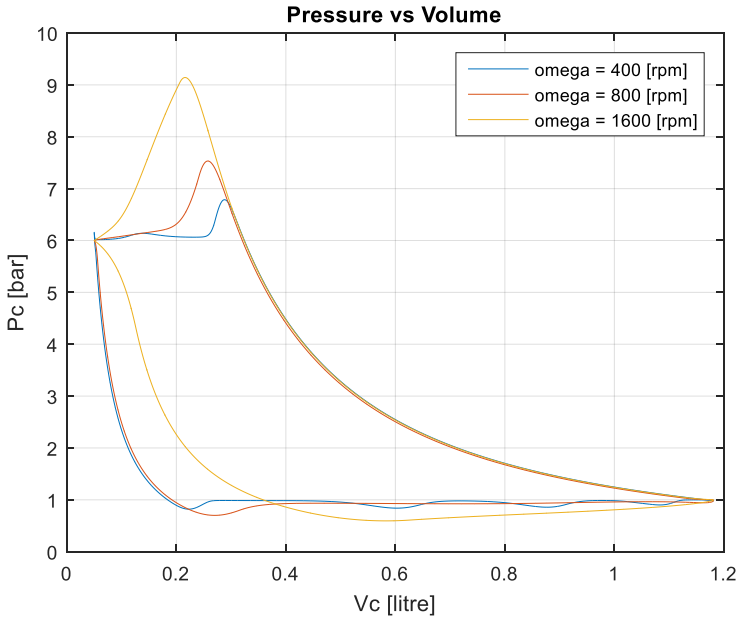

Figure 3.4. P-V Diagram for the Parametric Analysis of Motor Speed

As seen in the P-V diagram, when the motor speed decreases, losses at valves will decrease. However, a slower compressor compresses less gas per time. In other words, the capacity of the slower compressor is less.

Table 3.2 Results obtained for the Parametric Analysis of Motor Speed

Parameter	**Unit**	**Quantity**	**Value**		
			ω = 400 rpm	**ω = 800 rpm**	**ω=1600 rpm**
Chamber Pressure	[bar]	max	6.786	7.532	9.142
		min	0.82	0.7	0.594
		delta	5.966	6.832	8.548
		mean	2.229	2.248	2.511
		rms	2.948	3.008	3.438
Chamber Temperature	[°C]	max	245.8	267.1	318.8
		min	-5.3	-11.7	-13.9
		delta	251.2	278.9	332.7
		mean	76.9	81.1	100.4
		rms	108.5	113.7	137.5
Outlet Temperature	[°C]	max	228.9	234.9	254.8
		min	198.2	204.8	219.4
		delta	30.7	30.1	35.4
		mean	217.5	223.2	238.6
		rms	217.7	223.4	238.9
Shaft Torque	[Nm]	max	359.9	382.4	430.5
		min	-68.8	-72.9	-147.8

Table 3.2 (continued)

		delta	428.7	455.3	578.4
		mean	38.3	39.2	40.3
		rms	113.8	116.6	132
Heat Rate	[W]	max	164.65	291.93	560.98
		min	-939.65	-1856.34	-4034.95
		delta	1104.3	2148.27	4595.93
		mean	-52.78	-84.07	-236.9
		rms	271.24	519.15	1126.08
Mass Inlet	[g]	~	1.12247	1.08505	0.85945
Net Heat Transfer	[J]	~	-7.92	-6.29	-8.87
$\boldsymbol{W_{net}}$	[J]	~	240.93	246.49	252.83
$\boldsymbol{W_{net}^{pm}}$	[kJ/kg]	~	214.64	227.17	294.18
$\boldsymbol{\eta_{pm}^{iso}}$	[%]	~	70.2	66.32	51.22
$\boldsymbol{\eta_v}$	[%]	~	83.46	80.68	63.9
$\boldsymbol{cap}$	[m^3/hr]		22.65	43.8	69.38
$\boldsymbol{W_{pos}^{pm}}$	[kJ/kg]	~	326.29	341.84	467.36
$\boldsymbol{W_{abs}^{pm}}$	[kJ/kg]	~	437.94	456.52	640.54
$\boldsymbol{\eta_{pres}}$	[%]	~	64.96	60.13	41.16
$\boldsymbol{I_{fw}}$	kgm^2	~	6.07	1.54	0.42
$\boldsymbol{\Delta E_{fw}}$	[J]	~	266.45	269.44	297.86

3.4.2 Parametric Analysis for the Outlet Valve Diameter

The outlet valve diameter has been taken to be 40, 50 and 60 mm, while all other parameters have been kept at their nominal values. The P-V diagram is shown in Figure 3.5. Numerical results and the performance aspects are tabulated in Table 3.3.

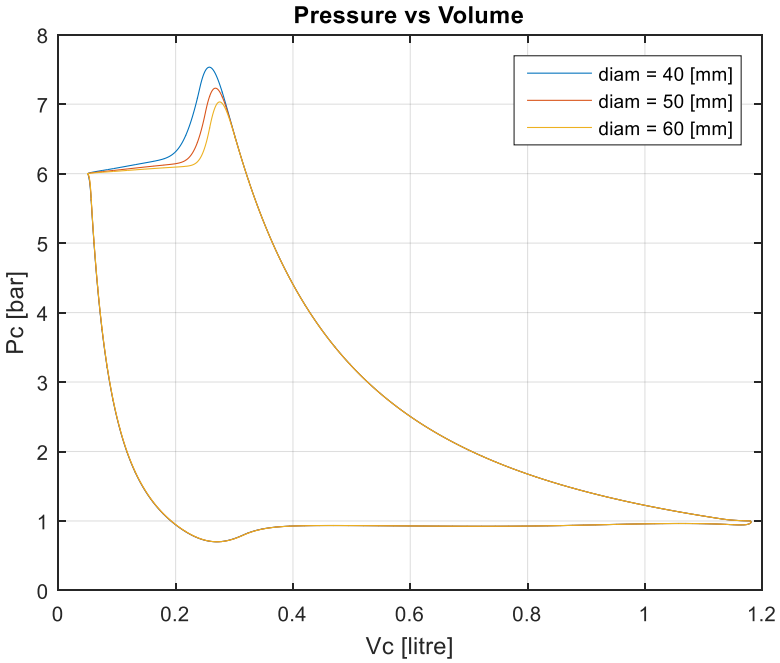

Figure 3.5. P-V Diagram for the Parametric Analysis of Outlet Valve Diameter

As seen in the P-V diagram, when the outlet diameter decreases, the losses at the discharge valve increase. Hence, it can be concluded that the outlet valve diameter should be as large as possible.

Table 3.3 Results obtained for the Parametric Analysis of Outlet Valve Diameter

Parameter	**Unit**	**Quantity**	**Value**		
			D_{vo} = 40mm	**D_{vo} = 50mm**	**D_{vo} = 60mm**
Chamber Pressure	[bar]	max	7.532	7.23	7.032
		min	0.7	0.7	0.701
		delta	6.832	6.53	6.331
		mean	2.248	2.235	2.227
		rms	3.008	2.978	2.961
Chamber Temperature	[°C]	max	267.1	261.1	257.1
		min	-11.7	-11.7	-11.7
		delta	278.9	272.9	268.8
		mean	81.1	80.7	80.6
		rms	113.7	113.1	112.7
Outlet Temperature	[°C]	max	234.9	234.8	234.8
		min	204.8	204.9	205
		delta	30.1	29.9	29.8
		mean	223.2	223.3	223.3
		rms	223.4	223.4	223.5
Shaft Torque	[Nm]	max	382.4	372.9	366.5
		min	-72.9	-73.1	-73.3
		delta	455.3	446	439.8
		mean	39.2	38.6	38.2

Table 3.3 (continued)

		rms	116.6	114.8	113.8
Heat Rate	[W]	max	291.93	290.38	289.53
		min	-1856.34	-1771.55	-1715.53
		delta	2148.27	2061.93	2005.06
		mean	-84.07	-80.45	-78.36
		rms	519.15	505.98	498.47
Mass Inlet	[g]	~	1.08505	1.08471	1.08428
Net Heat Transfer	[J]	~	-6.29	-6.02	-5.87
$\boldsymbol{W_{net}}$	[J]	~	246.49	242.39	239.99
$\boldsymbol{W_{net}^{pm}}$	[kJ/kg]	~	227.17	223.46	221.34
$\boldsymbol{\eta_{pm}^{iso}}$	[%]	~	66.32	67.43	68.07
$\boldsymbol{\eta_{v}}$	[%]	~	80.68	80.65	80.62
$\boldsymbol{cap}$	[m^3/hr]		43.8	43.78	43.77
$\boldsymbol{W_{pos}^{pm}}$	[kJ/kg]	~	341.84	338.25	336.25
$\boldsymbol{W_{abs}^{pm}}$	[kJ/kg]	~	456.52	453.04	451.17
$\boldsymbol{\eta_{pres}}$	[%]	~	60.13	62.19	63.41
$\boldsymbol{I_{fw}}$	kgm^2	~	1.54	1.52	1.51
$\boldsymbol{\Delta E_{fw}}$	[J]	~	269.44	266.82	265.33

3.4.3 Parametric Analysis for the Inlet Valve Diameter

The inlet valve diameter has been taken to be 40, 50 and 60 mm, while all other parameters have been kept at their nominal values. The P-V diagram is shown in Figure 3.6. Numerical results and the performance aspects are tabulated in Table 3.4.

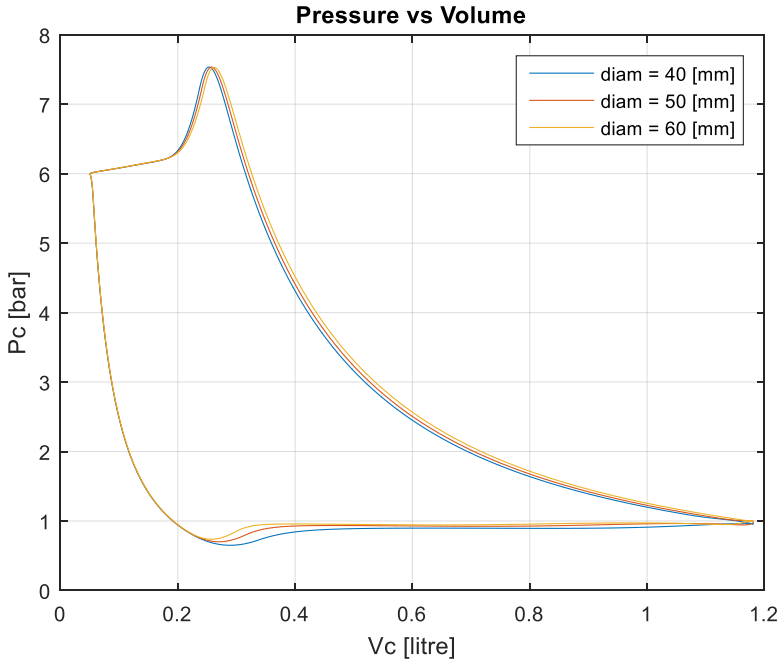

Figure 3.6. P-V Diagram for the Parametric Analysis of Inlet Valve Diameter

Similar to the outlet valve diameter analysis, the inlet valve diameter should be as large as possible so that the suction process occurs with less loss. It should be noted that, the cylinder bore diameter constrains the maximum sizes of the inlet and outlet valve areas.

Table 3.4 Results obtained for the Parametric Analysis of Inlet Valve Diameter

Parameter	**Unit**	**Quantity**	**Value**		
			D_{vi} = 40mm	**D_{vi} = 50mm**	**D_{vi} = 60mm**
Chamber Pressure	[bar]	max	7.534	7.532	7.528
		min	0.65	0.7	0.737
		delta	6.884	6.832	6.791
		mean	2.219	2.248	2.273
		rms	2.989	3.008	3.026
Chamber Temperature	[°C]	max	274.7	267.1	262.3
		min	-13.2	-11.7	-10.5
		delta	287.9	278.9	272.8
		mean	84	81.1	79.6
		rms	117.1	113.7	111.8
Outlet Temperature	[°C]	max	242	234.9	230.4
		min	211.1	204.8	200.8
		delta	30.9	30.1	29.5
		mean	230	223.2	218.9
		rms	230.2	223.4	219.1
Shaft Torque	[Nm]	max	379.8	382.4	385.1
		min	-72.7	-72.9	-73.1
		delta	452.5	455.3	458.2
		mean	39.2	39.2	39.6

Table 3.4 (continued)

		rms	115.1	116.6	118
Heat Rate	[W]	max	280.07	291.93	293.43
		min	-1880.67	-1856.34	-1839.87
		delta	2160.74	2148.27	2133.3
		mean	-85.82	-84.07	-87.97
		rms	523.44	519.15	514.96
Mass Inlet	[g]	~	1.04966	1.08505	1.11789
Net Heat Transfer	[J]	~	-6.43	-6.29	-6.59
$\boldsymbol{W_{net}}$	[J]	~	246.2	246.49	249.04
$\boldsymbol{W_{net}^{pm}}$	[kJ/kg]	~	234.56	227.17	222.77
$\boldsymbol{\eta_{pm}^{iso}}$	[%]	~	64.24	66.32	67.63
$\boldsymbol{\eta_v}$	[%]	~	78.04	80.68	83.12
$\boldsymbol{cap}$	[m^3/hr]		42.37	43.8	45.12
$\boldsymbol{W_{pos}^{pm}}$	[kJ/kg]	~	349	341.84	336.27
$\boldsymbol{W_{abs}^{pm}}$	[kJ/kg]	~	463.44	456.52	449.76
$\boldsymbol{\eta_{pres}}$	[%]	~	59.06	60.13	60.76
$\boldsymbol{I_{fw}}$	kgm^2	~	1.51	1.54	1.56
$\boldsymbol{\Delta E_{fw}}$	[J]	~	265.23	269.44	273.23

3.4.4 Parametric Analysis for the Outlet Valve Spring Constant

The outlet valve spring constant has been taken to be 2500, 5000 and 7500 N/m, while all other parameters have been kept at their nominal values. The P-V diagram is shown in Figure 3.7. Numerical results and the performance aspects are tabulated in Table 3.5.

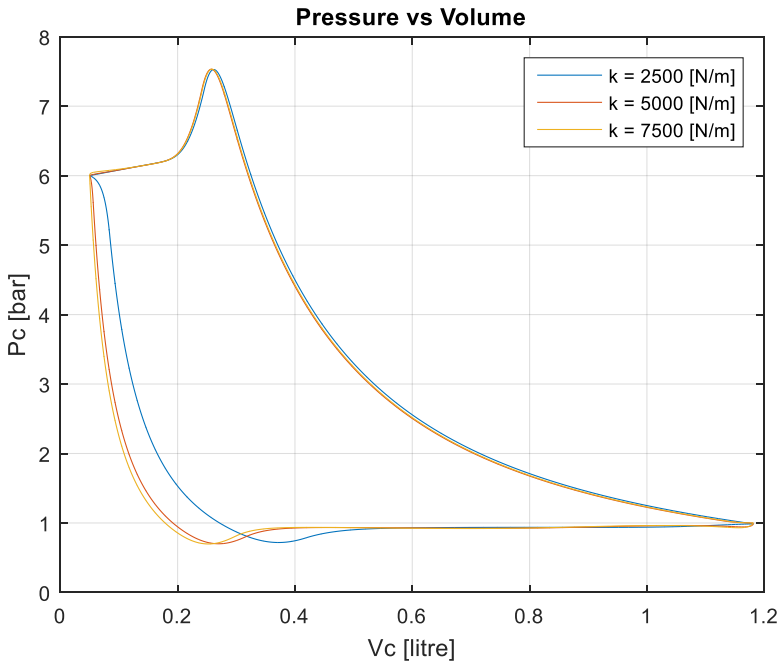

Figure 3.7. P-V Diagram for the Parametric Analysis of Outlet Valve Spring Constant

As seen in Figure 3.7 and Table 3.5, a stiffer spring for the outlet valve improves all performance aspects. However, the outlet temperature increases as the stiffness of the spring increases.

Table 3.5 Results obtained for the Parametric Analysis of Outlet Valve Spring Constant

Parameter	**Unit**	**Quantity**	**Value**		
			k_{vo} = 2500 N/m	**k_{vo} = 5000 N/m**	**k_{vo} = 7500 N/m**
Chamber Pressure	[bar]	max	7.527	7.532	7.532
		min	0.719	0.7	0.698
		delta	6.809	6.832	6.835
		mean	2.37	2.248	2.227
		rms	3.14	3.008	2.982
Chamber Temperature	[°C]	max	262.7	267.1	267.6
		min	-14	-11.7	-10.4
		delta	276.6	278.9	278
		mean	82.4	81.1	81
		rms	115.3	113.7	113.4
Outlet Temperature	[°C]	max	230.7	234.9	235.3
		min	196.4	204.8	209.4
		delta	34.3	30.1	25.9
		mean	216.5	223.2	225.4
		rms	216.8	223.4	225.5
Shaft Torque	[Nm]	max	384.7	382.4	382.9
		min	-117.6	-72.9	-66
		delta	502.3	455.3	448.9
		mean	37	39.2	39.9

Table 3.5 (continued)

		rms	119.5	116.6	116.6
Heat Rate	[W]	max	299.34	291.93	291.82
		min	-1813.25	-1856.34	-1862.32
		delta	2112.59	2148.27	2154.14
		mean	-105.76	-84.07	-78.85
		rms	521.55	519.15	511.32
Mass Inlet	[g]	~	1.01388	1.08505	1.10595
Net Heat Transfer	[J]	~	-7.93	-6.29	-5.91
$\boldsymbol{W_{net}}$	[J]	~	232.32	246.49	250.69
$\boldsymbol{W_{net}^{pm}}$	[kJ/kg]	~	229.14	227.17	226.67
$\boldsymbol{\eta_{pm}^{iso}}$	[%]	~	65.76	66.32	66.47
$\boldsymbol{\eta_{v}}$	[%]	~	75.38	80.68	82.23
$\boldsymbol{cap}$	[m^3/hr]		40.92	43.8	44.64
$\boldsymbol{W_{pos}^{pm}}$	[kJ/kg]	~	370.01	341.84	336.38
$\boldsymbol{W_{abs}^{pm}}$	[kJ/kg]	~	510.88	456.52	446.09
$\boldsymbol{\eta_{pres}}$	[%]	~	59.02	60.13	60.29
$\boldsymbol{I_{fw}}$	kgm^2	~	1.59	1.54	1.53
$\boldsymbol{\Delta E_{fw}}$	[J]	~	278.3	269.44	269.05

3.4.5 Parametric Analysis for the Inlet Valve Spring Constant

The inlet valve spring constant has been taken to be 2500, 5000 and 7500 N/m, while all other parameters have been kept at their nominal values. The P-V diagram is shown in Figure 3.8. Numerical results and the performance aspects are tabulated in Table 3.6.

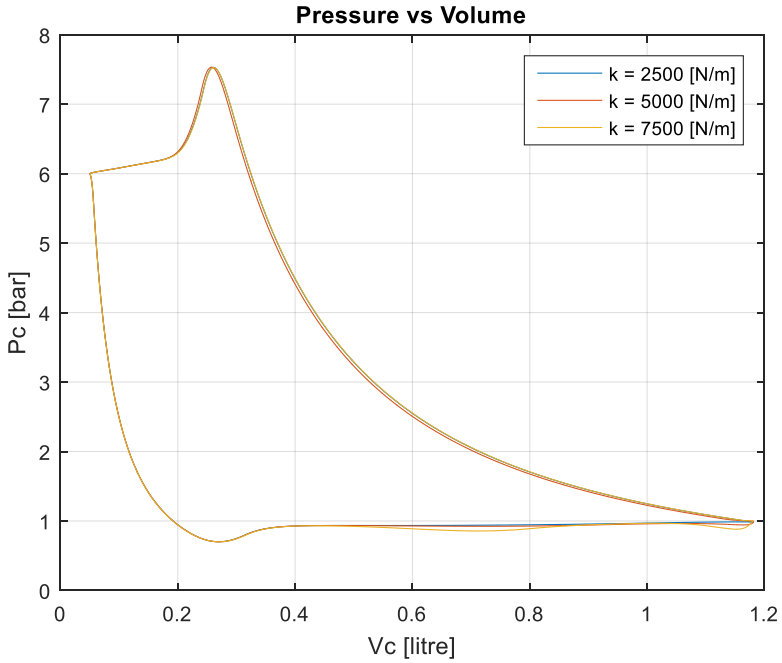

Figure 3.8. P-V Diagram for the Parametric Analysis of Inlet Valve Spring Constant

As seen in Figure 3.8 and Table 3.6, a soft spring for inlet valve improves all performance aspects. However, the improvements are quite marginal.

Table 3.6 Results obtained for the Parametric Analysis of Inlet Valve Spring Constant

Parameter	**Unit**	**Quantity**	**Value**		
			k_{vi} = 2500 N/m	**k_{vi} = 5000 N/m**	**k_{vi} = 7500 N/m**
Chamber Pressure	[bar]	max	7.529	7.532	7.526
		min	0.701	0.7	0.7
		delta	6.828	6.832	6.826
		mean	2.265	2.248	2.252
		rms	3.021	3.008	3.017
Chamber Temperature	[°C]	max	263.2	267.1	268.9
		min	-13.3	-11.7	-11
		delta	276.5	278.9	279.8
		mean	80	81.1	82.3
		rms	112.2	113.7	115.2
Outlet Temperature	[°C]	max	231.3	234.9	236.6
		min	201.6	204.8	206.3
		delta	29.6	30.1	30.3
		mean	219.8	223.2	224.9
		rms	219.9	223.4	225.1
Shaft Torque	[Nm]	max	384.4	382.4	384.4
		min	-73.1	-72.9	-72.9
		delta	457.5	455.3	457.3
		mean	39.6	39.2	40.2

Table 3.6 (continued)

		rms	117.5	116.6	117.4
Heat Rate	[W]	max	282.98	291.93	304.07
		min	-1840.85	-1856.34	-1864.49
		delta	2123.83	2148.27	2168.56
		mean	-98.35	-84.07	-94.27
		rms	510.26	519.15	519.92
Mass Inlet	[g]	~	1.10969	1.08505	1.09935
Net Heat Transfer	[J]	~	-7.36	-6.29	-7.06
$\boldsymbol{W_{net}}$	[J]	~	249.02	246.49	252.3
$\boldsymbol{W_{net}^{pm}}$	[kJ/kg]	~	224.41	227.17	229.5
$\boldsymbol{\eta_{pm}^{iso}}$	[%]	~	67.14	66.32	65.65
$\boldsymbol{\eta_{v}}$	[%]	~	82.51	80.68	81.74
$\boldsymbol{cap}$	[m^3/hr]		44.79	43.8	44.37
$\boldsymbol{W_{pos}^{pm}}$	[kJ/kg]	~	337.52	341.84	340.9
$\boldsymbol{W_{abs}^{pm}}$	[kJ/kg]	~	450.64	456.52	452.29
$\boldsymbol{\eta_{pres}}$	[%]	~	60.43	60.13	59.73
$\boldsymbol{I_{fw}}$	kgm^2	~	1.55	1.54	1.54
$\boldsymbol{\Delta E_{fw}}$	[J]	~	271.98	269.44	271.04

3.4.6 Parametric Analysis for the Percentage of the Clearance Volume

The clearance volume has been taken to be 0.025, 0.050 and 0.100 L., while all other parameters have been kept at their nominal values. The P-V diagram is shown in Figure 3.9. Numerical results and the performance aspects are tabulated in Table 3.7. Furthermore, in studies [12] and [21], percent clearance volume, V_{pcl}, (see equation (2.40)) is used in comparison of compressors, Hence, in Table 3.7, corresponding V_{pcl} are also given.

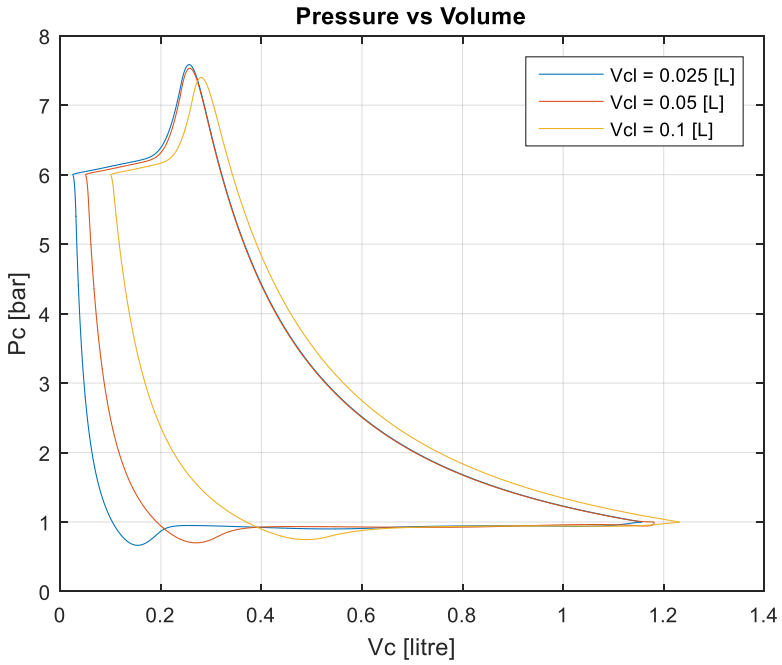

Figure 3.9. P-V Diagram for the Parametric Analysis of Clearance Volume

In order to obtain better compressor performance, the clearance volume should be "small". However, it cannot be too small (because otherwise the piston and the head of the cylinder would collide). Furthermore, the mechanical assemblies of the inlet and outlet valves also require a certain amount of clearance volume. Hence, the clearance volume should be as small as the mechanical constraints allow.

Table 3.7 Results obtained for the Parametric Analysis of Clearance Volume

Parameter	**Unit**	**Quantity**	**Value**		
			$\boldsymbol{V_{cl} = 0.025\ L}$ $\boldsymbol{V_{pcl} = 2.16\%}$	$\boldsymbol{V_{cl} = 0.050\ L}$ $\boldsymbol{V_{pcl} = 4.23\%}$	$\boldsymbol{V_{cl} = 0.100\ L}$ $\boldsymbol{V_{pcl} = 8.12\%}$
Chamber Pressure	[bar]	max	7.584	7.532	7.398
		min	0.665	0.7	0.746
		delta	6.92	6.832	6.652
		mean	2.238	2.248	2.315
		rms	3.013	3.008	3.044
Chamber Temperature	[°C]	max	266.2	267.1	263.6
		min	-22.8	-11.7	-2.2
		delta	288.9	278.9	265.7
		mean	78.4	81.1	85.9
		rms	111.3	113.7	117
Outlet Temperature	[°C]	max	233	234.9	234
		min	188.1	204.8	215.5
		delta	45	30.1	18.5
		mean	217.8	223.2	225.9
		rms	218.2	223.4	226
Shaft Torque	[Nm]	max	399.1	382.4	357.9
		min	-57.8	-72.9	-96.7

Table 3.7 (continued)

		delta	457	455.3	454.5
		mean	42.9	39.2	35.2
		rms	120.3	116.6	114.7
Heat Rate	[W]	max	270.73	291.93	309.97
		min	-1922.44	-1856.34	-1725.49
		delta	2193.17	2148.27	2035.46
		mean	-103.3	-84.07	-82.58
		rms	524.13	519.15	498.02
Mass Inlet	[g]	~	1.19638	1.08505	0.97061
Net Heat Transfer	[J]	~	-7.74	-6.29	-6.18
$\boldsymbol{W_{net}}$	[J]	~	269.4	246.49	221.16
$\boldsymbol{W_{net}^{pm}}$	[kJ/kg]	~	225.18	227.17	227.85
$\boldsymbol{\eta_{pm}^{iso}}$	[%]	~	66.91	66.32	66.13
$\boldsymbol{\eta_{v}}$	[%]	~	88.95	80.68	72.17
$\boldsymbol{cap}$	[m^3/hr]		48.29	43.8	39.18
$\boldsymbol{W_{pos}^{pm}}$	[kJ/kg]	~	322.18	341.84	373.73
$\boldsymbol{W_{abs}^{pm}}$	[kJ/kg]	~	419.18	456.52	519.6
$\boldsymbol{\eta_{pres}}$	[%]	~	60.29	60.13	60.09
$\boldsymbol{I_{fw}}$	kgm^2	~	1.57	1.54	1.54
$\boldsymbol{\Delta E_{fw}}$	[J]	~	275.69	269.44	269.68

3.4.7 Parametric Analysis for the Stroke

The stroke has been taken to be 0.05, 0.10 and 0.20 m., while all other parameters have been kept at their nominal values. The P-V diagram is shown in Figure 3.10. Numerical results and the performance aspects are tabulated in Table 3.8.

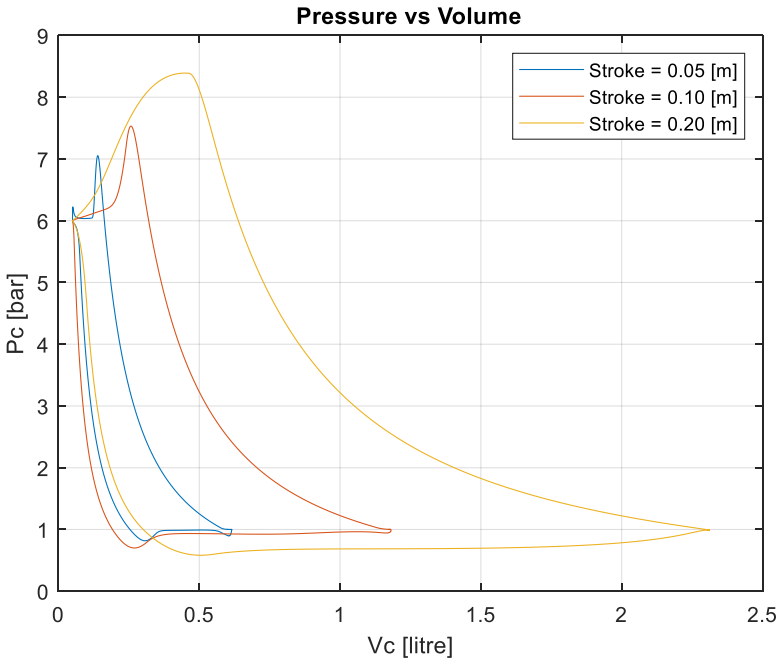

Figure 3.10. P-V Diagram for the Parametric Analysis of Stroke

The stroke of a reciprocating compressor is a crucial design parameter. Hence, in order to obtain the desired requirements, the stroke should be selected properly. Clearly, an increase in the stroke results in an increase in the capacity. An increase in the stroke, on the other hand, results in a decrease in the isothermal efficiency. Hence, one should select a compromising value for the stroke.

Table 3.8 Results obtained for the Parametric Analysis of Stroke

Parameter	**Unit**	**Quantity**	**Value**		
			$\boldsymbol{S = 0.05\ m}$	$\boldsymbol{S = 0.10\ m}$	$\boldsymbol{S = 0.20\ m}$
Chamber Pressure	[bar]	max	7.054	7.532	8.391
		min	0.817	0.7	0.583
		delta	6.237	6.832	7.808
		mean	2.518	2.248	2.162
		rms	3.246	3.008	3.094
Chamber Temperature	[°C]	max	240.9	267.1	317.4
		min	-6.9	-11.7	-16.4
		delta	247.7	278.9	333.8
		mean	81.7	81.1	92.7
		rms	113.7	113.7	129.1
Outlet Temperature	[°C]	max	218.8	234.9	266.3
		min	194.5	204.8	216.6
		delta	24.4	30.1	49.7
		mean	207.7	223.2	246.9
		rms	207.8	223.4	247.4
Shaft Torque	[Nm]	max	157.7	382.4	1006
		min	-69.8	-72.9	-210.5
		delta	227.5	455.3	1216.6
		mean	13.2	39.2	96.9

Table 3.8 (continued)

		rms	55.2	116.6	284.6
Heat Rate	[W]	max	143.73	291.93	710.73
		min	-772.62	-1856.34	-5007.16
		delta	916.35	2148.27	5717.89
		mean	-63.73	-84.07	-204.08
		rms	257.92	519.15	1303.45
Mass Inlet	[g]	~	0.37727	1.08505	2.11857
Net Heat Transfer	[J]	~	-4.78	-6.29	-15.29
$\boldsymbol{W_{net}}$	[J]	~	83.18	246.49	608.56
$\boldsymbol{W_{net}^{pm}}$	[kJ/kg]	~	220.49	227.17	287.25
$\boldsymbol{\eta_{pm}^{iso}}$	[%]	~	68.34	66.32	52.45
$\boldsymbol{\eta_{v}}$	[%]	~	56.1	80.68	78.76
$\boldsymbol{cap}$	[m^3/hr]		15.23	43.8	85.51
$\boldsymbol{W_{pos}^{pm}}$	[kJ/kg]	~	455.89	341.84	388.59
$\boldsymbol{W_{abs}^{pm}}$	[kJ/kg]	~	691.3	456.52	489.92
$\boldsymbol{\eta_{pres}}$	[%]	~	61.46	60.13	44.79
$\boldsymbol{I_{fw}}$	kgm^2	~	0.77	1.54	3.5
$\boldsymbol{\Delta E_{fw}}$	[J]	~	134.71	269.44	614.2

3.4.8 Parametric Analysis for the Piston Diameter

The piston diameter has been taken to be 0.10, 0.12 and 0.14 m., while all other parameters have been kept at their nominal values. The P-V diagram is shown in Figure 3.11. Numerical results and the performance aspects are tabulated in Table 3.9.

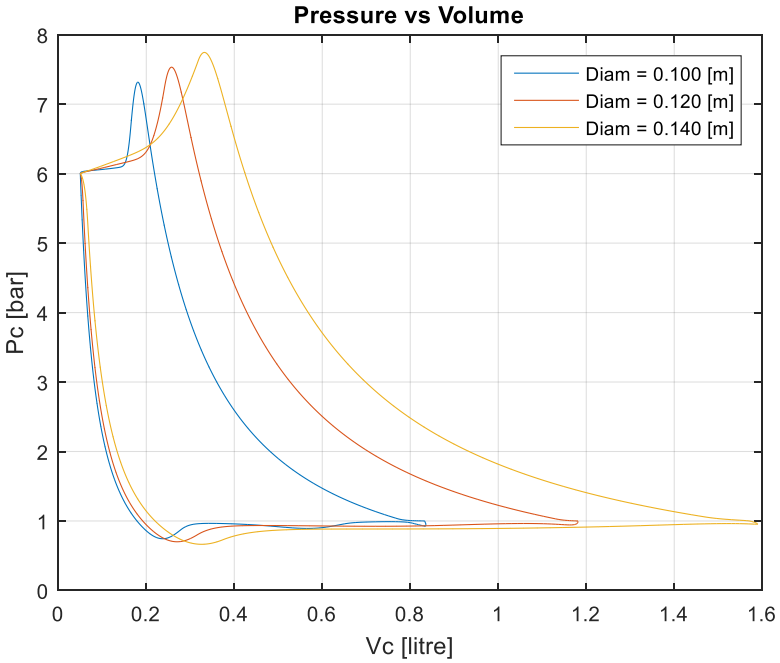

Figure 3.11. P-V Diagram for the Parametric Analysis of Piston Diameter

The diameter of the piston is another crucial design parameter. Similar to the stroke, a larger piston diameter leads to an increase in capacity. However, the isothermal efficiency decreases when the piston diameter increases.

Table 3.9 Results obtained for the Parametric Analysis of Piston Diameter

Parameter	**Unit**	**Quantity**	**Value**		
			D_{cyl} = 0.100 m	**D_{cyl} = 0.120 m**	**D_{cyl} = 0.140 m**
Chamber Pressure	[bar]	max	7.316	7.532	7.745
		min	0.744	0.7	0.664
		delta	6.572	6.832	7.08
		mean	2.211	2.248	2.256
		rms	2.939	3.008	3.059
Chamber Temperature	[°C]	max	263.6	267.1	275.6
		min	-3.8	-11.7	-16.7
		delta	267.5	278.9	292.3
		mean	81.1	81.1	82.3
		rms	113	113.7	116.3
Outlet Temperature	[°C]	max	235.7	234.9	238.9
		min	214	204.8	200.8
		delta	21.8	30.1	38.1
		mean	226.7	223.2	224.6
		rms	226.8	223.4	224.9
Shaft Torque	[Nm]	max	249.3	382.4	535
		min	-54.7	-72.9	-103.5
		delta	304.1	455.3	638.4
		mean	24.4	39.2	55.3

Table 3.9 (continued)

		rms	77.1	116.6	161.5
Heat Rate	[W]	max	243.63	291.93	340.09
		min	-1326.28	-1856.34	-2481.11
		delta	1569.92	2148.27	2821.2
		mean	-44.03	-84.07	-130.49
		rms	365.97	519.15	699.58
Mass Inlet	[g]	~	0.68474	1.08505	1.46372
Net Heat Transfer	[J]	~	-3.29	-6.29	-9.77
$\boldsymbol{W_{net}}$	[J]	~	153.41	246.49	347.37
$\boldsymbol{W_{net}^{pm}}$	[kJ/kg]	~	224.05	227.17	237.32
$\boldsymbol{\eta_{pm}^{iso}}$	[%]	~	67.25	66.32	63.49
$\boldsymbol{\eta_v}$	[%]	~	73.31	80.68	79.96
$\boldsymbol{cap}$	[m^3/hr]		27.64	43.8	59.08
$\boldsymbol{W_{pos}^{pm}}$	[kJ/kg]	~	356.31	341.84	349.37
$\boldsymbol{W_{abs}^{pm}}$	[kJ/kg]	~	488.58	456.52	461.43
$\boldsymbol{\eta_{pres}}$	[%]	~	62	60.13	56.67
$\boldsymbol{I_{fw}}$	kgm^2	~	1.03	1.54	2.11
$\boldsymbol{\Delta E_{fw}}$	[J]	~	179.97	269.44	369.58

3.4.9 Parametric Analysis for the Wall Temperature

The wall temperature has been calculated as 83°C using the method described in the previous chapter. Hence, the nominal value of T_w has been taken to be 83°C in this analysis; and T_w has been taken to be 50, 83 and 120 °C, while all other parameters have been kept at their nominal values. The P-V diagram is shown in Figure 3.12. Numerical results and the performance aspects are tabulated in Table 3.10.

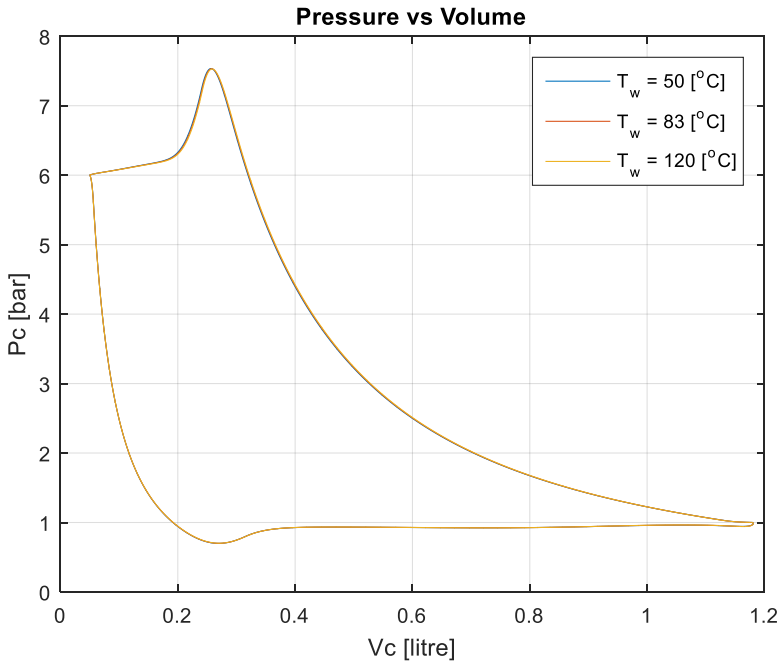

Figure 3.12. P-V Diagram for the Parametric Analysis of Wall Temperature

The wall temperature can be controlled, to a certain extent, by cooling the cylinder. It is observed that by proper cooling, the compressor will have a better performance.

Table 3.10 Results obtained for the Parametric Analysis of Wall Temperature

Parameter	**Unit**	**Quantity**	**Value**		
			$T_w = 50$ ℃	$T_w = 83$ ℃	$T_w = 120$ ℃
Chamber Pressure	[bar]	max	7.535	7.532	7.529
		min	0.699	0.701	0.702
		delta	6.836	6.831	6.827
		mean	2.247	2.248	2.249
		rms	3.007	3.008	3.009
Chamber Temperature	[°C]	max	256.5	267.8	280.6
		min	-19.9	-11.2	-1.4
		delta	276.4	279	282
		mean	74.4	81.5	89.5
		rms	107.3	114.1	122
Outlet Temperature	[°C]	max	225.1	235.5	247.3
		min	191.2	205.7	222.1
		delta	33.9	29.9	25.2
		mean	211.9	223.9	237.5
		rms	212.2	224.1	237.6
Shaft Torque	[Nm]	max	382	382.4	382.9
		min	-73	-72.9	-72.9
		delta	455	455.4	455.7
		mean	39.2	39.2	39.3

Table 3.10 (continued)

		rms	116.5	116.6	116.7
Heat Rate	[W]	max	156.65	300.65	465.47
		min	-2081.17	-1842.48	-1582.3
		delta	2237.82	2143.13	2047.77
		mean	-190.18	-77.51	46.33
		rms	566.98	516.89	492.98
Mass Inlet	[g]	~	1.10056	1.08409	1.06581
Net Heat Transfer	[J]	~	-14.25	-5.8	3.48
$\boldsymbol{W_{net}}$	[J]	~	246.17	246.51	246.87
$\boldsymbol{W_{net}^{pm}}$	[kJ/kg]	~	223.68	227.39	231.63
$\boldsymbol{\eta_{pm}^{iso}}$	[%]	~	67.36	66.26	65.05
$\boldsymbol{\eta_v}$	[%]	~	81.83	80.6	79.25
$\boldsymbol{cap}$	[m^3/hr]		44.42	43.76	43.02
$\boldsymbol{W_{pos}^{pm}}$	[kJ/kg]	~	336.7	342.17	348.42
$\boldsymbol{W_{abs}^{pm}}$	[kJ/kg]	~	449.71	456.95	465.2
$\boldsymbol{\eta_{pres}}$	[%]	~	59.77	60.15	60.57
$\boldsymbol{I_{fw}}$	kgm^2	~	1.53	1.54	1.54
$\boldsymbol{\Delta E_{fw}}$	[J]	~	269.18	269.45	269.74

3.5 Analysis of Reciprocating Compressors with Cam Motion Curves Regardless of the Mechanism

The slider crank mechanism that is utilized in a conventional reciprocating compressor converts a rotational motion into a translational motion (or, vice versa). The piston motion can change in a restricted manner for a reciprocating compressor employing a slider crank mechanism. In the MinFaS-TaR mechanism, the translational and rotational motions can be related to each other in any desired manner. Clearly, this is not possible in the slider crank mechanism.

Before the optimization of the piston motion for a reciprocating compressor employing a MinFaS-TaR mechanism, the piston motion is analysed regardless of the mechanism. In order to see the effects of the piston motion on the performance of a reciprocating compressor, basic cam motion curves will be used as the piston motion regardless of the mechanism. The piston motion can be adjusted using several rise, dwell and return motions. An example of a dwell-rise-dwell-return type cam motion curve is shown in Figure 3.13.

Figure 3.13. A D-R-D-R Type Cam Motion Curve

3.5.1 Basic Cam Motion Curves

There are various motion curves defined for cams. In this study, the cycloidal and modified trapezoidal acceleration motion curves will be utilized since the first, second and third derivatives (velocity, acceleration and jerk) are finite.

3.5.1.1 Cycloidal Motion Curve

The cycloidal motion curve is usually preferred for high speed applications. It gives a finite acceleration throughout the motion; and zero acceleration at the start and end points. The displacement (x), velocity (v) and acceleration (a), with respect to the rotation angle (θ), are given by the following three equations

$$x = \frac{H}{\pi}\left(\frac{\pi\theta}{\beta} - \frac{1}{2}sin\left(\frac{2\pi\theta}{\beta}\right)\right) \tag{3.44}$$

$$v = \frac{H}{\beta}\left(1 - cos\left(\frac{2\pi\theta}{\beta}\right)\right) \tag{3.45}$$

$$a = \frac{2H\pi}{\beta^2}sin\left(\frac{2\pi\theta}{\beta}\right) \tag{3.46}$$

In equations (3.44) - (3.46), H is the total follower rise, and β is the rotation angle of the cam corresponding to H. For a unit rise (i.e., for H = 1) and for cycloidal motion, the follower position, velocity and acceleration curves will be as shown in Figure 3.14.

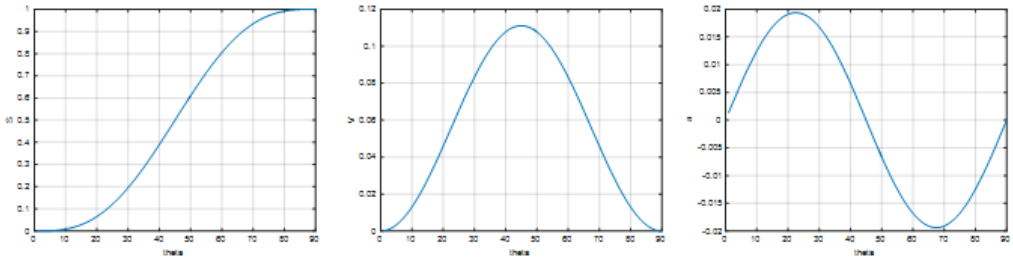

Figure 3.14. Cycloidal Motion Position, Velocity and Acceleration Curves

3.5.1.2 Modified Trapezoidal Acceleration Curve

The modified trapezoidal acceleration motion is composed of constant acceleration motion curves and cycloidal motion curves. The motion equations for the modified trapezoidal curve are given by Harold et al. (see [19]). Since these equations are too long, they are not given in this thesis. Cycloidal and modified trapezoidal curves are shown in Figure 3.15.

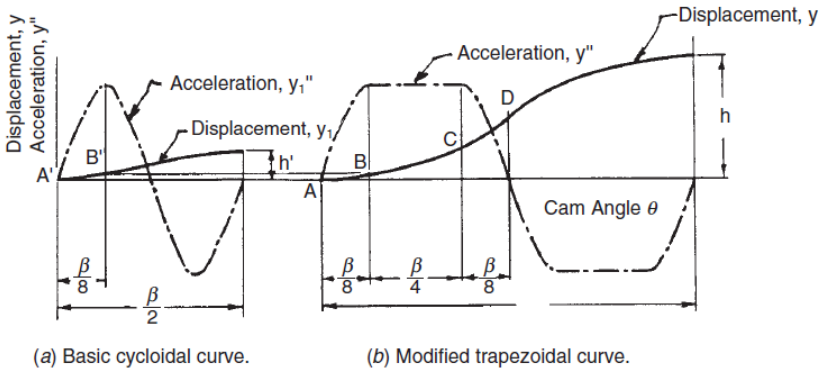

Figure 3.15. The Modified Trapezoidal Motion Curve [19]

3.5.2 Rise-Return Motion Profile for the Reciprocating Compressor Regardless of the Mechanism

An example of a rise and return type motion curve is given in Figure 3.16. The slider crank provides a rise and return type motion. In the slider crank mechanism, the stroke can be adjusted by changing the kinematic dimensions. However, the

angle β_1 (See Figure 3.16) cannot be adjusted. In other words, β_1 will always be 180º for an inline slider crank mechanism.

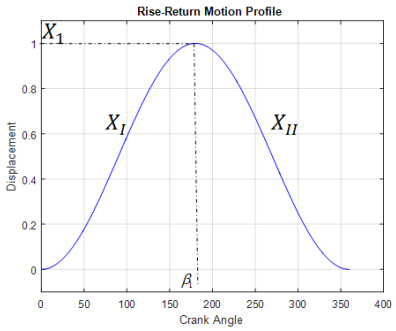

Figure 3.16. Rise Return Motion Profile

In the analysis of the reciprocating compressor, the stroke is taken to be constant which is equal to the stroke of the conventional reciprocating compressor (See numerical values in Table 2.1). While the stroke is constant, the angle β_1 is changed in order to observe its effects on the performance of the compressor.

In order to analyse the effects of β_1 on the performance, a physically meaningful variable, $(X')_{avg}$, has been introduced via equation (3.47).

$$(X')_{avg} \triangleq \frac{\Delta x}{\Delta \theta} \tag{3.47}$$

$(X')_{avg}$ can be considered to be the average piston velocity. The average velocities for the rise and return motions (namely, $(X_I')_{avg}$ and $(X_{II}')_{avg}$) are given by equations (3.48) and (3.49), respectively.

$$(X_I')_{avg} = \frac{|X_1|}{\beta_1} \tag{3.48}$$

$$(X_{II}')_{avg} = \frac{|0 - X_1|}{2\pi - \beta_1} \tag{3.49}$$

Rather than investigate the effects of $(X_I')_{avg}$ and $(X_{II}')_{avg}$ on the performance of the compressor separately, it is more convenient to investigate the effect of the

dimensionless ratio $(X'_{II})_{avg}/(X'_{I})_{avg}$ on the compressor efficiency. The isothermal efficiency vs. $(X'_{II})_{avg}/(X'_{I})_{avg}$ graphs for the cycloidal motion curve (CMC) and the modified trapezoidal acceleration motion curve are given in Figure 3.17. The isothermal efficiency for the reciprocating compressor employing the slider crank mechanism is also shown in the same figure.

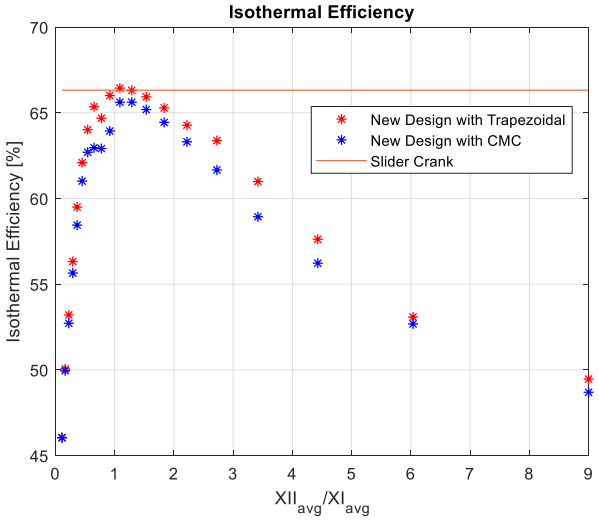

Figure 3.17. Isothermal Efficiency versus $(X'_{II})_{avg}/(X'_{I})_{avg}$

As seen in the figure, the modified trapezoidal acceleration motion profile is slightly better than the slider crank motion profile for some $\frac{(X'_{II})_{avg}}{(X'_{I})_{avg}}$ values which are slightly higher than 1. $\frac{(X'_{II})_{avg}}{(X'_{I})_{avg}} > 1$ implies that the compression process is faster than the expansion process. Therefore, it can be said that the piston motion profile should be designed such that the compression process is faster than the expansion process.

3.6 Effects of Valve Losses and Heat Transfer

This section is devoted to observing the effects of valve losses, heat transfer and piston motion profile on the performance of a reciprocating compressor. In order to

observe these effects, firstly four different valve loss and heat transfer combinations, to be used in the simulations, have been suggested (See Table 3.11). Furthermore, six different motion profiles, also to be used in the simulations, have been created (See Table 3.12).

Table 3.11 Valve and Heat Transfer Cases for the Simulation

Name	**Heat Transfer**	**Valve**
A1	Adiabatic[(3)]	Normal[(1)]
A2	Adiabatic	Ideal[(2)]
A3	Non-Adiabatic[(3)]	Normal
A4	Non-Adiabatic	Ideal

[(1)]Normal valve means that valve is modeled as the spring mass model.
[(2)]Ideal valve means that valves are immediately and fully opened when the pressure difference is positive and closed when the pressure difference is negative. (i.e. There is no spring or damping).
[(3)]Adiabatic means that there is no heat transfer, Non-Adiabatic means that there exists heat transfer.

Table 3.12 The Motion Profile Cases for the Simulation

Name	**Motion Profile**
M1	Slider Crank
M2	Trapezoidal Acceleration Motion Curve with $\frac{(X_{II}')_{avg}}{(X_{I}')_{avg}} = 0.5$
M3	Trapezoidal Acceleration Motion Curve with $\frac{(X_{II}')_{avg}}{(X_{I}')_{avg}} = 0.8$
M4	Trapezoidal Acceleration Motion Curve with $\frac{(X_{II}')_{avg}}{(X_{I}')_{avg}} = 1.0$
M5	Trapezoidal Acceleration Motion Curve with $\frac{(X_{II}')_{avg}}{(X_{I}')_{avg}} = 1.2$
M6	Trapezoidal Acceleration Motion Curve with $\frac{(X_{II}')_{avg}}{(X_{I}')_{avg}} = 1.5$

By combining the four cases presented in Table 3.11 with the 6 cases presented in Table 3.12, $4 \times 6 = 24$ simulations have been realized. The results are presented in Appendix C in detail. When these results are analyzed, it can be concluded that in

order to improve the performance of a compressor, the valve losses must be minimized (as much as possible).

Although cases A2 and A4 in Table 3.12 refer to ideal valves (without any springs, or damping), it should be noted that the area of a valve is another important parameter that leads to losses during the discharge and suction phases. In order to test this claim, another simulation case, A5, has been considered. In case A5, the compressor is non-adiabatic, the valves are ideal and the valve diameters are 5 times as large (indeed, this case is not physically implementable due to the bore diameter restriction). The results of this simulation indicate that although the valve losses are reduced, they are not eliminated completely.

In conclusion, it can be stated that the piston motion curve should be designed such that the valve losses are minimized. Furthermore, it has been observed that it is possible to obtain a more efficient compressor by using a modified trapezoidal acceleration rise-return motion curve. It has also been observed that the modified trapezoidal acceleration rise-return motion does not increase the efficiency of the compressor significantly.

CHAPTER 4

OPTIMIZATION OF RECIPROCATING COMPRESSOR

4.1 Introduction

The design of any machine starts by specifying the requirements. For reciprocating compressors, the inlet pressure, the outlet pressure and the capacity may be considered to be the main requirements that can be specified. Indeed, there may be other requirements regarding the diameter of the cylinder, the stroke, etc.

In this study, the nominal values of the inlet pressure, the outlet pressure and the capacity are taken to be identical with the conventional, slider crank based reciprocating compressor (see the related simulations and results given in chapters 2 and 3). Hence, the nominal values of the inlet pressure, the outlet pressure and the capacity that are employed in this study are as follows.

- $P_i = 1$ bar
- $P_o = 6$ bar
- cap $= 43.8\ m^3/hr$

After the requirements are specified, one may optimize the compressor according to any desired objective function which will be related to the performance aspects discussed in the previous chapter. In this study, the energy consumption (of the motor) per compressed mass will be minimized. It should be recalled that, depending upon the motor type, the energy consumption can be computed using three different approaches (see section 3.2.5)

Clearly, one should have some design parameters which can be changed for the purposes of optimization. In this study, the piston motion curve, the diameter of the cylinder, the diameters of the inlet and outlet valves and the motor speed (which is

assumed to be constant) are selected as design parameters. Hence, a design parameter vector, $\overrightarrow{DP}$, is defined as given below.

$$\overrightarrow{DP} = [x_p(\theta); D_{cyl}; D_{vi}; D_{vo}; \omega] \tag{4.1}$$

In definition (4.1), it should be noted that $x_p(\theta)$ is a "function", whereas, $D_{cyl}, D_{vi}, D_{vo}, \omega$ are "parameters". Note that, $\overrightarrow{DP}$ is, rigorously, not a physical vector that has a magnitude and a direction. In this study, $\overrightarrow{DP}$ is used, loosely, to represent a list of design parameters that consists of a function and some scalar parameters.

In this chapter, the optimization of a reciprocating compressor, with respect to the design parameter vector $\overrightarrow{DP}$, is discussed. The optimization with respect to the parameters D_{cyl}, D_{vi}, D_{vo} and ω is quite straight forward. However, tackling the optimization with respect to the function $x_p(\theta)$, is somewhat complicated. To this purpose, two different methods are utilized. In the first method, the piston motion function, $x_p(\theta)$, is taken to be the design function (which is parametrized using cam motion curves). The corresponding chamber pressure function, $P_c(\theta)$, on the other hand, is obtained via simulation (of the compression process). In the second method, the chamber pressure function, $P_c(\theta)$, is taken to be the design function (which is parametrized using cam motion curves). The corresponding piston motion function, $x_p(\theta)$, on the other hand, is obtained via simulation (of the compression process).

In the following sections, these two methods are explained in detail.

4.1.1 Parametrization of the Piston Motion Function, $x_p(\theta)$

In chapter 3, the piston motion function $x_p(\theta)$ has been parametrized by utilizing some common cam motion profiles. It should be recalled that the parametrized piston motion function utilized in Chapter 3 was composed of two portions,

namely, rise and return parts (leading to a so-called rise-return cam motion profile). Clearly, if the parametrized piston motion function involves more rises and/or returns and/or dwells, the optimization will lead to much better results. Therefore, in this chapter, a more complicated piston motion profile is proposed. The proposed motion profile consists of 4 polynomial curves (of degrees 6, 5, 6 and 5, respectively). Hence, it is labelled as the 6-5-6-5 polynomial motion curve. The derivation of the equations yielding this motion curve is given in Appendix D. Figure 4.1 shows a typical 6-5-6-5 motion curve and the notation that is utilized.

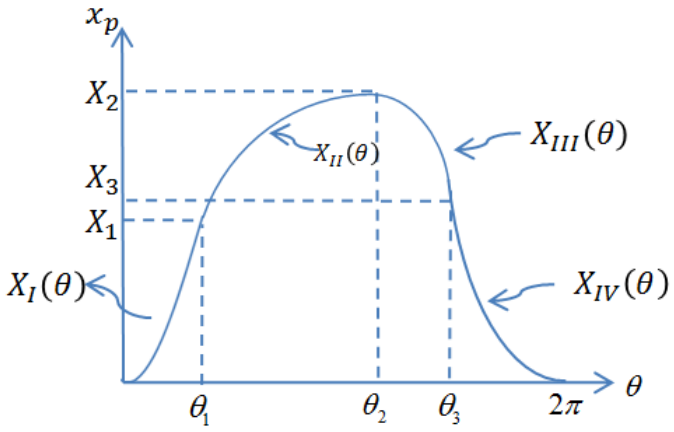

Figure 4.1. An Example of 6-5-6-5 Motion Curve

The $x_p - \theta$ curve shown in Figure 4.1 is uniquely defined by the six components of the $\vec{P}_{6565}$ vector which is defined by the equation below.

$$\vec{P}_{6565} = [\theta_1; X_1; \theta_2; X_2; \theta_3; X_3] \tag{4.2}$$

Note that, (θ_1, X_1), (θ_2, X_2) and (θ_3, X_3) correspond to the coordinates of three points on the motion curve. $X_I(\theta)$, $X_{II}(\theta)$, $X_{III}(\theta)$ and $X_{IV}(\theta)$, on the other hand, designate four different polynomials of orders 6, 5, 6 and 5, respectively. Although the $x_p - \theta$ curve shown in Figure 4.1 may be uniquely defined by the six components of the $\vec{P}_{6565}$ vector, it is more convenient to describe the $x_p - \theta$ curve via six different parameters that are physically more meaningful. These 6 physically more meaningful parameters are the six average "velocities" $(X'_{I+II})_{avg}$,

$(X'_{III+IV})_{avg}$, $(X'_{I})_{avg}$, $(X'_{II})_{avg}$, $(X'_{III})_{avg}$, and $(X'_{IV})_{avg}$ which are defined via equations (4.3) - (4.8). It should be noted that, in this study $X' = \frac{dx_p}{d\theta}$ is termed as a "velocity" (which has the units "piston displacement per crank rotation").

$$(X'_{I+II})_{avg} \triangleq \frac{\int_o^{\theta_2} X'(\theta)\, d\theta}{\theta_2 - 0} = \frac{X_2}{\theta_2} \tag{4.3}$$

$$(X'_{III+IV})_{avg} \triangleq \frac{\int_{\theta_2}^{2\pi} X'(\theta)\, d\theta}{2\pi - \theta_2} = \frac{0 - X_2}{2\pi - \theta_2} \tag{4.4}$$

$$(X'_{I})_{avg} \triangleq \frac{\int_o^{\theta_1} X'(\theta)\, d\theta}{\theta_1 - 0} = \frac{X_1}{\theta_1} \tag{4.5}$$

$$(X'_{II})_{avg} \triangleq \frac{\int_{\theta_1}^{\theta_2} X'(\theta)\, d\theta}{\theta_2 - \theta_1} = \frac{X_2 - X_1}{\theta_2 - \theta_1} \tag{4.6}$$

$$(X'_{III})_{avg} \triangleq \frac{\int_{\theta_2}^{\theta_3} X'(\theta)\, d\theta}{\theta_3 - \theta_2} = \frac{X_3 - X_2}{\theta_3 - \theta_2} \tag{4.7}$$

$$(X'_{IV})_{avg} \triangleq \frac{\int_{\theta_3}^{2\pi} X'(\theta)\, d\theta}{2\pi - \theta_3} = \frac{0 - X_3}{2\pi - \theta_3} \tag{4.8}$$

where

$(X'_{I})_{avg}$: Average velocity associated with f $X_I(\theta)$

$(X'_{II})_{avg}$: Average velocity associated with f $X_{II}(\theta)$

$(X'_{III})_{avg}$: Average velocity associated with $X_{III}(\theta)$

$(X'_{IV})_{avg}$: Aaverage velocity associated with $X_{IV}(\theta)$

$(X'_{I+II})_{avg}$: Average velocity associated with $X_I(\theta)$ and $X_{II}(\theta)$

$(X'_{III+IV})_{avg}$: Average velocity associated with $X_{III}(\theta)$ and $X_{IV}(\theta)$

The six average velocities defined via equations (4.3) - (4.8) are the elements of the vector $\vec{P}^*_{6565}$ which is defined via the equation below.

$$\vec{P}^*_{6565} = [(X'_{I+II})_{avg}; (X'_{III+IV})_{avg}; (X'_I)_{avg}; (X'_{II})_{avg}; (X'_{III})_{avg}; (X'_{IV})_{avg}] \tag{4.9}$$

The design parameter vector $\overrightarrow{DP}$, on the other hand, is given by equation (4.1). Combining $\vec{P}^*_{6565}$ and $\overrightarrow{DP}$, a new design parameter vector, $\overrightarrow{DP}_{x_p}$, can be defined as shown below.

$$\overrightarrow{DP}_{x_p} = [(X'_{I+II})_{avg}; (X'_{III+IV})_{avg}; (X'_I)_{avg}; (X'_{II})_{avg}; (X'_{III})_{avg}; (X'_{IV})_{avg}; D_{cyl}; D_{vi}; D_{vo}; \omega] \tag{4.10}$$

Note that, $\overrightarrow{DP}_{x_p}$ denotes the design parameter vector that utilizes $x_p(\theta)$ as the design function. Since $\overrightarrow{DP}_{x_p}$ has 10 parameters, one ends up with a nonlinear optimization problem with 10 design variables. Clearly, such an optimization problem will be quite challenging. In order to show this challenging problem, a method of optimization with the design function $x_p(\theta)$ and a numerical case study will be shown following section.

4.1.1.1 Optimization Problem with the Design Function $x_p(\theta)$

In order to reduce the execution time for the optimization, firstly, a brute force search will be performed. The brute force search results will then be used as initial guesses for an appropriate optimization algorithm. The design function for the optimization is taken to be $x_p(\theta)$.

In this section, the brute force search in the design parameter space and the consequent optimization are explained in detail. Firstly, a search area in the design

parameter space is described. Secondly, the search and the optimization algorithms are discussed with a numerical example.

4.1.1.1.1 Search Area for Design Parameters of 6-5-6-5 Polynomial

In order to obtain the type of $x_p - \theta$ curve shown in Figure 4.1, $\theta_1,\ \theta_2,\ \theta_3\ X_1, X_2,$ X_3 should satisfy the following constraints.

$$0 < \theta_1 < \theta_2 < \theta_3 < 2\pi \tag{4.11}$$

$$0 < X_1 < X_2 \tag{4.12}$$

$$0 < X_3 < X_2 \tag{4.13}$$

Using constraints above and the equations between (4.3) and (4.8), a new inequality set can be obtained in terms of parameters in $\vec{P}^*_{6565}$ (from equation (4.9)). One can obtain the inequality set by Mathematica as follows

$$(X'_{I+II})_{avg} > 0 \tag{4.14}$$

$$(X'_{III+IV})_{avg} < 0 \tag{4.15}$$

$$\begin{aligned}\left[(X'_I)_{avg} > (X'_{I+II})_{avg}\ \&\&\ 0 < (X'_{II})_{avg} < (X'_{I+II})_{avg}\right] \mid\mid \left[(X'_{II})_{avg}\right. \\ \left. > (X'_{I+II})_{avg}\ \&\&\ 0 < (X'_I)_{avg} < (X'_{I+II})_{avg}\right]\end{aligned} \tag{4.16}$$

$$\left[(X'_{IV})_{avg} < (X'_{III+IV})_{avg} \;\&\&\; (X'_{III+IV})_{avg} < (X'_{III})_{avg} < 0\right] \;||\; \left[(X'_{III})_{avg} < (X'_{III+IV})_{avg} \;\&\&\; (X'_{III+IV})_{avg} < (X'_{IV})_{avg} < 0\right] \tag{4.17}$$

The inequality set between (4.14) and (4.17) yields the allowable region in $(X'_I)_{avg} - (X'_{II})_{avg}$ plane and $(X'_{III})_{avg} - (X'_{IV})_{avg}$ plane as shown in Figure 4.2.

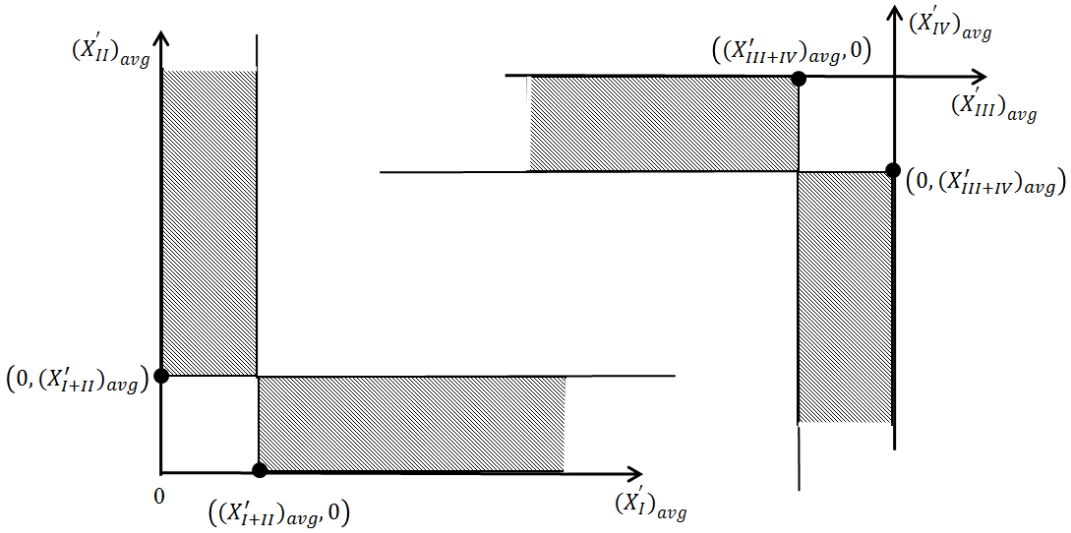

Figure 4.2. 6-5-6-5 Polynomial Allowable Regions

It should be noted that the inequality set defined between (4.14) and (4.17) are necessary, but not sufficient. One should also make sure that $X_I, X_{II}, X_{III}, X_{IV}$ do not have any local minimum and maxiumum (in the intervals that they are used). To check this situation higher order derivative test or general derivative test can be used.

In order to perform a brute force search, points as in Figure 4.3 are formed. For example, 16 points are shown in Figure 4.3.

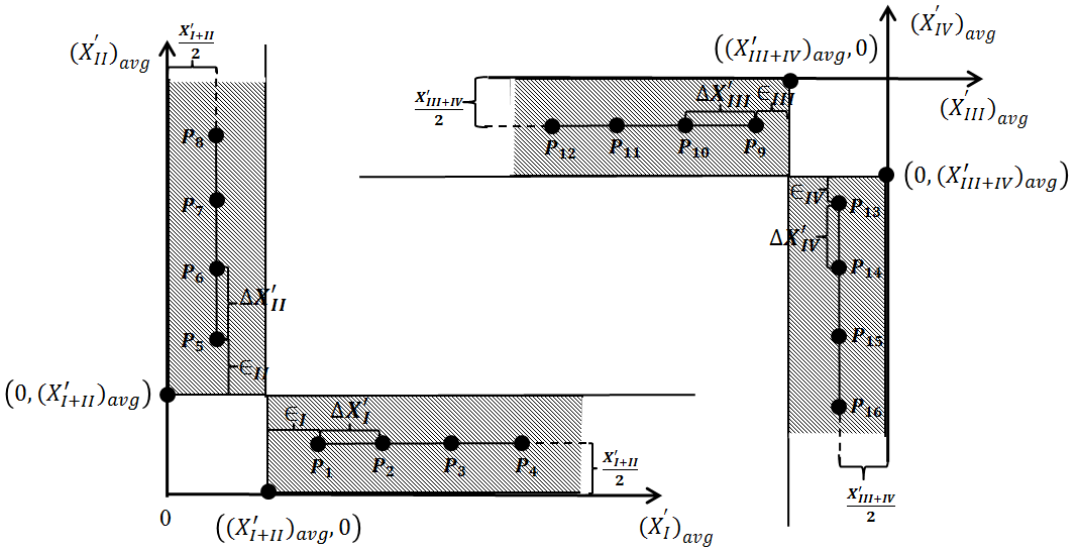

Figure 4.3. 6-5-6-5 Polynomial Brute Force Search Points

In order to obtain these 16 points, the variables $((X'_{I+II})_{avg}$, $(X'_{III+IV})_{avg}$, $\Delta X'_I$, $\Delta X'_{II}$, $\Delta X'_{III}$, $\Delta X'_{IV}$,$\in_I$,$\in_{II}$,$\in_{III}$,$\in_{IV})$ should be specified. Alternatively, rather than selecting $\Delta X'$ values, one could select a multiplier "m" such that

$$\left[(X'_I)_{avg}\ of\ P_2\right] = m * \left[(X'_I)_{avg}\ of\ P_1\right]$$

$$\left[(X'_I)_{avg}\ of\ P_3\right] = m * \left[(X'_I)_{avg}\ of\ P_2\right]$$

$$\left[(X'_I)_{avg}\ of\ P_4\right] = m * \left[(X'_I)_{avg}\ of\ P_3\right]$$

where m = 2 or 3 or 4 etc. Other points can be found similarly.

In this search method, the number of points, values of $\Delta X'$ or m and $\in$ values are user specified parameters. After brute force search points are formed, these points are used to form piston motion profiles. Next, obtained piston motion profiles and other design parameters in $\overrightarrow{DP}_{x_p}$ are used in the compressor simulation defined in chapter 2. According to the objective of optimization, related outputs are saved.

4.1.1.1.2 The Search and The Optimization Algorithms with a Numerical Example

For a numerical example, in the search algorithm, the multiplier method is used. Furthermore, to specify $(X'_{I+II})_{avg}$ and $(X'_{III+IV})_{avg}$, X_2 is taken to be equal to the stroke of slider crank based compressor and θ_2 is taken [160º 170º 180º 190º 200º 210º 220º]. It should be noted that the motor speed, the cylinder diameter, diameters of valves are also taken to be equal to corresponding values of the slider crank based compressor.

16 points defined as in previous section are formed and simulations of them are performed. If results are compared according to net work done per mass, the minimum value of net work done per mass is obtained when $\vec{P}^*_{6565}$ is as below.

$$\vec{P}^*_{6565} = [0.0273; -0.0382;\ 0.0307; 0.0136; -0.0191;\ -0.0389] \qquad (4.18)$$

Table 4.1 Optimum Results Obtained by the Brute Force Search Method for 6-5-6-5 Piston Motion Curve

Parameter	**Unit**	**Value**	
		Slider Crank Based	**6-5-6-5 Piston Motion Based**
$\boldsymbol{W^{pm}_{net}}$	[kJ/kg]	227,17	226,69
cap	[m^3/hr]	43,8	45,22

The optimum $\vec{P}^*_{6565}$ vector (given by equation (4.18)) is used as initial guess for an appropriate optimization algorithm. The objective of optimization is taken minimization of net work done per mass. The design parameter vector that uses $x_p(\theta)$ as the design function has been given in (4.10). However, In order to reduce the execution time for the optimization, D_{cyl}, D_{vi} and D_{vo} are taken to be equal to corresponding values of slider crank based compressor. Hence, the new design parameter vector becomes

$$\overrightarrow{DP}^{*}_{x_p} = [(X'_{I+II})_{avg}; (X'_{III+IV})_{avg}; (X'_{I})_{avg}; (X'_{II})_{avg}; (X'_{III})_{avg}; (X'_{IV})_{avg}; \omega] \quad (4.19)$$

3 optimization problems are solved with 3 initial guesses which are

1^{st} Inial guess of $\overrightarrow{DP}^{*}_{x_p} = [0.0273, -0.0382, 0.0307, 0.0136, -0.0191, -0.0389, 700]$

2^{nd} Inial guess of $\overrightarrow{DP}^{*}_{x_p} = [0.0273, -0.0382, 0.0307, 0.0136, -0.0191, -0.0389, 800]$

3^{rd} Inial guess of $\overrightarrow{DP}^{*}_{x_p} = [0.0273, -0.0382, 0.0307, 0.0136, -0.0191, -0.0389, 900]$

At the end of the optimization,

$$optimum\ \overrightarrow{DP}^{*}_{x_p} = [0.0280 \quad -0.0380 \quad 0.0365 \quad 0.0133 \quad -0.0186 \quad -0.0391 \quad 717.99]$$

is found and the net work done per mass is obtained as 224.60 kJ/kg. It means that the energy consumption is less than %1.13 of the slider crank based compressor.

By changing search points, this optimization can be performed many times. However, as seen the example some of design parameters are taken as constant to reduce the execution time for optimization and to reduce nonlinearities. It can be said that it is not enough to obtain an effective optimization. Hence, clearly, if $x_p(\theta)$ is selected to be the design function, it is difficult, if not impossible, to predict the "shape" of the optimal design function. Hence, determination of the optimal $x_p(\theta)$, via a nonlinear optimization, will be quite cumbersome.

4.1.2 Parametrization of the Chamber Pressure Function, $P_c(\theta)$

It is said that if $x_p(\theta)$ is selected to be the design function, it is difficult to predict the "shape" of the optimal design function. However, prediction of the optimal "shape" of the chamber pressure function, $P_c(\theta)$, is quite intuitive. In order to minimize the valve losses, the chamber pressure must be constant during the suction and discharge periods. Hence, when the chamber pressure function, $P_c(\theta)$, is taken to be the design function, $P_c(\theta)$ is assumed to be as shown in Figure 4.4.

Here, it should be recalled that when the chamber pressure function, $P_c(\theta)$, is taken to be the design function, the corresponding piston motion function, $x_p(\theta)$ may be obtained via simulation (of the compression process). The assumed chamber pressure function shown in Figure 4.4 can be described via the five parameters (θ_a, θ_b, θ_c, ΔP_o, ΔP_i). In the figure, the non-constant parts of $P_c(\theta)$ are modelled by using suitable (one or more) cam motion curves.

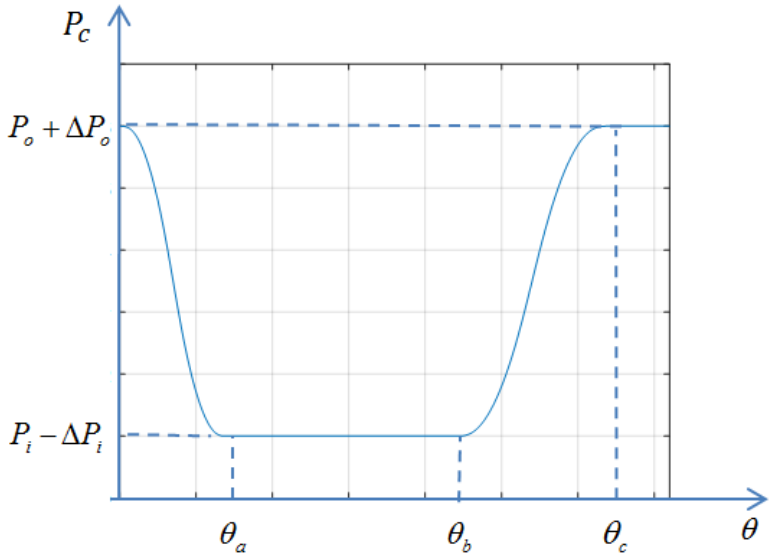

Figure 4.4. Assumed Optimal Chamber Pressure Function for a Reciprocating Compressor

As seen in Figure 4.4 the valve losses at the suction and the discharge states have been eliminated. ΔP_i and ΔP_o are pressure difference which between chamber and suction plenum, chamber and discharge plenum, respectively. ΔP_i and ΔP_o are required to open valves. They can be taken as optimization parameters. However, to reduce the number of optimization parameters ΔP_i and ΔP_o are taken to be constant pressures which open the valves fully. Hence, ΔP_i and ΔP_o are obtained from the valve parameters. ΔP_i and ΔP_o are defined via the equations

$$\Delta P_i = \frac{k_{vi} L_{vi}}{\frac{\pi D_{vi}^2}{4}} \tag{4.20}$$

$$\Delta P_o = \frac{k_{vo} L_{vo}}{\frac{\pi D_{vo}^2}{4}} \tag{4.21}$$

where L_{vi} and L_{vo} are the maximum opening of the inlet valve and the outlet valve, respectively. As seen in equations (4.20) and (4.21), force in springs for the maximum opening of the valves are divided to area of valves and ΔP_i and ΔP_o are obtained.

As stated before, the "curves" for the compression and the expansion processes may be modelled as cam motion curves. In this study, each of these curves is modelled by using a single modifed trapezoidal acceleration cam motion profile. Hence, the pressure function in terms of the crank angle is defined via the equation

$$P_c(\theta) = \begin{cases} f_a(\theta) & 0 < \theta < \theta_a \\ P_i - \Delta P_i & \theta_a < \theta < \theta_b \\ f_b(\theta) & \theta_b < \theta < \theta_c \\ P_o + \Delta P_o & \theta_c < \theta < 2\pi \end{cases} \tag{4.22}$$

where $f_a(\theta)$ and $f_b(\theta)$ are functions that define the modifed trapezoidal acceleration cam motion profile (see section 3.5.1.2).

The design parameter vector for this method, $\overrightarrow{DP_{pres}}$, is given by the equation below

$$\overrightarrow{DP_{pres}} = [\theta_a; \theta_b; \theta_c; D_{cyl}; D_{vi}; D_{vo}; \omega] \tag{4.23}$$

Here, $\overrightarrow{DP_{pres}}$ is the design parameter vector that uses $P_c(\theta)$ as the design function.

In the assumed optimal chamber pressure function shown in Figure 4.4, the pressures at the suction and discharge states are constant. Because of this property, the expressions for the inlet and outlet mass flow rates and the capacity (i.e., $\dot{m}_i$, $\dot{m}_o$ and cap) may be simplified. In the rest of this section, these simplifications will be derived.

The inlet mass flow rate, $\dot{m}_i$, can be determined via equation (2.34). Using the fact that P_i is constant, one may rerarrange this equation , yielding

$$\dot{m}_i = c_1 A_{vi} P_c^{c_4} \sqrt{1 - c_2 P_c^{c_3}} \tag{4.24}$$

where c_1, c_2, c_3 and c_4 are four constants given by the equations

$$c_1 = C_{di} \rho_i \left(\frac{1}{P_i}\right)^{\frac{1}{\gamma}} \sqrt{2 \frac{\gamma}{\gamma - 1} \frac{P_i}{\rho_i}} \tag{4.25}$$

$$c_2 = \left(\frac{1}{P_i}\right)^{\frac{\gamma - 1}{\gamma}} \tag{4.26}$$

$$c_3 = \frac{\gamma - 1}{\gamma} \tag{4.27}$$

$$c_4 = \frac{1}{\gamma} \tag{4.28}$$

If it is assumed that the inlet valve opens and closes immediately, A_{vi} will also be constant, yielding

$$A_{vi} = \pi D_{vi} L_{vi} \tag{4.29}$$

when the valve is fully open. As seen in Figure 4.4, in the suction phase (between θ_a and θ_b), the chamber pressure is constant at $(P_i - \Delta P_i)$. Hence, equation (4.24) yields

$$\dot{m}_i = c_1 A_{vi} (P_i - \Delta P_i)^{c_4} \sqrt{1 - c_2 (P_i - \Delta P_i)^{c_3}} \tag{4.30}$$

where ΔP_i is defined by equation (4.20). After some manipulations, ΔP_i can be expressed as

$$\Delta P_i = \frac{c_5}{D_{vi}^2} \tag{4.31}$$

where

$$c_5 = \frac{4k_{vi}L_{vi}}{\pi} = constant \tag{4.32}$$

From equations (4.30) and (4.31), it follows that $\dot{m}_i$ is a function of D_{vi} only (and hence, constant), i.e.,

$$\dot{m}_i = f(D_{vi}) = constant \tag{4.33}$$

The capacity, on the other hand, can be expressed in terms of the inlet mass flow rate via the equation

$$cap = \frac{\int_0^T \dot{m}_i(t)dt}{T} \tag{4.34}$$

where

$$T = \frac{2\pi}{\omega} \tag{4.35}$$

When the inlet valve is closed, $\dot{m}_i = 0$. Hence, equation (4.34) yields

$$cap = \frac{\int_{t_1}^{t_2} \dot{m}_i(t)dt}{T} \tag{4.36}$$

where t_1 and t_2 designate the times at which the inlet valve opens and closes, respectively. Since $\dot{m}_i(t)$ is constant between t_1 and t_2, the capacity can be found via equation (4.36) , yielding

$$cap = \frac{\dot{m}_i * (t_2 - t_1)}{\frac{2\pi}{\omega}} \tag{4.37}$$

If it is assumed that the inlet valve opens and closes immediately at θ_a and θ_b respectively, equation (4.37) simplifies to

$$cap = \frac{\dot{m}_i * (\theta_b - \theta_a)}{2\pi} \tag{4.38}$$

One of the design parameters can be eliminated by using equation (4.38). For instance, one may solve θ_b (in terms of θ_a, cap and $\dot{m}_i$) from equation(4.38), yielding

$$\theta_b = \theta_a + \frac{cap * 2\pi}{\dot{m}_i} \tag{4.39}$$

Note that, $\dot{m}_i$ is function of D_{vi}.

Recall that, during the derivation of equation (4.38) the inlet valve has been assumed to open and close immediately. Hence, the actual capacity will not be exactly equal to the value calculated from equation (4.38) [because of the transient behaviors during the opening and closing processes of the inlet valve]. However, equation (4.38) will still be used to eliminate the design parameter θ_b, via equation (4.39), since this elimination decreases the number of design variables by one (hence, simplifying the optimization process). As a result, the desired capacity will be obtained only approximately.

Similarly, the expression for $\dot{m}_o$ given by equation (2.35) can also be simplified, yielding.

$$\dot{m}_o = \frac{d_1 A_{vo} P_c^{d_4} \sqrt{T_c - d_2 T_c P_c^{d_3}}}{T_c} \tag{4.40}$$

where d_1, d_2, d_3, d_4 are four constants given by equations (4.41) - (4.44). In equation (4.40), it should be noted that, $\dot{m}_o$ depends upon not only the chamber pressure, but the chamber temperature as well.

$$d_1 = C_{do} \rho_i (P_o)^{\frac{1}{\gamma}} \sqrt{2 \frac{\gamma}{\gamma - 1} \frac{1}{R}} \tag{4.41}$$

$$d_2 = (P_o)^{\frac{\gamma - 1}{\gamma}} \tag{4.42}$$

$$d_3 = -\frac{\gamma - 1}{\gamma} \tag{4.43}$$

$$d_4 = \frac{\gamma - 1}{\gamma} \tag{4.44}$$

If it is assumed that the outlet valve opens and closes immediately, A_{vo} will be a constant value given by

$$A_{vo} = \pi D_{vo} L \tag{4.45}$$

for the fully opened position of the outlet valve. As seen in Figure 4.4, in the discharge phase (between θ_c and 2π), pressure is given constant at $(P_o + \Delta P_o)$. Hence, the equation (4.40) will be changed as below.

$$\dot{m}_o = \frac{d_1 A_{vo} (P_o + \Delta P_o)^{d_4} \sqrt{T_c - d_2 T_c (P_o + \Delta P_o)^{d_3}}}{T_c} \tag{4.46}$$

where ΔP_o is defined by equation (4.21). After some manipulations, ΔP_o can be expressed as

$$\Delta P_o = \frac{d_5}{D_{vo}^2} \tag{4.47}$$

where

$$d_5 = \frac{4 k_{vo} L}{\pi} = constant \tag{4.48}$$

Hence $\dot{m}_o$ is only function of D_{vo} and $T_c(t)$.

From equations (4.46) and (4.47), it follows that $\dot{m}_o$ is a function of D_{vo} and $T_c(t)$, i.e.,

$$\dot{m}_o = f(T_c(t), D_{vo}) \tag{4.49}$$

The capacity, on the other hand, can be expressed in terms of the outlet mass flow rate via the equation

$$cap = \frac{\int_0^T \dot{m}_o(t)dt}{T} \tag{4.50}$$

When the outlet valve is closed, $\dot{m}_o = 0$. Hence, equation (4.50) yields

$$cap = \frac{\int_{t_3}^{t_4} \dot{m}_o(t)dt}{T} \tag{4.51}$$

where t_3 and t_4 designate the times at which the outlet valve opens and closes, respectively. If it is assumed that $T_c(t)$ is constant, $\dot{m}_o(t)$ will be constant between t_3 and t_4. Since $\dot{m}_o(t)$ is constant between t_3 and t_4, the capacity can be found via equation (4.51), yielding

$$cap = \frac{\dot{m}_o * (t_4 - t_3)}{\frac{2\pi}{\omega}} \tag{4.52}$$

If it is assumed that the outlet valve opens and closes immediately at θ_c and 2π respectively, equation (4.52)(4.37) simplifies to

$$cap = \frac{\dot{m}_o * (2\pi - \theta_c)}{2\pi} \tag{4.53}$$

In order to obtain equation (4.53), $T_c(t)$ has been assumed to be constant, which, clearly, is not true. However, by using this constant temperature assumption, equation (4.53) may be used to determine the lower and upper bounds on θ_c. To be more explicit, if one uses equation (4.49) to calculate $\dot{m}_o$ by using the predicted minimum and maximum values of T_c; substitute the result into equation (4.53) and then solve for θ_c, the lower and upper bounds on θ_c can be obtained.

It has already been stated that the design parameters vector includes D_{cyl}, D_{vi} and D_{vo}. In the parametric analysis, on the other hand, it has been observed that the inlet and outlet valve areas should be as large as possible. Hence, it is necessary to place upper bounds on D_{vi} and D_{vo} which, implicitly, are provided via the equality constraint

$$D_{vi} + D_{vo} = \mu D_{cyl} \tag{4.54}$$

where μ is a specified parameter subject to the constraint $0 < \mu < 1$. Indeed, it is possible to consider μ as one of the design parameters. However, in order to keep the number of design parameters to be as small as possible, μ is taken to be 0.75 (based on the slider crank based compressor design presented in Chapter 2). In other words, in this study, the constraint given by the equation

$$D_{vi} + D_{vo} = 0.75 D_{cyl} \tag{4.55}$$

will be used. Now, using equation (4.54), one may eliminate the design parameter D_{vo} [by replacing D_{vo} with the right hand side of equation (4.56)].

$$D_{vo} = 0.75 D_{cyl} - D_{vi} \tag{4.56}$$

Hence, the number of design variables reduces by 2, yielding the new design parameter vector, $\overrightarrow{DP^*_{pres}}$, defined below.

$$\overrightarrow{DP^*_{pres}} = [\theta_a; \theta_c; D_{cyl}; D_{vi}; \omega] \tag{4.57}$$

4.1.2.1 Solving Thermo-Fluid Model of a Reciprocating Compressor using $P_c(\theta)$ as the Input

In chapter 2, the reciprocating compressor has been mathematically modelled. In this model, the piston motion, $x_p(\theta)$, has been taken to be the input. A new simulation model, by using $P_c(\theta)$ as the input this time, is presented in Figure 4.5.

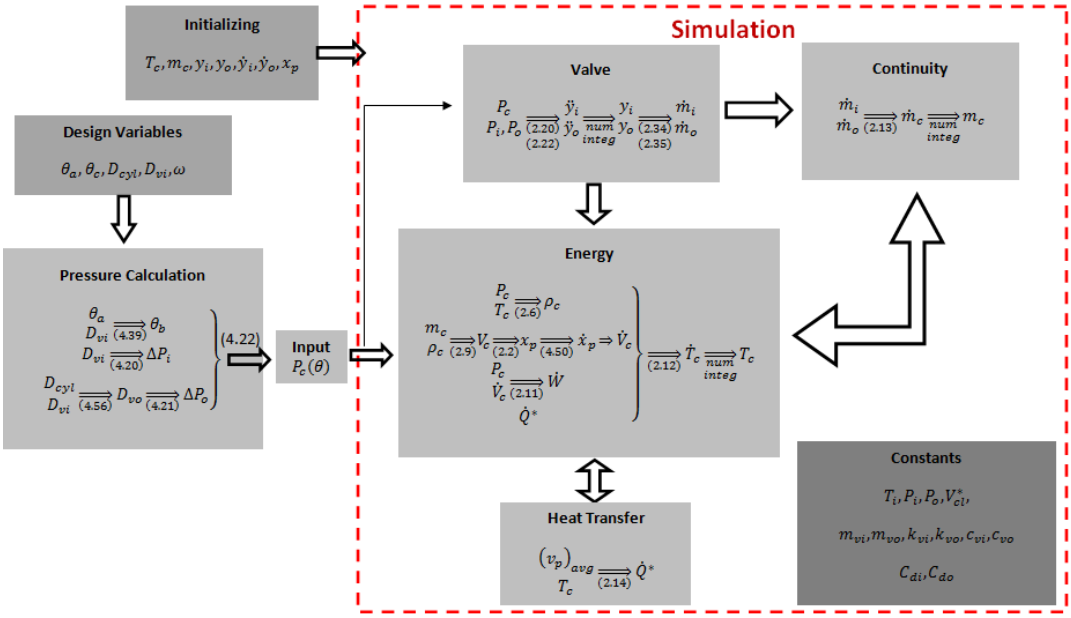

Figure 4.5. Simulation Block Diagram for the Thermo-Fluid Model of a Reciprocating Compressor using the Pressure, $P_c(\theta)$, as the Input

Similar to the previous simulation, there are four differential equations [namely, energy equation (2.12), continuity equation (2.13) and the equations of motion for the inlet and outlet valves (2.20) and (2.22)]. Furthermore, there is one more differential equation for the piston motion which is defined via the equation

$$\dot{x}_p = \frac{\mathrm{d}x_p}{\mathrm{dt}} \tag{4.58}$$

This mathematical model is solved via a code developed in Simulink. The fourth order Runge-Kutta is chosen as the solver and the time step is taken to be 10^{-5} seconds.

Since there are 3 first order and 2 second order differential equations in the mathematical model, 7 initial conditions are required. The initial conditions for $T_c, m_c, y_i, y_o, \dot{y}_i, \dot{y}_o$ are calculated using the iterative approach that has been introduced in Section 2.3 . The initial condition for x_p, on the other hand, is taken to be zero.

At the end of the simulation, $x_p(\theta)$ is obtained in a discrete manner (i.e., the solution is obtained in the form of "points" in the x_p - θ plane). In order to obtain a continuous motion profile, a curve is fitted to the "points" that have been obtained at the end of the solution. To this purpose, a Fourier-8 type fit is applied (using the nonlinear least squares method provided in MATLAB). Fourier-8 fit can be defined via the equation

$$x_p(\theta) = a_0 + a_1\cos(\theta w) + b_1\sin(\theta w) + a_2\cos(2\theta w) + b_2\sin(2\theta w) + \cdots + a_8\cos(8\theta w) + b_8\sin(8\theta w) \quad (4.59)$$

The w term is a measure of period. $2\pi/w$ converts to the period. Hence w is set to 1, since the period of motion profile is 2π. The coefficients $a_0, a_1, \ldots, a_8$ and $b_0, b_1, \ldots, b_8$ are calculated by the MATLAB curve fitting tool.

On the other hand, it is possible to obtain a continuous motion profile using a cubic spline curve fit utilized at the start and end of the motion. For the original discrete solution, a cubic spline curve fit is also utilized at the start and end of the motion in order to satisfy the periodicity of the motion. It is applied only a few data at the start and end of the motion. As seen in Figure 4.6, blue dot points represent the original discrete solution. The left side is the end of motion and the right side is the start of motion. These small parts are combined by utilizing a cubic spline curve fit. This method is named as discrete motion with cubic spline patching.

The effects of these two different curve fit methods will be discussed in a numerical case study, in section 4.2.4.

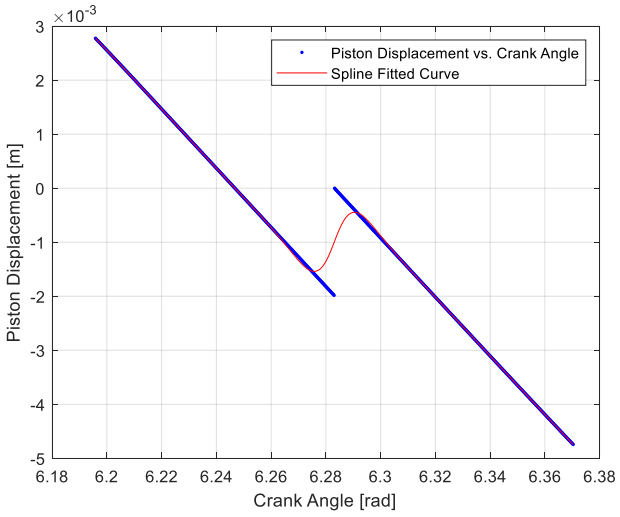

Figure 4.6. Spline Fit for the Periodicity

Since the piston motion is unknown in the beginning of the simulation, the computation of $\dot{Q}$ and V_{cl} require recursive procedures. In order to emphasise the iterative determination of $\dot{Q}$ and V_{cl}, $\dot{Q}$ and V_{cl} are denoted as $\dot{Q}^*$ and V_{cl}^* in the simulation block diagram given in Figure 4.5. Next, the aforementioned recursive procedures will be explained in detail.

4.1.2.1.1 Recursive Procedure for Determining $\dot{Q}^*$

In order to calculate the heat transfer $\dot{Q}^*$, the average piston velocity is required. When the pressure is given as the input, the average piston velocity is not known in the beginning (since the piston motion is, yet, unknown). For this reason, an iterative algorithm is used to calculate the average piston velocity. The steps of this algorithm are listed below

1) Take the average piston velocity to be equal to the average piston velocity of the slider crank based compressor discussed in chapter 2.

2) Run the simulation.

3) Determine the average piston velocity corresponding to the piston motion found at the end of the simulation.

4) Compute the difference between the average piston velocity found in step 3 and the average piston velocity used in the previous iteration. If this difference is below a user specified tolerance, stop. Otherwise, go to step 2.

4.1.2.1.2 Recursive Procedure for Determining V_{cl}^{*}

When the pressure variation, with respect to θ, is taken to be the input, the piston displacement, x_p can take negative values. Hence, the clearance volume can be smaller than the user specified lower limit of the clearance volume (which is related to the mechanical constraints associated with the inlet and outlet valves). In this study, the user specified lower limit of the clearance volume is taken to be the clearance volume of the slider crank based compressor analyzed in Chapter 2. In addition to the lower limit, since the percentage of the clearance volume has an effect on the performance of a reciprocating compressor, it should be constant along the optimization. The percentage of the clearance is taken to be equal to corresponding value of the slider crank based compressor due to fair comparison (i.e., not to add another effect on performance of compressor). Therefore, an iterative algorithm, similar to the calculation of the piston average velocity, is used to obtain a constant percentage of the clearance volume. The steps of this algorithm are listed below. It should be noted that percentage of the clearance volume, V_{pcl}, has been defined in equation (2.40).

1) Take the percentage of the clearance volume to be equal to the percentage of the clearance volume of the slider crank based compressor discussed in chapter 2.

2) Run the simulation.

3) Determine the percentage of the clearance volume corresponding to the piston motion found at the end of the simulation.

4) Compute the difference between the percentage of the clearance volume found in step 3 and step 1. If this difference is below a user specified tolerance, go to step 5. Otherwise, go to step 2.

5) If the clearance volume obtained is smaller than the user specified lower limit, set the clearance volume to the lower limit and stop. (the lower limit of the clearance volume is related to the mechanical constraints associated with the inlet and outlet valves)

4.1.3 Additional Design Parameters in a MinFaS-TaR Based Compressor

In a MinFaS-TaR based compressor, there are 2 additional design parameters which are the masses of links 3 and 5 (see Figure 4.7.). Recall that inertial effects associated with a slider crank based compressor are neglected in this study. For the MinFaS-TaR based compressors, on the other hand, the inertial effects are taken into consideration. A schematic diagram of the MinFaS-TaR mechanism is given in Figure 4.7.

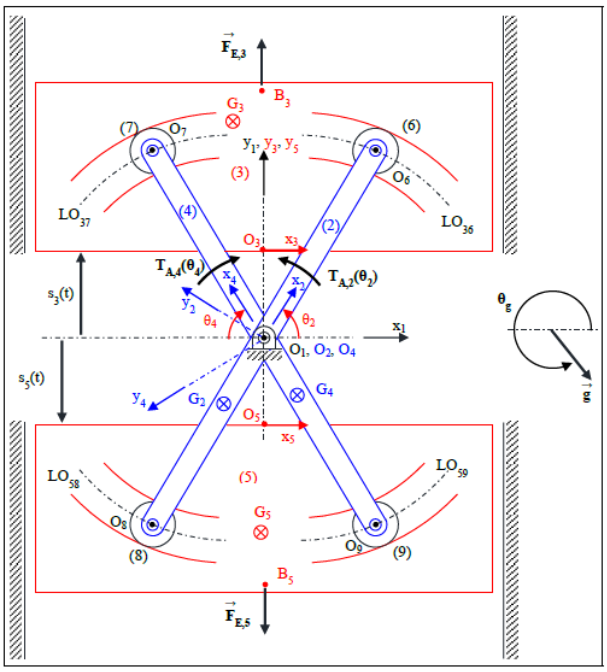

Figure 4.7. Schematic diagram of the TaR mechanism [3]

The properties of a MinFaS-TaR mechanism are given below.

- Link 2 and 4:

$$m_2 = m_4 \tag{4.60}$$

$$\theta_2 = \theta_4 \tag{4.61}$$

$$T_{A,4} = T_{A,2} \tag{4.62}$$

- Link 3 and 5:

$$m_3 = m_5 \tag{4.63}$$

$$s_3 = s_5 \tag{4.64}$$

$$F_{E,3} = F_{E,5} \tag{4.65}$$

- Link 6,7,8 and 9 (rollers):

$$m_6 = m_7 = m_8 = m_9 \tag{4.66}$$

$$r_6 = r_7 = r_8 = r_9 \tag{4.67}$$

where

$T_{A,2}, T_{A,4}$: Actuator torques applied on links 2 and 4, respectively.

θ_2, θ_4 : Angular positons of links 2 and 4, respectively.

s_3, s_5 : Linear positons of links 3 and 5, respectively.

$F_{E,3}, F_{E,5}$: External forces applied on links 3 and 5, respectively.

$m_2, m_3, m_4, m_5,$: Masses of links 2,3,4 and 5, respectively.

$m_6, m_7, m_8, m_9,$: Masses of rollers 6,7,8 and 9, respectively.

$r_6, r_7, r_8, r_9,$: Radius of rollers 6,7,8 and 9, respectively.

Total motor (actuator) torque, τ_m is defined via equation

$$\tau_m = T_{A,2} + T_{A,4} \tag{4.68}$$

Furthermore, inertial parameters of

- links 2 and 4,
- links 3 and 5,
- links 6,7,8 and 9

are identical to each other.

In this study, the inertia of the rotating arms 2, 4 and the inertia of the rollers are neglected. Hence, using D'Alembert's principle, the virtual power equation yields.

$$\tau_m \dot{\theta}_2 + 2F_{E,3}\dot{s}_3 - 2m_3\ddot{s}_3\dot{s}_3 = 0 \tag{4.69}$$

The total motor torque may be solved from equation (4.69), yielding.

$$\tau_m = -\frac{2F_{E,3}\dot{s}_3 - 2m_3 a_{13}\dot{s}_3}{\dot{\theta}_2} \tag{4.70}$$

where

$$\dot{\theta}_2 = \omega \tag{4.71}$$

Hence, using equations (4.70) and (4.71), the total motor torque is given by the equation

$$\tau_m = -\frac{2F_{E,3}\dot{s}_3 - 2m_3 \dot{s}_3 \ddot{s}_3}{\omega} \tag{4.72}$$

$s_3, \dot{s}_3 \; and \; \ddot{s}_3$ can be obtained via the position, velocity and acceleration analysis of the MinFaS-TaR mechanism (in terms of θ_2 and ω, when ω is constant). $F_{E,3}$ and $F_{E,5}$, on the other hand, are the pressure forces due to the fluid inside the cylinder. The total motor torque can be conveniently seperated into two parts (which are due to the pressure and inertial forces) i.e.,

$$\tau_m = \tau_{iner} + \tau_{press} \tag{4.73}$$

where

$$\tau_{iner} = \frac{2m_3 \dot{s}_3 \ddot{s}_3}{\omega} \tag{4.74}$$

$$\tau_{pres} = \frac{-2F_{E,3}\dot{s}_3}{\omega} \tag{4.75}$$

Clearly, τ_{pres} is obtained from the simulation of the compressor. τ_{iner}, on the other hand, is dependent on m_3. Hence, by selecting m_3 appropriately, the motor torque characteristics of the compressor can be " designed " to a certain extent. Such a design can be useful for the flywheel sizing. Therefore, m_3 can be considered to be a design parameter (which is used after the optimization of $\overrightarrow{DP}^*_{pres}$ is completed). Since m_3 is not necessary for the compressor simulation, its introduction as an additional design parameter does not affect the execution time for the optimization

extensively. It should be noted that, the work done by the motor can then be calculated by using equations (3.29) - (3.40) and equation (4.72).

It should be noted that $\dot{s}_3$ and $\ddot{s}_3$ in equation (4.74) correspond to $\dot{x}_p$ and $\ddot{x}_p$, respectively. Furthermore, according to the notation that is employed, $\dot{s}_3 = -\dot{x}_p$ and $\ddot{s}_3 = -\ddot{x}_p$.

4.2 Optimization of the Performance of a Reciprocating Compressor

The optimization of the performance of a reciprocating compressor is time consuming and complicated due to the following reasons. (i) The problem is nonlinear (with nonlinear equality and inequality constraints). (ii) The number of design variables is large. (iii) The evaluation of the objective function takes a considerable amount of time (since it requires that the compressor is simulated in order to obtain the steady state operating conditions). In order to reduce the execution time for the optimization, firstly, a brute force search will be performed. The brute force search results will then be used as initial guesses for an appropriate optimization algorithm.

In this section, the brute force search in the design parameter space and the consequent optimization are explained in detail. The design function for the optimization is taken to be $P_c(\theta)$; whereas $x_p(\theta)$ is obtained as a result of the optimization. Firstly, a search area in the design parameter space is described. Secondly, the objective functions that are utilized are introduced. Thirdly, the search and the optimization algorithms are discussed. Lastly, a numerical case study is presented in detail.

4.2.1 Search Area

In order to obtain an effective search area, one can manipulate the equations that have been obtained for the compressor model. As a result, one obtains several

equalities and inequalities which constrain the design parameters. During these manipulations, the following two assumptions are made

- The inlet valve opens and closes immediately at θ_a and θ_b, respectively (see Figure 4.4)
- The outlet valve opens and closes immediately at θ_c and 2π, respectively.

Considering conservation of mass, it is clear that

$$m_i = m_o \tag{4.76}$$

Since $\dot{m}_i$ is constant (see equation (4.33)), the inlet mass, m_i, may be expressed as follows.

$$m_i = \int_0^T \dot{m}_i \, dt = \dot{m}_i (t_2 - t_1) = \frac{\dot{m}_i (\theta_b - \theta_a)}{\omega} \tag{4.77}$$

The outlet mass, m_o, on the other hand, is given by the following equation.

$$m_o = \int_0^T \dot{m}_o \, dt = C \int_{t_3}^T \frac{1}{\sqrt{T_c(t)}} dt \tag{4.78}$$

where $C = f(D_{vo})$ is defined via the equation

$$C = d_1 A_{vo} \left(P_o + \frac{d_5}{D_{vo}^2} \right)^{d_4} \sqrt{1 - d_2 \left(P_o + \frac{d_5}{D_{vo}^2} \right)^{d_3}} \tag{4.79}$$

Substituting $dt = \frac{d\theta}{\omega}$ into the equation (4.78), one obtains

$$m_o = \frac{C}{\omega} \int_{\theta_c}^{2\pi} \frac{1}{\sqrt{T_c(\theta)}} d\theta \tag{4.80}$$

Now, substituting equations (4.77) and (4.80) into equation (4.76) one obtains

$$\frac{\dot{m}_i(\theta_b - \theta_a)}{\omega} = \frac{C}{\omega}\int_{\theta_c}^{2\pi} \frac{1}{\sqrt{T_c(\theta)}}d\theta \tag{4.81}$$

which simplifies to

$$\frac{\dot{m}_i(\theta_b - \theta_a)}{C} = \int_{\theta_c}^{2\pi} \frac{1}{\sqrt{T_c(\theta)}}d\theta \tag{4.82}$$

If T_c is constant, equation (4.82) yields

$$\frac{\dot{m}_i(\theta_b - \theta_a)}{C} = \frac{(2\pi - \theta_c)}{\sqrt{T_c}} \tag{4.83}$$

which can be arranged as:

$$\frac{\dot{m}_i(\theta_b - \theta_a)}{C(2\pi - \theta_c)} = \frac{1}{\sqrt{T_c}} \tag{4.84}$$

Now, let $(T_c)_{min}$ and $(T_c)_{max}$ denote the minimum and maximum values of T_c. Hence, equation (4.84) leads to the 2 inequalities given by the equation

$$\frac{1}{\sqrt{(T_c)_{max}}} < \frac{\dot{m}_i(\theta_b - \theta_a)}{C(2\pi - \theta_c)} < \frac{1}{\sqrt{(T_c)_{min}}} \tag{4.85}$$

which can be expressed as

$$\frac{1}{\sqrt{(T_c)_{max}}} < D < \frac{1}{\sqrt{(T_c)_{min}}} \tag{4.86}$$

where D is defined by the equation

$$D = f(\theta_a, \theta_b, \theta_c, D_{vi}, D_{vo}) = \frac{\dot{m}_i(\theta_b - \theta_a)}{C(2\pi - \theta_c)} \tag{4.87}$$

In order to obtain a physically realizable system, it is clear that the design parameters must satisfy the following 10 inequalities.

$$0 < \theta_a \tag{4.88}$$

$$\theta_a < \theta_b \tag{4.89}$$

$$\theta_b < \theta_c \tag{4.90}$$

$$\theta_c < 2\pi \tag{4.91}$$

$$0 < D_{vi} \tag{4.92}$$

$$D_{vi} < \mu D_{cyl} \tag{4.93}$$

$$0 < D_{v0} \tag{4.94}$$

$$D_{v0} < \mu D_{cyl} \tag{4.95}$$

$$0 < D_{cyl} \tag{4.96}$$

$$0 < \omega \tag{4.97}$$

Due to practical considerations, it is also convenient to put lower bounds on D_{vi} and D_{vo}; and lower and upper bounds on D_{cyl} and ω leading to the following six inequality constraints.

$$(D_{vi})_{min} < D_{vi} \tag{4.98}$$

$$(D_{vo})_{min} < D_{vo} \tag{4.99}$$

$$\left(D_{cyl}\right)_{min} < D_{cyl} \tag{4.100}$$

$$(\omega)_{min} < \omega \tag{4.101}$$

$$\omega < (\omega)_{max} \tag{4.102}$$

$$D_{cyl} < \left(D_{cyl}\right)_{max} \tag{4.103}$$

where, $(D_{vi})_{min}, (D_{vo})_{min}, \left(D_{cyl}\right)_{min}, (\omega)_{min}, \left(D_{cyl}\right)_{max}, (\omega)_{max}$ are user specified, positive numbers. Note that inequalities (4.98) and (4.99) replace inequalities (4.92) and (4.94), respectively.

The last 2 inequalities are due to 2 radicands that appear in the expressions for $\dot{m}_i$ and $\dot{m}_o$ [see equations (4.30) and (4.46)]. Clearly, both of these radicands must be positive, i.e.,

$$0 < 1 - c_2(P_i - \Delta P_i)^{c_3} \tag{4.104}$$

$$0 < T_c - d_2 T_c (P_o + \Delta P_o)^{d_3} \tag{4.105}$$

so that $\dot{m}_i$ and $\dot{m}_o$ are real numbers (rather than complex numbers).

As a result, one obtains 16 inequalities on the 5 design variables. Two of these inequalities are due to equation (4.86) and the remaining 14 inequalities are given by equations (4.88), (4.89), (4.90), (4.91), (4.93), (4.95), (4.98), (4.99), (4.100), (4.101), (4.102), (4.103), (4.104) and (4.105). The aforementioned 16 inequalities may be combined into a single inequality set defined by the equation below.

$$\begin{aligned} Inequality\ set \triangleq\ eq((4.86), (4.88), (4.89), (4.90), (4.91), (4.93), (4.95), \\ (4.98), (4.99), (4.100), (4.101), (4.102), (4.103), (4.104), (4.105)) \end{aligned} \tag{4.106}$$

When the 16 inequalities are examined, it can be observed that they are conveniently decoupled since some of the inequalities involve the design parameters D_{vi} and D_{cyl} only. Hence, the problem of determining the allowable

region in the design parameter space is simplified extensively if the allowable region in the D_{vi} - D_{cyl} plane is determined firstly.

It should be noted that the inequality set given by equation (4.106) does not guarantee a periodic cycle. In other words, the chamber mass, the chamber temperature and the piston position should be the same at the start and end of the cycle. Hence, in order to ensure that the cycle is periodic, the following inequality is introduced

$$Periodicity \triangleq \left(\frac{m_c(end) - m_c(start)}{m_c(start)}\right)^2 + \left(\frac{T_c(end) - T_c(start)}{T_c(start)}\right)^2 < tol \qquad (4.107)$$

In equation (4.107), $m_c(end)$ and $T_c(end)$ indicate that the chamber mass and the chamber temperature at the "end" of simulation, respectively. On the other hand, $m_c(start)$ and $T_c(start)$ indicate that the chamber mass and the chamber temperature at the "start" of simulation, respectively. Furthermore, tol is user specified tolerance value. It should be noted that when the chamber mass and temperature are periodic, the periodicity of the piston motion is guaranteed. It should also be noted that it is necessary to simulate the compressor cycle before checking the inequality given by equation (4.107).

Lastly, it is convenient to assign lower and upper bounds for the design parameter m_3 for practical purposes, i.e.,

$$(m_3)_{min} < m_3 < (m_3)_{max} \qquad (4.108)$$

To summarize, the inequalities to be satisfied by the components of the design parameter vector $\overrightarrow{DP}^*_{pres}$ (see equation (4.57)) are given by equations (4.106), (4.107) and (4.108). Based on these inequalities, a search region, in the design parameter space, can be defined. In order to determine the aforementioned search region, the following lower and upper bounds on the 6 design parameters θ_a, θ_c, D_{vi}, D_{cyl}, ω and m_3 are considered

$$(\theta_a)_{min}, (\theta_a)_{max}, (\theta_c)_{min}, (\theta_c)_{max}, (D_{vi})_{min}, (D_{vi})_{max},$$

$$\left(D_{cyl}\right)_{min}, \left(D_{cyl}\right)_{max}, (\omega)_{min}, (\omega)_{max}, (m_3)_{min}, (m_3)_{max}$$

Next, equally spaced grids are introduced into the search region. The " width " of the grids along the θ_a, θ_c, D_{vi}, D_{cyl}, ω and m_3 "axes" are given by the user specified parameters $\Delta\theta_a$, $\Delta\theta_c$, ΔD_{vi}, ΔD_{cyl}, $\Delta\omega$ and Δm_3. Then, each " point " at the " corners " of the grid is tested (to see whether the inequalities given by equations (4.106) and (4.108) are satisfied or not). The "points" that do not satisfy the inequalities are eliminated (so that they are not used for simulating the compression cycle).

4.2.2 Objective of Optimization

In this study, depending upon the motor type (See section 3.2.5), three objective functions have been defined for minimizing the energy consumption of a reciprocating compressor. These objective functions are listed below

$$obj_1 = W_{net}^{pm} = f_1(\theta_a, \theta_c, D_{vi}, D_{cyl}, \omega, m_3) \tag{4.109}$$

$$obj_2 = W_{pos}^{pm} = f_2(\theta_a, \theta_c, D_{vi}, D_{cyl}, \omega, m_3) \tag{4.110}$$

$$obj_3 = W_{abs}^{pm} = f_3(\theta_a, \theta_c, D_{vi}, D_{cyl}, \omega, m_3) \tag{4.111}$$

At the outset, it appears that obj_1 is function of m_3. In reality, however, obj_1(i.e. the net work done per mass) is not dependent on m_3 due to the nature of the inertia forces. Hence, one replaces the definition given by (4.109) with the following definition

$$obj_1 = f_1(\theta_a, \theta_c, D_{vi}, D_{cyl}, \omega) \tag{4.112}$$

The values of the 3 objective functions for the slider crank based, single cylinder reciprocating compressor is given in Table 4.2.

Table 4.2 The Values of the 3 Objective Functions for the Slider Crank Based, Single Cylinder Reciprocating Compressor

		Unit	Value
$\boldsymbol{obj_1}$		[kJ/kg]	227.29
$\boldsymbol{obj_2}$		[kJ/kg]	342.04
$\boldsymbol{obj_3}$		[kJ/kg]	456.77
cap		[m^3/hr]	43.8
Design Variables	D_{vi}	[mm]	50
	D_{cyl}	[mm]	120
	ω	[rpm]	800

4.2.3 Optimization Algorithm

The objective functions that will be minimized are defined by equations ((4.110), (4.111), (4.112)). The steps of the brute force optimization algorithm that will be used to determine the optimal values of the objective functions are given below.

1) Input the design requirements (i.e., the inlet pressure, the outlet pressure and the capacity)
2) Input the lower and upper bounds for the design parameters, i.e., specify

$$(\theta_a)_{min}, (\theta_a)_{max}, (\theta_c)_{min}, (\theta_c)_{max}, (D_{vi})_{min}, (D_{vi})_{max},$$

$$(D_{cyl})_{min}, (D_{cyl})_{max}, (\omega)_{min}, (\omega)_{max}, (m_3)_{min}, (m_3)_{max}$$

3) Input the "width" of the grids in the design parameter space, i.e., specify

$$\Delta\theta_a, \Delta\theta_c, \Delta D_{vi}, \Delta D_{cyl}, \Delta\omega, \Delta m_3$$

4) Determine the points at the "corners" of the grid in the design parameter space (see section 4.2.1).

5) For each point obtained in step 4, check whether the inequality set defined by equation (4.106) is satisfied, or not.
6) Let NPT denote the number of points that satisfy inequality set (4.95) in step 5. If NPT is considered to be insufficient, replace $\Delta\theta_a$, $\Delta\theta_c$ with halves of their previous values; and repeat steps 4 and 5 until NPT is sufficiently large.
7) Besides the inequality set (4.106), the periodicity requirement (see equation (4.107)) should also be satisfied by the candidate "corner" points. Hence, the compressor simulation is run at this stage.
8) For each point obtained at the end of step 6, check whether the periodicity requirement given by (4.107) is satisfied, or not.
9) It is expected that NPT decreases after the periodicity check. Let the new number of points that satisfy inequality set (4.106) and the periodicity requirement be denoted as NPT*. If NPT* is not sufficiently large, then decrease $\Delta\theta_a, \Delta\theta_c$ to halve of their previous values; and repeat steps 4 to 8 until NPT* is sufficiently large.
10) For each point which satisfy inequality set (4.106) and the periodicity requirement, one should record the following items.
    i. The piston motion, $x_p(\theta)$.
    ii. In order to obtain a continuous motion profile, the Fourier-8 type curve fitting defined by equation (4.59) or cubic spline patching applied. The coefficients associated with this fit are recorded.
    iii. The actuator torque due to the pressure force, $\tau_{pres}(t)$.
    iv. The net work done per mass, which is objective function obj_1 (which does not depend on the inertia forces).
    v. Obtained capacity.
11) Using the m_3 value corresponding to the grid point, determine τ_{iner} via equation (4.74). Note that $\dot{s}_3$ and $\ddot{s}_3$ in equation (4.74) correspond to $\dot{x}_p$ and $\ddot{x}_p$, respectively. Furthermore, according to the notation that is employed, $\dot{s}_3 = -\dot{x}_p$ and $\ddot{s}_3 = -\ddot{x}_p$.

12) For each point which satisfy inequality set (4.106) and the periodicity requirement and for each m_3 in the grid, determine and save obj_2 and obj_3. In other words, determine and save obj_2 and obj_3 for each "corner" point in the allowable $[\theta_a, \theta_c, D_{vi}, D_{cyl}, \omega, m_3]$ space.
13) At this stage, the values of the 3 objective functions obj_1, obj_2 and obj_3 have been determined for each "corner" point (which satisfy inequality set (4.106) and the periodicity requirement) in the allowable $[\theta_a, \theta_c, D_{vi}, D_{cyl}, \omega, m_3]$ space. Therefore, the minimum of each objective function (and the corresponding optimal corner point in the $[\theta_a, \theta_c, D_{vi}, D_{cyl}, \omega, m_3]$ space) can simply be found by sorting the values of the 3 objective functions.

After running the brute force optimization algorithm described above, one obtains the minimum values of the 3 objective functions obj_1, obj_2 and obj_3 and the corresponding optimal corner points in the $[\theta_a, \theta_c, D_{vi}, D_{cyl}, \omega, m_3]$ space. These optimal corner points are then used as the initial guesses for a constrained nonlinear multivariable optimization problem. The MATLAB function "fmincon" is used to solve the aforementioned constrained nonlinear multivariable optimization problem. $Periodicity$ is defined as a nonlinear constraint in the fmincon function. In addition to this nonlinear constraint, the lower and upper bounds of the design parameters are also inputted.

In order to find the global minimum of objectives, a "GlobalSearch" object is defined in MATLAB. Using this object and the "fmincon" function (as a local solver), the minimum of objective can be found. In the GlobalSearch options, maximum iteration, maximum time etc. can be defined. In this global search method, based on defined options, local solver (fmincon) is run repeatedly.

4.2.4 Numerical Case Study

Using the algorithm introduced in the previous section, a numerical case study will be realized in this section. All parameters, other than the design parameters, are taken to be the same with the parameters of the conventional reciprocating compressor discussed in chapter 2. The steps of the procedure that has been followed for the numerical case study are presented below.

1) The design requirements are specified as below.

$$\mathrm{P_i} = 1 \text{ bar}$$

$$\mathrm{P_o} = 6 \text{ bar}$$

$$\text{cap} = 43.8 \text{ m}^3/\text{hr}$$

2) The lower and upper bounds for the design parameters are specified as below.

$$(\theta_a)_{min} = 0°$$
$$(\theta_a)_{max} = 360°$$
$$(\theta_c)_{min} = 0°$$
$$(\theta_c)_{max} = 360°$$
$$\left(D_{cyl}\right)_{min} = 60mm$$
$$\left(D_{cyl}\right)_{max} = 180mm$$
$$(D_{vi})_{min} = (D_{vo})_{min} = 10mm$$
$$(D_{vi})_{max} = \mu\left(D_{cyl}\right)_{max} - (D_{vo})_{min} = 125mm$$
$$(\omega)_{min} = 100rpm$$
$$(\omega)_{max} = 800rpm$$
$$(m_3)_{min} = 0.1kg$$
$$(m_3)_{max} = 5kg$$

Note that, μ is taken to be 0.75 as in the conventional slider crank based compressor.

3) The " width " of the grids (used to discretize the design parameters) are specified as given below.

$$\Delta\theta_a = \Delta\theta_c = 10°$$

$$\Delta D_{vi} = \Delta D_{cyl} = 20mm$$

$$\Delta\omega = 100rpm$$

$$\Delta m_3 = 0.1kg$$

4) The gridded design parameters space is formed.
5) Each "corner" point of the gridded design parameter space is checked to see whether it satisfies the inequality set defined in section 4.2.1, or not.

As stated previously, firstly, the inequalities involving only D_{vi} and D_{cyl} are checked. The feasible points that have been obtained are shown in Figure 4.8.

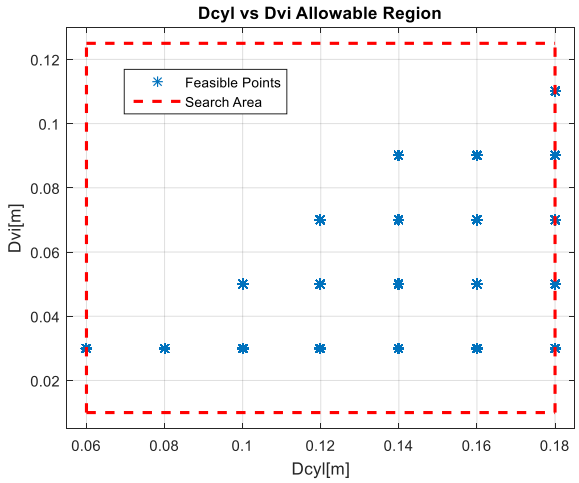

Figure 4.8. Check for the Inequalities involving only D_{vi} and D_{cyl}

For each feasible point in the D_{vi} - D_{cyl} plane, the remaining inequalities are also checked. For example, for a feasible point in the D_{vi} - D_{cyl} plane, the corresponding feasible points in the θ_a - θ_c plane are shown in Figure 4.9.

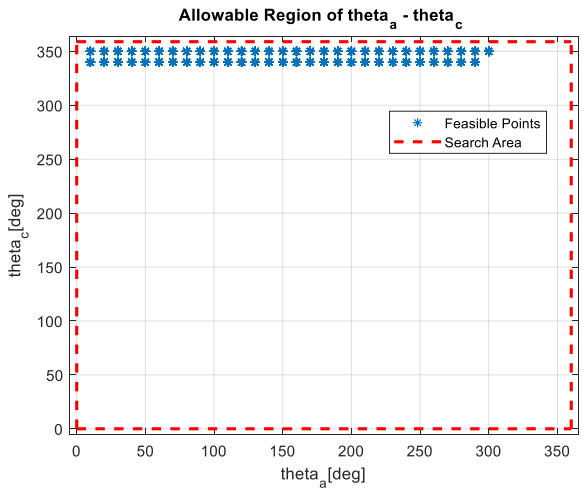

Figure 4.9. Feasible Points in the θ_a - θ_c Plane

As seen in Figure 4.9, the number of feasible points in the θ_a - θ_c plane is very small. Hence, the lower and upper bounds specified for θ_a and θ_c, in step 1 are modified and steps 2-5 are repeated once more. Hence, one obtains the four steps which are labelled as steps 2^*, 3^*, 4^* and 5^* below.

2*) The lower and upper bounds for θ_a and θ_c are modified as below.

$$(\theta_a)_{min} = 1°$$

$$(\theta_a)_{max} = 311°$$

$$(\theta_c)_{min} = 335°$$

$$(\theta_c)_{max} = 359°$$

3*) The "width" of the grids for θ_a and θ_c are modified as shown below.

$$\Delta\theta_a = 10$$

$$\Delta\theta_c = 1°$$

4*) The gridded design parameter space is formed.

5*) Each "corner" point of the gridded design parameter space is checked to see whether it satisfies the inequality set defined in section 4.2.1, or not.

The feasible points that have been obtained are shown in Figure 4.10.

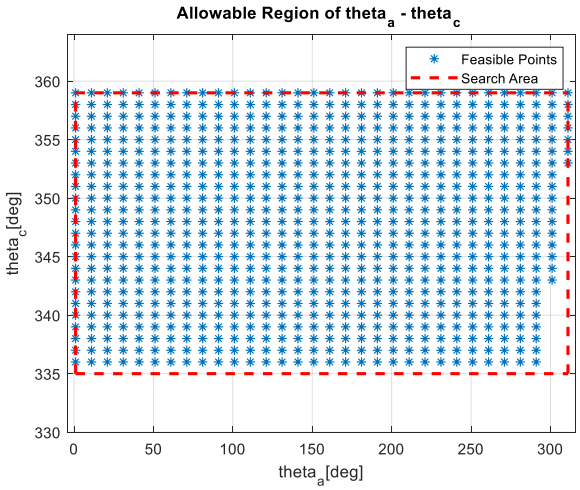

Figure 4.10. The Feasible θ_a and θ_c Points

6) Let NPT denote the number of points that satisfy inequality set (4.106) in step 5. If NPT is considered to be insufficient, replace $\Delta\theta_a$, $\Delta\theta_c$ with halve of their previous values; and repeat steps 4 and 5 until NPT is sufficiently large.

The total number of points in search area is 268800 for $\theta_a, \theta_c, D_{vi}, D_{cyl}, \omega$. After the inequality set check, NPT is found 117984. Hence, it can be said that NPT is sufficient.

7) Besides the inequality set (4.106), the periodicity requirement (see equation (4.107)) should also be satisfied by the candidate "corner" points. Hence, the compressor simulation is run at this stage.
8) For each point obtained at the end of step 6, check whether the periodicity requirement given by (4.107) is satisfied, or not.
9) It is expected that NPT decreases after the periodicity check. Let the new number of points that satisfy inequality set (4.106) and the periodicity requirement be denoted as NPT*. If NPT* is not sufficiently large, then decrease $\Delta\theta_a, \Delta\theta_c$ to halve of their previous values; and repeat steps 4 to 8 until NPT* is sufficiently large

After periodicity check, NPT* is found 4065.

10) For each point which satisfy inequality set (4.106) and the periodicity requirement, one should record the following items.
    i. The piston motion, $x_p(\theta)$.

ii. In order to obtain a continuous motion profile, the Fourier-8 type curve fitting defined by equation (4.59) or cubic spline patching is applied. The coefficients associated with this fit are recorded.

For example, a Fourier-8 type fit on the data is shown in Figure 4.11.

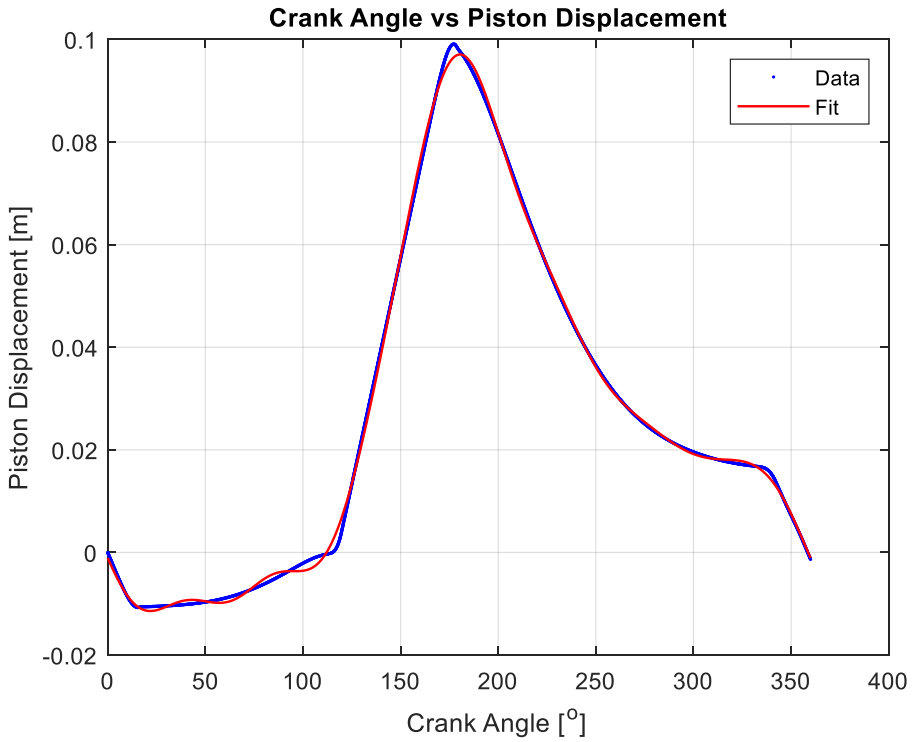

Figure 4.11. Fourier Curve Fit on the Data

iii. The actuator torque due to the pressure force, $\tau_{pres}(t)$.

iv. The net work done per mass, which is objective function obj_1 (which does not depend on the inertia forces).

v. Obtained capacity.

11) Using the m_3 value corresponding to the grid point, determine τ_{iner} via equation (4.74). Note that $\dot{s}_3$ and $\ddot{s}_3$ in equation (4.74) correspond to $\dot{x}_p$ and $\ddot{x}_p$, respectively. Furthermore, according to the notation that is employed, $\dot{s}_3 = -\dot{x}_p$ and $\ddot{s}_3 = -\ddot{x}_p$

12) For each point which satisfy inequality set (4.106) and the periodicity requirement and for each m_3 in the grid, determine and save obj_2 and obj_3. In other words, determine and save obj_2 and obj_3 for each "corner" point in the allowable $[\theta_a, \theta_c, D_{vi}, D_{cyl}, \omega, m_3]$ space

13) At this stage, the values of the 3 objective functions obj_1, obj_2 and obj_3 have been determined for each "corner" point (which satisfy inequality set (4.106) and the periodicity requirement) in the allowable $[\theta_a, \theta_c, D_{vi}, D_{cyl}, \omega, m_3]$ space. Therefore, the minimum of each objective function (and the corresponding optimal corner point in the $[\theta_a, \theta_c, D_{vi}, D_{cyl}, \omega, m_3]$ space) can simply be found by sorting the values of the 3 objective functions

Hence the minima of the objective functions are tabulated in Table 4.3. Optimal DV values (which minimizing the objective) are also given in Table 4.3. DV denotes design variables.

Table 4.3 Optimization Results Obtained by the Brute Force Search Method

			Objective Function		
		Unit	**Minimum of obj_1**	**Minimum of obj_2**	**Minimum of obj_3**
Value		[kJ/kg]	205.01	303.99	393.96
cap		[m^3/hr]	58.04	71.18	73.80
Optimal DV Values	θ_a	[°]	121	101	61
	θ_c	[°]	355	342	344
	D_{vi}	[mm]	90	50	50
	D_{cyl}	[mm]	180	180	160
	ω	[rpm]	200	100	100
	m_3	[kg]	~	5	5

As seen in Table 4.3, the optimum results are achieved at the upper limit of D_{cyl} and at the lower limit of ω. Therefore, in order to see the effects of larger D_{cyl} and smaller ω values, a new design parameter space is formed according to the data given below. Since a theoretical limit is searched, D_{cyl} is taken up to 1 m (it is not practical).

$$\left(D_{cyl}\right)_{min} = 200mm, \qquad \left(D_{cyl}\right)_{max} = 1000mm, \qquad \Delta D_{cyl} = 100mm$$

$$\left(D_{vi}\right)_{min} = 100mm, \qquad \left(D_{vi}\right)_{max} = 700mm, \qquad \Delta D_{vi} = 100mm$$

$$\left(\omega\right)_{min} = 100rpm, \qquad \left(\omega\right)_{max} = 800rpm, \qquad \Delta\omega = 100rpm$$

Note that, besides the regular grid generated for ω as described by the data above, ω = 5 rpm, ω = 10 rpm and ω = 50 rpm grid lines are also considered in the grid generated for ω.

Furthermore, optimal m_3 values are also achieved at the upper limit. However, the effect of m_3 on the objective functions is not significant at low speeds. Therefore, the upper limit of m_3 has not been increased. The minima of the objective functions that are obtained for the aforementioned, modified lower and upper bounds are shown in Table 4.4.

Table 4.4 Optimization Results Obtained by the Brute Force Search Method (with Modified Lower and Upper Bounds for D_{cyl} and ω)

			Objective Function		
		Unit	**Minimum of obj_1**	**Minimum of obj_2**	**Minimum of obj_3**
Value		[kJ/kg]	198.92	297.42	388.26
cap		[m^3/hr]	44.51	64.92	66.51
Optimal DV Values	θ_a	[°]	141	31	31
	θ_c	[°]	344	355	356
	D_{vi}	[mm]	500	100	90
	D_{cyl}	[mm]	1000	200	180
	ω	[rpm]	10	50	50
	m_3	[kg]	~	0.1	0.1

Table 4.4 indicates that there are still some minima which lie on the boundaries of the search region. Hence, in order to investigate this situation further, D_{cyl} is kept constant (at 200 mm and 1000 mm); and the variation of the objective function W_{net}^{pm} (with respect to , θ_a and θ_c) is investigated. Variation of W_{net}^{pm} (for $D_{cyl} = 200mm$) is presented in Figure 4.12.

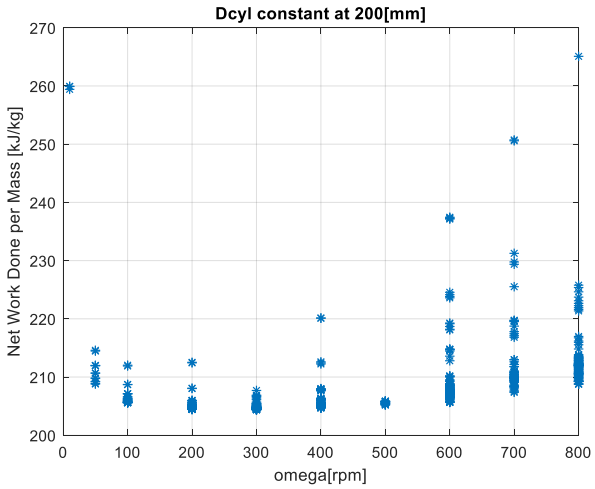

Figure 4.12. Variation of W_{net}^{pm} with respect to , θ_a and θ_c for D_{cyl} = 200 mm

In Figure 4.12, different W_{net}^{pm} values for the same ω correspond to different (θ_a , θ_c) pairs. Since each (θ_a, θ_c) pair corresponds to a different $x_p(\theta)$ motion profile, it follows that the different W_{net}^{pm} values in Figure 4.12 correspond to different $x_p(\theta)$ motion profiles. Hence, Figure 4.12 depicts the variation of W_{net}^{pm}, with respect to the design function $x_p(\theta)$, for various ω values.

Now, let $\left(W_{net}^{pm}\right)_{min}[\omega]$ and $\left(W_{net}^{pm}\right)_{max}[\omega]$ denote the minimum and maximum value of W_{net}^{pm} corresponding to a given ω value in Figure 4.12. Furthermore, let $sav[\omega]$ defined by the equation

$$sav[\omega] = \frac{\left(W_{net}^{pm}\right)_{max}[\omega] - \left(W_{net}^{pm}\right)_{min}[\omega]}{\left(W_{net}^{pm}\right)_{max}[\omega]} \times 100 \tag{4.113}$$

designates the percent savings in W_{net}^{pm} (due to the changes in motion profile) corresponding to a given ω value. Hence, using the data shown in Figure 4.12, one obtains sav[50] = 2.70 , sav[100] = 3.05 , sav[200] = 3.81 , sav[300] = 1.59 sav[400] =7.00 , sav[500] = 0.33 sav[600] = 13.40, sav[700] = 17.29, sav[800] = 21.25. The maximum saving occurs at ω = 800 rpm, yielding sav[800] = 21.25. Clearly, it can be said that the changes in motion profile have a huge effect for savings of energy.

In Figure 4.12, the minimum of W_{net}^{pm} occurs at 200 rpm. However, if a larger diameter is selected, the minimum of W_{net}^{pm} occurs at a smaller speed. For instance, for $D_{cyl} = 1000mm$, the variation of W_{net}^{pm} is shown in Figure 4.12.

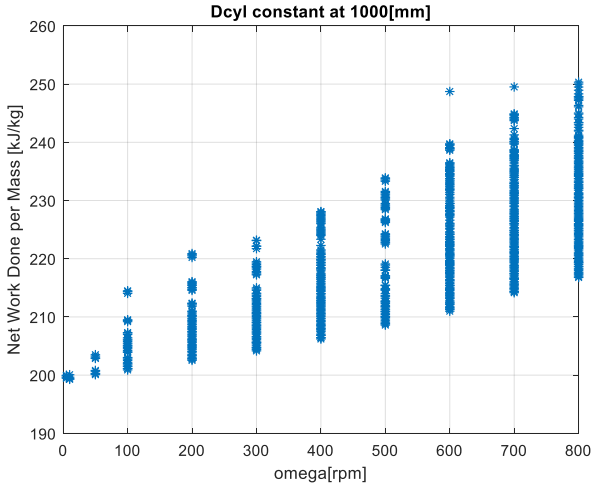

Figure 4.13. Variation of W_{net}^{pm} with respect to , θ_a and θ_c for D_{cyl} = 1000 mm

In Figure 4.13, the minimum of W_{net}^{pm} occurs at 10 rpm. Hence, it appears that when the upper limit of the cylinder diameter is increased, the minimum of W_{net}^{pm} is obtained at a slower speed. Similar trends have also been observed when the positive work done and the absolute work done are considered to be the objective function.

Although a cylinder diameter as large as 1000 mm; and an angular speed as low as 5 rpm have been considered in some of the case studies; it is clear that cylinder diameters which are too large and angular speeds which are too small are not practical. Hence, considering such practical limitations, the following data have been utilized throughout the rest of the case studies in this study.

$$\left(D_{cyl}\right)_{min} = 60mm, \qquad \left(D_{cyl}\right)_{max} = 180mm, \qquad \Delta D_{cyl} = 20mm$$

$$\left(D_{vi}\right)_{min} = 10mm, \qquad \left(D_{vi}\right)_{max} = 125mm, \qquad \Delta D_{vi} = 20mm$$

$$\left(\omega\right)_{min} = 100rpm, \qquad \left(\omega\right)_{max} = 800rpm, \qquad \Delta\omega = 100rpm$$

As mentioned before (see the optimization algorithm section), the optima that have been obtained via the brute force search are refined by using an optimization algorithm. For this algorithm, the optimal design variables shown in Table 4.3 are

used as initial guesses. It has already been observed that in order to minimize the objective function, D_{cyl} and ω tend to increase and decrease, respectively. Hence, in order to reduce the execution time necessary for the optimization, the 3 design variables D_{cyl}, D_{vi} and ω are taken to be constant. Thus, only θ_a and θ_c are used as the design parameters in the optimization algorithm.

In order to illustrate the procedure that is followed, consider the following example where the minimum value of obj_1 (obtained via the brute force search method) is to be minimized, further, by using an optimization algorithm. Firstly, the lower and upper bounds of $[\theta_a, \theta_c]$ are selected as shown below.

$$Lower\ Bound = [111°, 354°]$$

$$Upper\ Bound = [131°, 356°]$$

The initial guesses for the θ_a and θ_c are taken to be $121°$ and $355°$, respectively, from Table 4.3. Hence, by using the "fmincon" function readily available in MATLAB, the minimum of W_{net}^{pm} and the corresponding values of the optimal design parameters are obtained as shown in Table 4.5.

Table 4.5 Results of Optimization Based Upon the Initial Guess Provided by the Brute Force Method

			Objective Function
		Unit	**Minimum of obj_1**
W_{net}^{pm}		[kJ/kg]	204.99
cap		[m^3/hr]	56.96
Optimal *DV* Values	θ_a	[°]	130.10
	θ_c	[°]	354.37
	D_{vi}	[mm]	90
	D_{cyl}	[mm]	180
	ω	[rpm]	200
	m_3	[kg]	~

At the end of the simulation, the piston motion (in terms of the crank angle) is obtained discretely, i.e., in the form of a set of points in the x_p-θ plane. In order to convert the piston motion into a continuous function, a curve fit is utilized. The effect of this curve fit on the accuracy of the results can be observed in Table 4.6, where the results due to the original discrete solution with cubic spline patching and the Fourier curve fitted solution are given. As can be observed from Table 4.6, there is no significant difference between the results of the discrete and curve fitted piston motions. Although, effect of curve fit on performance is not significant, the chamber pressure is very sensitive of the motion profile. This situation is shown in Figure 4.14. However, in some cases, the Fourier-8 type curve fit can be insufficient.

Table 4.6 The Results Due to the Discrete Motion and Fourier Curve Fitted Piston Motion

		Unit	**Discrete Motion with Cubic Spline Patching**	**Fourier-8 Type Curve Fitted Motion**
$\boldsymbol{W_{net}^{pm}}$		[kJ/kg]	205.47	204.99
cap		[m^3/hr]	57.68	56.96
Optimal DV Values	θ_a	[°]	130.10	130.10
	θ_c	[°]	354.37	354.37
	D_{vi}	[mm]	90	90
	D_{cyl}	[mm]	180	180
	ω	[rpm]	200	200
	m_3	[kg]	~	~

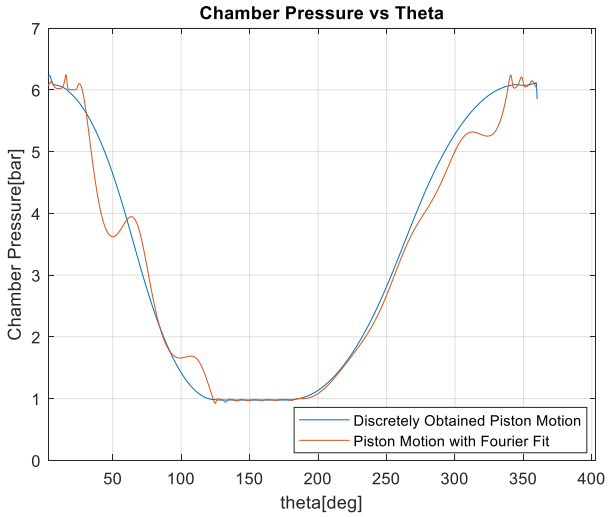

Figure 4.14. The Chamber Pressure for Fourier Fitted Motion and Discrete Motion

From Table 4.5, it is observed that the capacity that is obtained is more than the desired capacity. This is due to the assumptions that have been made while formulating the equality and the inequality constraints that are used to solve the piston motion (using the pressure as the input). In order to obtain the desired capacity, the motor's speed can be adjusted after the optimization. In other words, the speed of the motor can be decreased in order to obtain the desired capacity (while all other parameters and the piston motion are fixed). Since there is an approximate linear relationship between capacity and motor speed, the motor speed may be decreased by a factor of $\frac{cap_{desired}}{cap_{obtained}} = \frac{43.8}{56.96}$. Hence, the new motor speed becomes *153.8 rpm*. The results due to this reduced speed are tabulated in Table 4.7.

Therefore, an optimum reciprocating compressor is obtained. $x_p(\theta)$, PV diagram and the motor torque of the optimum reciprocating compressor thus obtained are shown in Figure 4.15, Figure 4.16 and Figure 4.17. In the same figures, slider crank based reciprocating compressors with original design variables and with optimal design variables (D_{vi}, D_{cyl} and ω are changed according to Table 4.7) are also given for comparison purposes.

Table 4.7 Results Obtained by Reducing the Motor Speed in Table 4.5

			Objective Function
		Unit	**Minimum obj_1**
W_{net}^{pm}		[kJ/kg]	204.41
cap		[m^3/hr]	43.91
Optimal *DV* Values	θ_a	[°]	130.10
	θ_c	[°]	354.37
	D_{vi}	[mm]	90
	D_{cyl}	[mm]	180
	ω	[rpm]	153.80
	m_3	[kg]	~

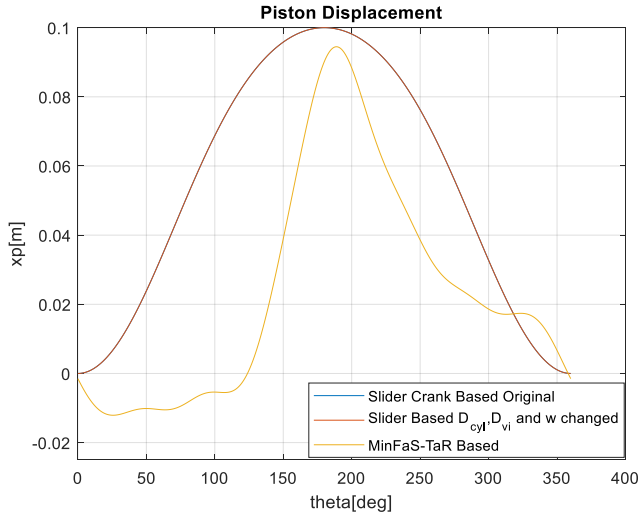

Figure 4.15. The Piston Displacements of the Optimum MinFaS-TaR based Compressor and the Slider Crank Based Compressors

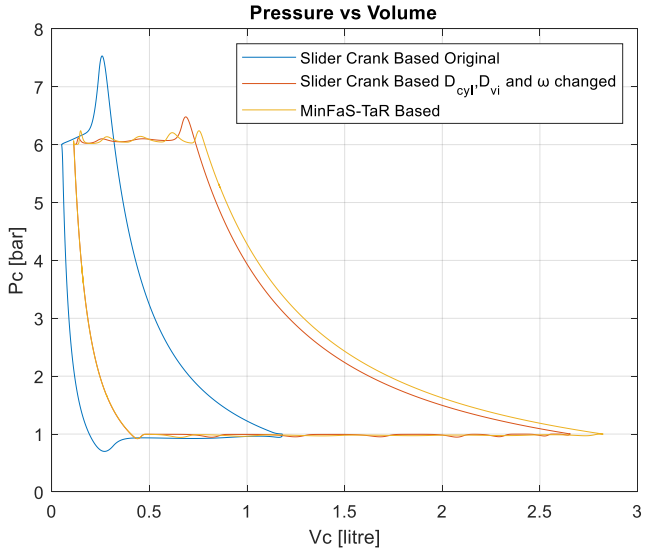

Figure 4.16. The PV Diagrams of the Optimum MinFaS-TaR based Compressor and the Slider Crank Based Compressors

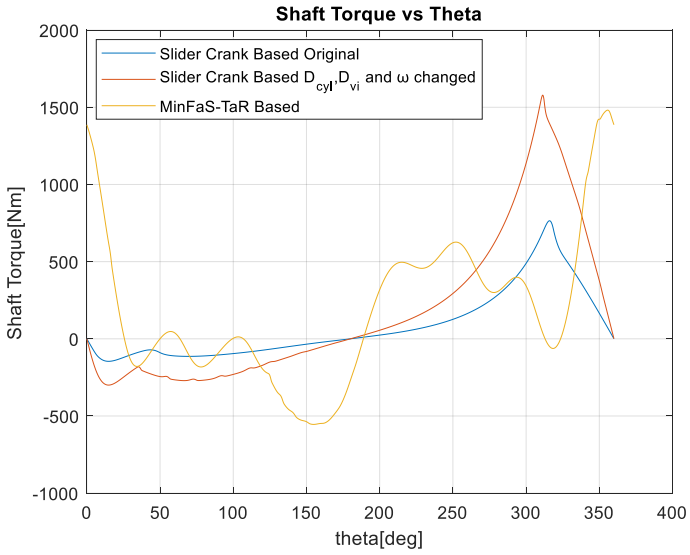

Figure 4.17. The Motor Torques of the Optimum MinFaS-TaR based Compressor and the Slider Crank Based Compressors

In order to visululize the piston motion, some snapshots from the simulation are presented in Figure 4.18.

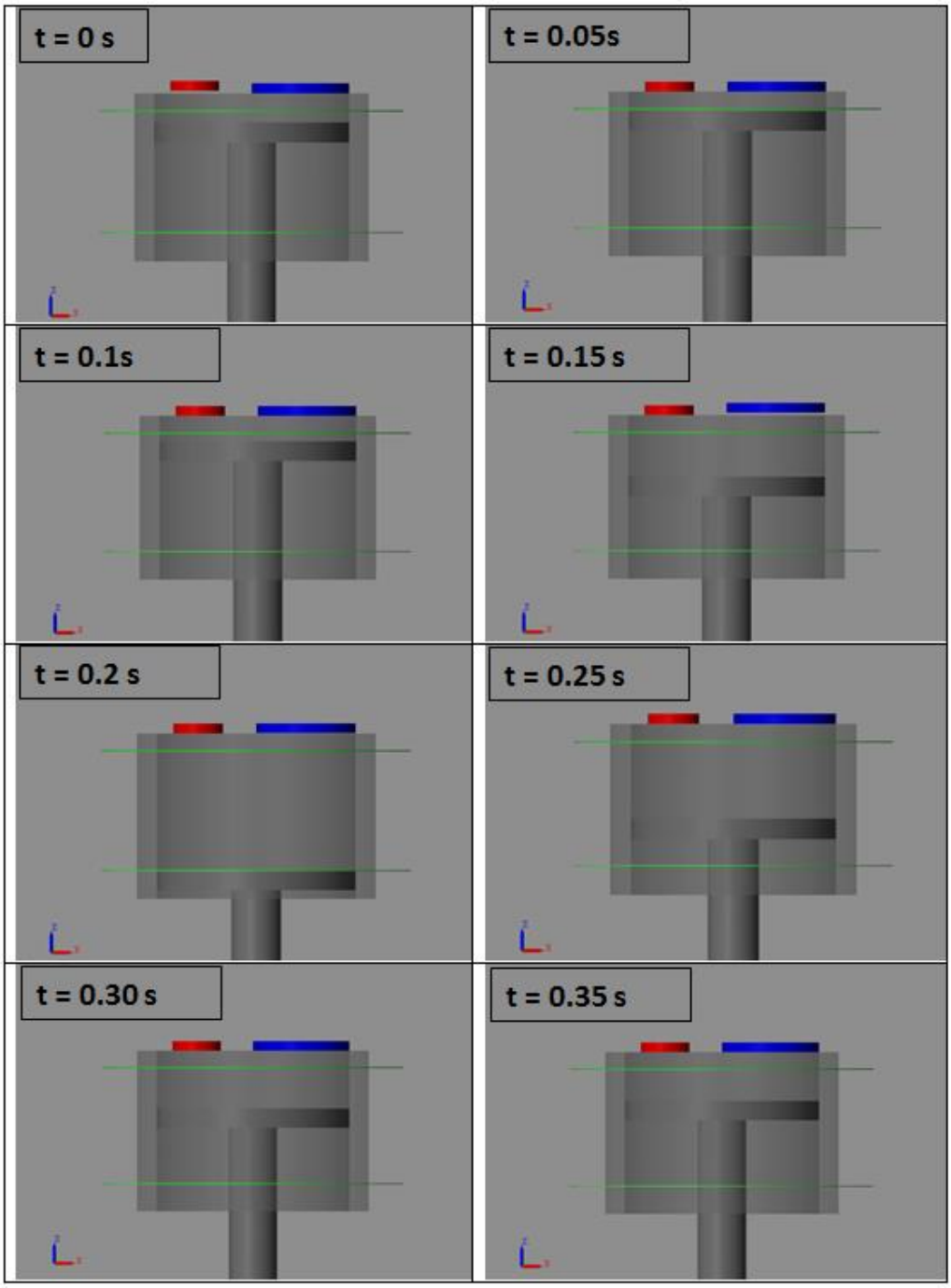

Figure 4.18. Snapshots of the Visual Simulation of the MinFaS-TaR based Compressor Cylinder

In Figure 4.18, the outlet and the inlet valves are red and blue, respectively. Green lines, on the other hand, represent BDC and TDC.

4.3 Optimization of Single-Stage Reciprocating Compressors with Different Capacities and Multi-Stage Reciprocating Compressors

Minimization of the energy consumption of reciprocating compressors has been discussed in the previous sections. A numerical case study for a one cylinder, single stage reciprocating compressor has also been presented in detail. In this section, the effects of required capacity, on the energy consumption of single stage reciprocating compressors, will be investigated. Furthermore, energy consumption of multi-stage compressors will also be considered. To this purpose, 7 different case studies will be considered. The definitions of these 7 case studies are given in Table 4.8. Minimizations of the energy consumption for the 7 cases described in this table are presented in the following sections.

Table 4.8 Case Studies Definitions

Case-1	One cylinder, single stage reciprocating compressor which compresses air from 1 to 6 bar with the reference capacity*.
Case-2	One cylinder, single stage reciprocating compressor which compresses air from 1 to 6 bar with half of the reference capacity*.
Case-3	One cylinder, single stage reciprocating compressor which compresses air from 1 bar to 6 bar with twice the reference capacity*.
Case-4	One cylinder, two-stage reciprocating compressor which compresses air from 1 to 6 bar in the first stage; and from 6 to 36 bar in the second stage (with an intercooler).
Case-5	One cylinder, two-stage reciprocating compressor which compresses air from 1 to 6 bar in the first stage; and from 6 to 36 bar in the second stage (without an intercooler).
Case-6	One cylinder, single stage reciprocating compressor which compresses air from 1 to 36 bar .
Case-7	Multi-cylinder single-stage reciprocating compressor which compresses air from 1 to 6 bar.

*the reference capacity is taken to be the capacity of the slider crank based reciprocating compressor given in chapters 2 and 3, i.e. the reference capacity is taken 43.8 m^3/hr.

4.3.1 One Cylinder, Single-Stage Reciprocating Compressors (Case-1, Case-2, Case-3, Case-6)

In this section, one cylinder, single stage reciprocating compressors with different capacities are optimized. A conventional reciprocating compressor with a specified capacity of 43.8 m^3/hr has already been presented in Section 3. For the new designs, the conventional reciprocating compressor's capacity is taken to be the reference capacity. In cases 1-3, reciprocating compressors are designed for the reference capacity, half of the reference capacity and twice of the reference capacity. In these 3 cases, air is compressed from 1 to 6 bar., In Case-6, on the other hand, air is compressed from 1 to 36 bar in one stage (with capacity being equal to the reference capacity).

Considering Case-1, optimal MinFaS-TaR based compressors, minimizing objective functions obj_1, obj_2 and obj_3, have been obtained. The results are presented in Table 4.9, Table 4.10 and Table 4.11, respectively. Here, one should recall that a MinFaS-TaR based compressor, by nature, has 2 pistons, connected to links 3 and 5 (and thus, 2 cylinders). A slider crank based compressor, on the other hand, has a single piston (and thus a single cylinder). In these tables, the data corresponding to the original slider crank based compressor and the so called modified slider crank based compressor are also presented (for comparison purposes). Here, the modified slider crank based compressor is defined to be a slider crank based compressor that has the same D_{cyl}, D_{vi} and ω values with the corresponding, optimal MinFaS-TaR based compressor. In these tables, it should be noted that ΔE_{fw} and I_{fw} refer to the change in energy in flywheel sizing and flywheel inertia corresponding to both shafts (i.e., links 2 and 4) of the MinFaS-TaR based compressor. In other words, the inertia of the flywheel mounted on one of the shafts is I_{fw} / 2. Furthermore, I_{fw} is found using speed of compressor side of shaft. On the other hand, if inertia of flywheel is found using speed of motor side of shaft, it will be less than other. In order to compare inertia of flywheel, it is assumed that 2000 rpm motor is used and flywheel is assembled right after motor.

This new flywheel inertia is shown with $I_{fw}^{2000rpm}$. The optimum piston motions for MinFaS-TaR based reciprocating compressor for Case-1 (corresponding to the design variables in Table 4.9, Table 4.10 and Table 4.11) are given in Appendix F.

Table 4.9 Optimal MinFaS-TaR Based Compressor for Case-1 (objective function = obj_1)

		Unit	New Design MinFaS-TaR	Slider Crank	
				$^{(1)}\boldsymbol{SC_{org}}$	$^{(2)}\boldsymbol{SC_{mod}}$
$\boldsymbol{obj_1}$ ($\boldsymbol{W_{net}^{pm}}$)		[kJ/kg]	204.41	227.29	206.29
cap		[m^3/hr]	43.91	43.8	20.10
$\boldsymbol{\Delta E_{fw}}$		[J]	1147	269.42	602.79
$\boldsymbol{I_{fw}}$		[kgm^2]	178	1.54	92.96
$\boldsymbol{I_{fw}^{2000rpm}}$		[kgm^2]	1.04	0.25	0.54
$\boldsymbol{\eta_{pres}}$		%	68.29	60.10	67.25
Optimal *DV* Values	θ_a	[°]	130.10	~	~
	θ_c	[°]	354.37	~	~
	D_{vi}	[mm]	90	50	90
	D_{cyl}	[mm]	180	120	180
	ω	[rpm]	153	800	153
	m_3	[kg]	5	~	~

$^{(1)}\boldsymbol{SC_{org}}$ is the original slider crank based reciprocating compressor.
$^{(2)}\boldsymbol{SC_{mod}}$ is the modified slider crank based reciprocating compressor according to optimal design variables.

Table 4.10 Optimal MinFaS-TaR Based Compressor for Case-1 (objective function = obj_2)

		Unit	MinFaS-TaR Based	Slider Crank Based	
				$^{(1)}SC_{org}$	$^{(2)}SC_{mod}$
obj_2 (W_{pos}^{pm})		[kJ/kg]	302.66	342.03	317.44
cap		[m^3/hr]	44.2	43.8	8.05
ΔE_{fw}		[J]	2604	269.42	600
I_{fw}		[kgm^2]	2506	1.54	577
$I_{fw}^{2000rpm}$		[kgm^2]	2.41	0.25	0.55
η_{pres}		%	67.6	60.10	67.7
Optimal DV Values	θ_a	[°]	104.20	~	~
	θ_c	[°]	342.85	~	~
	D_{vi}	[mm]	50	50	50
	D_{cyl}	[mm]	180	120	180
	ω	[rpm]	62	800	62
	m_3	[kg]	5	~	~

$^{(1)}SC_{org}$ is the original slider crank based reciprocating compressor.
$^{(2)}SC_{mod}$ is the modified slider crank based reciprocating compressor according to optimal design variables.

Table 4.11 Optimal MinFaS-TaR Based Compressor for Case-1 (objective function = obj_3)

		Unit	MinFaS-TaR Based	Slider Crank Based	
				$^{(1)}SC_{org}$	$^{(2)}SC_{mod}$
obj_3 (W_{abs}^{pm})		[kJ/kg]	392.69	456.77	426.18
cap		[m^3/hr]	44.20	43.8	6.16
ΔE_{fw}		[J]	2382	269.42	473.9
I_{fw}		[kgm^2]	2467	1.54	490.76
$I_{fw}^{2000rpm}$		[kgm^2]	2.17	0.25	0.43
η_{pres}		%	67.1	60.10	67.71
Optimal DV Values	θ_a	[°]	58.54	~	~
	θ_c	[°]	343.15	~	~
	D_{vi}	[mm]	50	50	50
	D_{cyl}	[mm]	160	120	160
	ω	[rpm]	59.3	800	59.3
	m_3	[kg]	5	~	~

$^{(1)}SC_{org}$ is the original slider crank based reciprocating compressor.
$^{(2)}SC_{mod}$ is the modified slider crank based reciprocating compressor according to optimal design variables.

Considering Case-2, optimal MinFaS-TaR based compressors, minimizing objective functions obj_1, obj_2 and obj_3, have been obtained. The results are presented in Table 4.12. Since there is no corresponding slider crank based compressor data, only the MinFaS-TaR based compressor results are shown. It should be noted that, in the optimization of Case-2, Fourier fit did not work properly. It has been observed that the capacity obtained from Fourier fitted motion is far away from the capacity obtained from discrete motion. Hence, the results given in Table 4.12 correspond to discrete motion with cubic spline patching results. The optimum piston motions for MinFaS-TaR based reciprocating compressor for Case-2 (corresponding to the design variables in Table 4.12) are given in Appendix F.

Table 4.12 Optimal MinFaS-TaR Based Compressor for Case-2

Objective			**Minimum of obj_1**	**Minimum of obj_2**	**Minimum of obj_3**
Value of Objective		[kJ/kg]	204.54	302.84	396.49
cap		[m^3/hr]	20.43	22.09	21.90
ΔE_{fw}		[J]	858.04	1720	1727
I_{fw}		[kgm^2]	339.2	3338	3352
$I_{fw}^{2000rpm}$		[kgm^2]	0.78	1.56	1.56
η_{pres}		%	70.9	70.4	70.5
Optimal *DV* Values	θ_a	[°]	110.99	91.57	96.81
	θ_c	[°]	358.31	356.65	356.46
	D_{vi}	[mm]	70	50	50
	D_{cyl}	[mm]	180	160	160
	ω	[rpm]	96	43.3	43.3
	m_3	[kg]	0.1	5	5

Considering Case-3, optimal MinFaS-TaR based compressors, minimizing objective functions obj_1, obj_2 and obj_3, have been obtained. The results are presented in Table 4.13. Since there is no corresponding slider crank based compressor data, only the MinFaS-TaR based compressor results are shown. The optimum piston motions for MinFaS-TaR based reciprocating compressor for Case-3 (corresponding to the design variables in Table 4.13) are given in Appendix F.

Table 4.13 Optimal MinFaS-TaR Based Compressor for Case-3

Objective			**Minimum of obj_1**	**Minimum of obj_2**	**Minimum of obj_3**
Value of Objective		[kJ/kg]	205.18	298.19	393.95
cap		[m^3/hr]	87.84	87.66	86.86
ΔE_{fw}		[J]	703.97	3901	3895
I_{fw}		[kgm^2]	36.08	2060	2127
$I_{fw}^{2000rpm}$		[kgm^2]	0.64	3.56	3.55
η_{pres}		%	67.9	68.6	67.5
Optimal *DV* Values	θ_a	[°]	124.49	88.34	75.35
	θ_c	[°]	329.81	331	330.08
	D_{vi}	[mm]	90	90	90
	D_{cyl}	[mm]	180	180	180
	ω	[rpm]	266.7	83.11	81.73
	m_3	[kg]	5	5	5

Considering Case-6, optimal MinFaS-TaR based compressors, minimizing objective functions obj_1, obj_2 and obj_3, have been obtained. The results are presented in Table 4.14. Since there is no corresponding slider crank based compressor data, only the MinFaS-TaR based compressor results are shown. It should be noted that, in the optimization of Case-6, Fourier fit did not work properly. It has been observed that the capacity obtained from Fourier fitted motion is far away from the capacity obtained from discrete motion. Hence, the results given in Table 4.14 correspond to discrete motion with cubic spline patching results. The optimum piston motions for MinFaS-TaR based reciprocating compressor for Case-6 (corresponding to the design variables in Table 4.14) are given in Appendix F.

Table 4.14 Optimal MinFaS-TaR Based Compressor for Case-6

Objective			**Minimum of obj_1**	**Minimum of obj_2**	**Minimum of obj_3**
Value of Objective		[kJ/kg]	572.01	1044	1468
cap		[m^3/hr]	43.86	43.34	44.8
ΔE_{fw}		[J]	3167	3075	7731
I_{fw}		[kgm^2]	202	231	9110
$I_{fw}^{2000rpm}$		[kgm^2]	2.88	2.80	6.89
η_{pres}		%	44.7	45.1	38.7
Optimal DV Values	θ_a	[°]	207.35	170.18	1.02
	θ_c	[°]	355.47	355.49	354
	D_{vi}	[mm]	90	90	90
	D_{cyl}	[mm]	180	180	180
	ω	[rpm]	239	220	55
	m_3	[kg]	0.2	1.5	0.1

4.3.2 Multi-Stage Reciprocating Compressors (Case-4, Case-5)

Multi-Stage compressors are used when a high compression ratio (i.e., P_o / P_i) is required. In multi-stage compressors, intercoolers are employed frequently. The intercoolers that are used between different stages decrease the temperature of air that is sent to the next stage. In this study, a two-stage reciprocating compressor is considered in Case-4 and Case-5. In Case-4, an intercooler is employed; whereas, in Case-5 there is no intercooler.

In multi-stage compressors, in order to minimize the consumed energy, the compression ratio corresponding to each stage is taken to be the same (see [20]). In other words, if the total pressure ratio is r_t, and there are n stages, the pressure ratio for each stage is taken to be $r_t^{1/n}$. For instance, for a two-stage compressor that has an inlet pressure of 1 bar and an outlet pressure of 36 bar, one obtains $r_t = \frac{36}{1}$. Hence, the pressure ratios for the first and second stages should be $r_1 = r_2 = 36^{1/2} = 6$.

In multi-stage compressors, intercoolers are used in order to decrease the temperature such that the inlet temperature of each stage is equal to the inlet temperature of the first stage. Thus, the consumed energy is minimized.

In this study, a two-stage compressor is considered such that the pressure is increased from 1 to 6 bar in the first stage; and from 6 to 36 bar in the second stage. The results of optimization for the first stage compressor have already been given in section (4.3.1). Now, the second stage compressor will be optimized. Two cases are considered for the second stage. Firstly, it is assumed that there is an intercooler (Case-4). Secondly, it is assumed that there is no intercooler (Case-5).

The slider crank based compressor is originally designed to increase the pressure from 1 bar to 6 bar. Here, however, it will also be used to increase the pressure from 6 bar to 36 bar (since the pressure ratio does not change).

Considering Case-4, optimal MinFaS-TaR based compressors, minimizing objective functions obj_1, obj_2 and obj_3, have been obtained. The results are presented in Table 4.15, Table 4.16 and Table 4.17, respectively. The optimum piston motions for MinFaS-TaR based reciprocating compressor for Case-4 (corresponding to the design variables in Table 4.15, Table 4.16 and Table 4.17) are given in Appendix F.

Table 4.15 Optimal MinFaS-TaR Based Compressor for Second Stage of Two-Stage Compressor for Case-4 (objective function = obj_1)

		Unit	**MinFaS-TaR Based**	**Slider Crank Based**	
				$^{(1)}\boldsymbol{SC_{org}}$	$^{(2)}\boldsymbol{SC_{mod}}$
$\boldsymbol{obj_1}$ **(** $\boldsymbol{W_{net}^{pm}}$ **)**		[kJ/kg]	199.89	216.27	202.31
cap		[m^3/hr]	44.47	44.08	26.59
$\Delta \boldsymbol{E_{fw}}$		[J]	6503	1644	3616
$\boldsymbol{I_{fw}}$		[kgm^2]	593.0	9.37	329.7
$\boldsymbol{I_{fw}^{2000rpm}}$		[kgm^2]	5.93	1.50	3.29
$\boldsymbol{\eta_{pres}}$		%	69.9	63.6	68.8
Optimal *DV* Values	θ_a	[°]	150.67	~	~
	θ_c	[°]	316	~	~
	D_{vi}	[mm]	90	50	90
	D_{cyl}	[mm]	180	120	180
	ω	[rpm]	200	800	200
	m_3	[kg]	0.1	~	~

$^{(1)}\boldsymbol{SC_{org}}$ is the original slider crank based reciprocating compressor.
$^{(2)}\boldsymbol{SC_{mod}}$ is the modified slider crank based reciprocating compressor according to optimal design variables.

Table 4.16 Optimal MinFaS-TaR Based Compressor for Second Stage of Two-Stage Compressor for Case-4 (objective function = obj_2)

		Unit	MinFaS-TaR Based	Slider Crank Based	
				$^{(1)}SC_{org}$	$^{(2)}SC_{mod}$
obj_2 (W_{pos}^{pm})		[kJ/kg]	295.36	341.18	315.32
cap		[m^3/hr]	43.60	44.08	5.13
ΔE_{fw}		[J]	12804	1644	1603
I_{fw}		[kgm^2]	6069	9.37	759
$I_{fw}^{2000rpm}$		[kgm^2]	11.67	1.50	1.46
η_{pres}		%	69.1	63.6	69.0
Optimal DV Values	θ_a	[°]	134.68	~	~
	θ_c	[°]	311.91	~	~
	D_{vi}	[mm]	50	50	50
	D_{cyl}	[mm]	120	120	120
	ω	[rpm]	87.7	800	87.7
	m_3	[kg]	5	~	~

$^{(1)}SC_{org}$ is the original slider crank based reciprocating compressor.
$^{(2)}SC_{mod}$ is the modified slider crank based reciprocating compressor according to optimal design variables.

Table 4.17 Optimal MinFaS-TaR Based Compressor for Second Stage of Two-Stage Compressor for Case-4 (objective function = obj_3)

		Unit	MinFaS-TaR Based	Slider Crank Based	
				$^{(1)}SC_{org}$	$^{(2)}SC_{mod}$
obj_3 (W_{abs}^{pm})		[kJ/kg]	386.89	466.08	427.59
cap		[m^3/hr]	43.59	44.08	5.13
ΔE_{fw}		[J]	12807	1644	1603
I_{fw}		[kgm^2]	6071	9.37	759
$I_{fw}^{2000rpm}$		[kgm^2]	11.67	1.50	1.46
η_{pres}		%	69.1	63.6	69.0
Optimal DV Values	θ_a	[°]	134.71	~	~
	θ_c	[°]	311.83	~	~
	D_{vi}	[mm]	50	50	50
	D_{cyl}	[mm]	120	120	120
	ω	[rpm]	87.7	800	87.7
	m_3	[kg]	5	~	~

$^{(1)}SC_{org}$ is the original slider crank based reciprocating compressor.
$^{(2)}SC_{mod}$ is the modified slider crank based reciprocating compressor according to optimal design variables.

Considering Case-5, optimal MinFaS-TaR based compressors, minimizing objective functions obj_1, obj_2 and obj_3, have been obtained. The results are presented in Table 4.18, Table 4.19 and, Table 4.20, respectively. The optimum piston motions for MinFaS-TaR based reciprocating compressor for Case-5 (corresponding to the design variables in Table 4.18, Table 4.19 and, Table 4.20) are given in Appendix F.

Table 4.18 Optimal MinFaS-TaR Based Compressor for Second Stage of Two-Stage Compressor for Case-5 (objective function = obj_1)

		Unit	**MinFaS-TaR Based**	**Slider Crank Based**	
				$^{(1)}\boldsymbol{SC_{org}}$	$^{(2)}\boldsymbol{SC_{mod}}$
$\boldsymbol{obj_1}$ ($\boldsymbol{W_{net}^{pm}}$)		[kJ/kg]	335.40	353.29	336.46
cap		[m^3/hr]	43.95	43.76	25.75
$\Delta \boldsymbol{E_{fw}}$		[J]	5998	1623	3591
$\boldsymbol{I_{fw}}$		[kgm^2]	594	9.25	356
$\boldsymbol{I_{fw}^{2000rpm}}$		[kgm^2]	5.47	1.50	3.28
$\boldsymbol{\eta_{pres}}$		%	69.8	64.8	68.6
Optimal DV Values	θ_a	[°]	118.52	~	~
	θ_c	[°]	326.01	~	~
	D_{vi}	[mm]	90	50	90
	D_{cyl}	[mm]	180	120	180
	ω	[rpm]	192	800	192
	m_3	[kg]	5	~	~

$^{(1)}\boldsymbol{SC_{org}}$ is the original slider crank based reciprocating compressor.
$^{(2)}\boldsymbol{SC_{mod}}$ is the modified slider crank based reciprocating compressor according to optimal design variables.

Table 4.19 Optimal MinFaS-TaR Based Compressor for Second Stage of Two-Stage Compressor for Case-5 (objective function = obj_2)

		Unit	MinFaS-TaR Based	Slider Crank Based	
				$^{(1)}SC_{org}$	$^{(2)}SC_{mod}$
obj_2 (W_{pos}^{pm})		[kJ/kg]	495.68	565.72	529.71
cap		[m^3/hr]	43.67	43.76	6.95
ΔE_{fw}		[J]	12145	1623	2180
I_{fw}		[kgm^2]	5713	9.25	1025
$I_{fw}^{2000rpm}$		[kgm^2]	11.06	1.50	1.98
η_{pres}		%	69.3	64.8	68.3
Optimal DV Values	θ_a	[°]	131.96	~	~
	θ_c	[°]	328.21	~	~
	D_{vi}	[mm]	70	50	70
	D_{cyl}	[mm]	140	120	140
	ω	[rpm]	88	800	88
	m_3	[kg]	5	~	~

$^{(1)}SC_{org}$ is the original slider crank based reciprocating compressor.
$^{(2)}SC_{mod}$ is the modified slider crank based reciprocating compressor according to optimal design variables.

Table 4.20 Optimal MinFaS-TaR Based Compressor for Second Stage of Two-Stage Compressor for Case-5 (objective function = obj_3)

		Unit	MinFaS-TaR Based	Slider Crank Based	
				$^{(1)}SC_{org}$	$^{(2)}SC_{mod}$
obj_3 (W_{abs}^{pm})		[kJ/kg]	648.73	778.15	713.63
cap		[m^3/hr]	43.34	43.76	4.90
ΔE_{fw}		[J]	12773	1623	1597
I_{fw}		[kgm^2]	6628	9.25	828
$I_{fw}^{2000rpm}$		[kgm^2]	11.69	1.50	1.46
η_{pres}		%	68.8	64.8	68.3
Optimal DV Values	θ_a	[°]	131.62	~	~
	θ_c	[°]	326.14	~	~
	D_{vi}	[mm]	50	50	50
	D_{cyl}	[mm]	120	120	120
	ω	[rpm]	84	800	4
	m_3	[kg]	5	~	~

$^{(1)}SC_{org}$ is the original slider crank based reciprocating compressor.
$^{(2)}SC_{mod}$ is the modified slider crank based reciprocating compressor according to optimal design variables.

Second stage of Case-4 and 5 have been shown above tables. On the other hand, in order to compare total of multi stage compressor, Case-1 results is taken as first stage of Case 4 and 5. Total work done per mass values of Case-4 and 5 are shown in Table 4.21. For comparison Case-6 is also shown in this table.

Table 4.21 Comparison Table for Multi-Stage Compressors

	Unit	Case-4		Case-5		Case-6
		MinFaS-TaR Based	Slider-Crank Based	MinFaS-TaR Based	Slider-Crank Based	MinFaS-TaR Based
obj_1	[kJ/kg]	404.3	443.56	539.81	580.58	572.01
obj_2	[kJ/kg]	598.02	683.95	798.34	908.49	1044
obj_3	[kJ/kg]	779.58	922.85	1041.42	1234.92	1468

4.3.3 Multi-Cylinder Reciprocating Compressors (Case-7)

There are several reasons for using a multi-cylinder compressor instead a of one-cylinder compressor. An n-cylinder, slider crank based reciprocating piston arrangement is shown in Figure 4.19.In the figure, $\varphi_2, \varphi_3, \ldots, \varphi_n$ indicate phase angles (with respect to the crank of the first cylinder). a_k , on the other hand, indicates the spacing of the k'th cylinder (measured from the first cylinder, along the crank shaft).

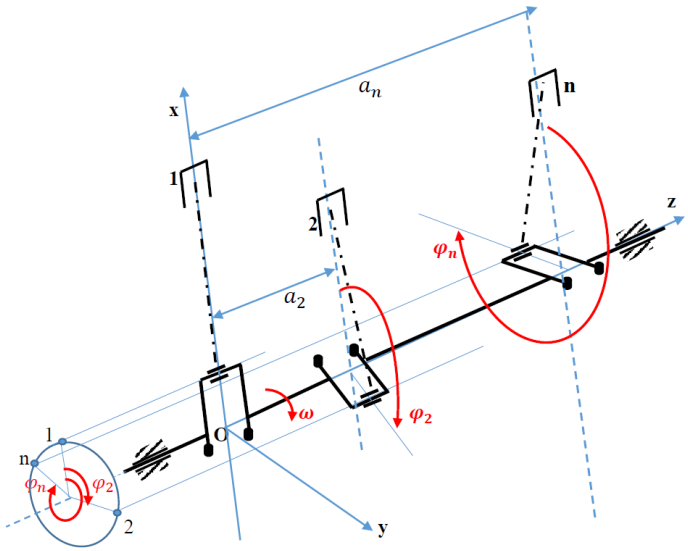

Figure 4.19. n-cylinder In-Line Reciprocating Piston Arrangement [22]

In slider-crank based reciprocating compressors, in order to reduce the shaking forces and moments, a_k and φ_k are utilized simultaneously. In general, φ_k's are selected, and a_k's are determined such that the shaking forces and moments are minimized.

In the case of an internal combustion engine, the crank arrangement affects not only the shaking forces and moments, but also the uniformity of the power output of the engine. The stroke type (two-stroke or four-stroke), on the other hand, affects the uniformity of power, but not the shaking forces and moments. For example, two different crank arrangements of an inline, 4-cylinder engine are compared in Table 4.22. The phase angles in the first and second case are (0º-180º-180º-0º) and (0º-90º-180º-270º), respectively. As can be observed from the table, the 2 crank arrangements behave differently for different objectives. In Table 4.22, first and second harmonic are related terms of shaking force and moments (see [23]).

Table 4.22 The Comparison of the Two Crank Arrangements of a 4-Cylinder Engine[22]

Crank Arrangement	Stroke Type	Uniformity of Power	Shaking			
			Forces		Moments	
			First Harmonic	Second Harmonic	First Harmonic	Second Harmonic
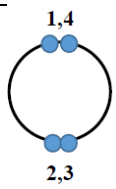	Two Stroke	👎	👍	👎	👍	👎
	Four Stroke	👍				
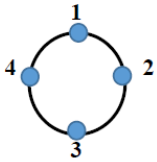	Two Stroke	👍	👍	👎	👎	👍
	Four Stroke	👎				

In a MinFaS-TaR based compressor, on the other hand, the shaking forces and moments are identically zero. Hence, the phase angles of a multi-cylinder MinFaS-TaR based compressor can be utilized to satisfy other requirements (such as obtaining a uniform flow rate, or a uniform motor torque). Here, one should recall that in the MinFaS-TaR based compressors, in addition to the shaking forces and moments (which are due to the inertia forces only), the shaking forces and moments acting on the ground due to the loading (i.e., due to the pressure forces) are also identically zero (at all times). Furthermore, the reaction forces and moments associated with all of the joints that connect the MinFaS-TaR based compressor to the ground are also identically zero at all times (regardless of the motion and the loading on the compressor).

Since the phase angles $\varphi_2, \varphi_3, \ldots, \varphi_n$ of an n cylinder MinFaS-TaR based compressor are not utilized for the purpose of minimizing the shaking forces and moments, these phase angles can be used to render the flow rate (or, the motor torque) of the compressor to be as uniform as possible. In the following section, 9 definitions, which will be useful in the solution of the aforementioned optimization problem, will be introduced.

Definition-1: $f(\theta)$ is a periodic function with period 2π, i.e.,

$$f(\theta + 2\pi) = f(\theta) \tag{4.114}$$

Definition-2: the mean value of $f(\theta)$, $\{f(\theta)\}_{avg}$, is defined via the equation

$$\{f(\theta)\}_{avg} \triangleq \frac{\int_{\theta=0}^{\theta=2\pi} f(\theta)d\theta}{2\pi} \tag{4.115}$$

Note that, the average value of $f(\theta)$ is defined as the mean value of $f(\theta)$ in this study.

Definition-3: the root mean square value of $f(\theta)$, $\{f(\theta)\}_{rms}$, is defined via the equation

$$\{f(\theta)\}_{rms} \triangleq \sqrt{\frac{\int_{\theta=0}^{\theta=2\pi}\left(f(\theta)\right)^2 d\theta}{2\pi}} \tag{4.116}$$

Definition-4: The deviation from the average value of $f(\theta)$, $\hat{f}(\theta)$, is defined via the equation

$$\hat{f}(\theta) \triangleq f(\theta) - \{f(\theta)\}_{avg} \tag{4.117}$$

Definition-5: The percent deviation from the average value of $f(\theta)$, $\{f(\theta)\}_{pdfa}$, is defined via the equation

$$\{f(\theta)\}_{pdfa} \triangleq \frac{\{\hat{f}(\theta)\}_{rms}}{\{f(\theta)\}_{avg}} * 100 \tag{4.118}$$

Definition-6: $f(\theta + \alpha_i)$ is a function which is obtained from $f(\theta)$ by shifting it by an amount of α_i along the θ axis. Since $f(\theta)$ is a periodic function with period 2π, it follows that $f(\theta + \alpha_i)$ is also periodic with period 2π , i.e.,

$$f(\theta + \alpha_i + 2\pi) = f(\theta + \alpha_i) \tag{4.119}$$

Note that the average value of $f(\theta + \alpha_i)$ can be obtained using the equation (4.115), yielding

$$\{f(\theta + \alpha_i)\}_{avg} = \frac{\int_{\theta=0}^{\theta=2\pi} f(\theta + \alpha_i) d\theta}{2\pi} \tag{4.120}$$

which implies that

$$\{f(\theta + \alpha_i)\}_{avg} = \{f(\theta)\}_{avg} \tag{4.121}$$

Definition-7: n denotes the number of MinFaS-TaR mechanisms used in the compressor.

Definition-8: α_i is the phase shift angle of link-2_{i+1} with respect to link-2_i (i = 1,2,..,n-1). Here, link-2_i denotes link 2 of the i^{th} MinFaS-TaR mechanism, MinFaS-

TaR_i . Note that, the phase shift angles α_1 , α_2 , …, α_{n-1} are defined in a similar manner to the phase angles $\varphi_2, \varphi_3, \ldots, \varphi_n$ (see Figure 4.19) defined for an n-cylinder, in-line reciprocating piston arrangement

Definition-9: $f_\Sigma(\theta)$ denotes the summation of the n functions consisting of $f_\Sigma(\theta)$ and its (n-1) "shifted" versions $f(\theta + \alpha_i)$ for i = 1,2, .., n-1 , i.e.,

$$f_\Sigma(\theta) \triangleq f(\theta) + \sum_{i=1}^{i=n-1} f(\theta + \alpha_i) \tag{4.122}$$

The average of $f_\Sigma(\theta)$ can be obtained from equation (4.115), yielding

$$\{f_\Sigma(\theta)\}_{avg} = \frac{\int_{\theta=0}^{\theta=2\pi} f_\Sigma(\theta) d\theta}{2\pi} \tag{4.123}$$

which, upon substituting equation (4.122), leads to

$$\{f_\Sigma(\theta)\}_{avg} = \frac{\int_{\theta=0}^{\theta=2\pi} f(\theta) d\theta}{2\pi} + \frac{\int_{\theta=0}^{\theta=2\pi} f(\theta+\alpha_1) d\theta}{2\pi} + \cdots + \frac{\int_{\theta=0}^{\theta=2\pi} f(\theta+\alpha_{n-1}) d\theta}{2\pi} \tag{4.124}$$

Hence, one obtains

$$\{f_\Sigma(\theta)\}_{avg} = n\{f(\theta)\}_{avg} \tag{4.125}$$

$\{f_\Sigma(\theta)\}_{pdfa}$,on the other hand, can be obtained from equation (4.118) as follows.

$$\{f_\Sigma(\theta)\}_{pdfa} = \frac{\{\hat{f}_\Sigma(\theta)\}_{rms}}{\{f_\Sigma(\theta)\}_{avg}} * 100 \tag{4.126}$$

which leads to

$$\{f_\Sigma(\theta)\}_{pdfa} = \frac{\sqrt{\frac{\int_{\theta=0}^{\theta=2\pi} [f_\Sigma(\theta) - n\{f(\theta)\}_{avg}]^2 d\theta}{2\pi}}}{n\{f(\theta)\}_{avg}} * 100 \tag{4.127}$$

Clearly, when $\{f_\Sigma(\theta)\}_{pdfa}$ = 0, one obtains $f(\theta) = \{f(\theta)\}_{avg}$ = constant.

While designing a MinFaS-TaR based compressor consisting of n MinFaS-TaR mechanisms, the phase angles, $\alpha_i's$, can be used as design variables [for the purpose of minimizing $\{f_\Sigma(\theta)\}_{pdfa}$, where $f(\theta)$ is taken to be either $\dot{m}_o(\theta)$ or $\tau(\theta)$]. Hence, the mass flow rate, $\dot{m}_o(\theta)$, or the motor torque, $\tau(\theta)$, may be compelled to be as uniform as possible.

Consider, now, a compressor consisting of two MinFaS-TaR mechanisms which involves only one design variable (which is α_1). Let each of the 2 MinFaS-TaR mechanisms be identical with the optimal MinFaS-TaR based compressor obtained for Case-1 where the objective function is obj_1 (see Table 4.9 for the properties of the optimal design). Hence, $\{f_\Sigma(\theta)\}_{pdfa}$, where $f(\theta)$ is $\dot{m}_o(\theta)$, is a function of only one design variable, α_1. Figure 4.20 shows $\{f_\Sigma(\theta)\}_{pdfa}$ as a function of α_1 . As can be observed from this figure, there are infinitely many α_1 values which yield the same global minimum for $\{f_\Sigma(\theta)\}_{pdfa}$. Note that for each optimal α_1 value, the mass flow rate corresponding to one of the MinFaS-TaR mechanism based compressors is zero when the mass flow rate corresponding to the remaining MinFaS-TaR mechanism based compressor is nonzero. Figure 4.21 shows the total mass flow rates for the cases where α_1 = 42.7° and α_1 = 317.3°.

Figure 4.22, on the other hand, shows $\{f_\Sigma(\theta)\}_{pdfa}$, where $f(\theta)$ is $\tau(\theta)$, as a function of α_1. As can be observed from this figure, there is a single minimum which occurs at α_1 = 180°. The maximum (i.e., the worst case), on the other hand, occurs at α_1 = 0° as expected.

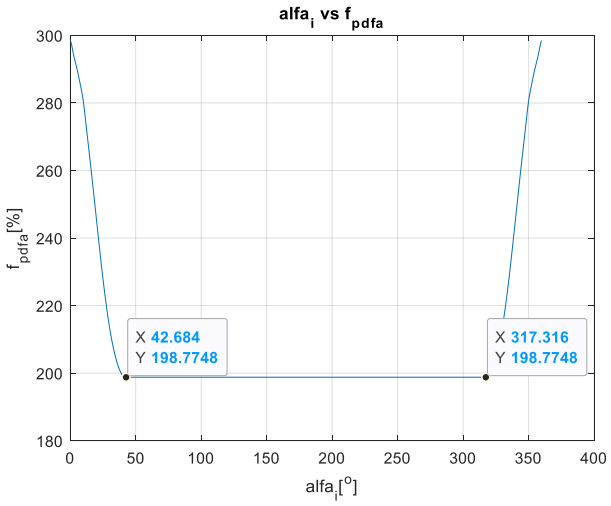

Figure 4.20. Variation of $\{f_{\Sigma}(\theta)\}_{pdfa}$, where $f(\theta)$ is $\dot{m}_o(\theta)$, for a Compressor Which Utilizes Two MinFaS-TaR Mechanisms

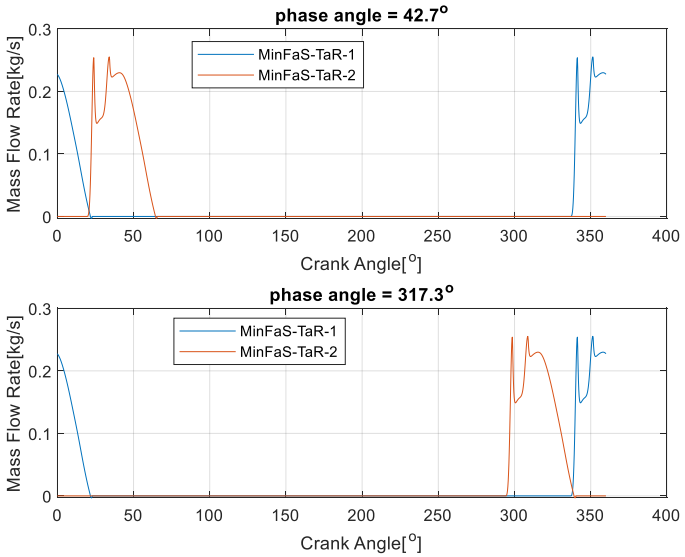

Figure 4.21. The Mass Flow Rate of a Compressor Which Utilizes Two MinFaS-TaR Mechanisms with Different Phase Angle Solutions

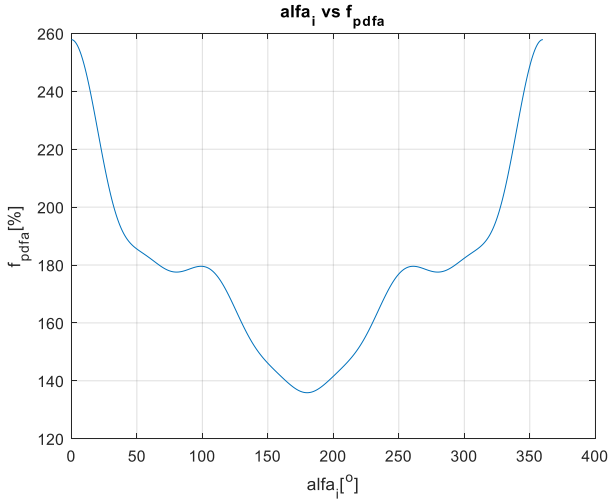

Figure 4.22. Variation of $\{f_\Sigma(\theta)\}_{pdfa}$, where $f(\theta)$ is $\tau(\theta)$, for a Compressor Which Utilizes Two MinFaS-TaR Mechanisms

For a compressor which utilizes n MinFaS-TaR mechanisms, the design variables will be α_1,α_2, …. ,α_{n-1}. Hence, for such a compressor, the minimization of $\{f_\Sigma(\theta)\}_{pdfa}$ requires solving an (n-1) dimensional optimization problem. The problem of minimizing $\{f_\Sigma(\theta)\}_{pdfa}$, where $f(\theta)$ is $\dot{m}_o(\theta)$, for the cases of n = 1, 2, 3, 4, 5 and 6 has been solved; and the results are presented in Figure 4.23. In this figure, in addition to the minimum values of $\{f_\Sigma(\theta)\}_{pdfa}$, the maximum values of $\{f_\Sigma(\theta)\}_{pdfa}$ are also shown for comparison purposes. As expected, the maximum values of $\{f_\Sigma(\theta)\}_{pdfa}$ occur when all of the phase angles, α_i's , are zero. In the same figure, the minimum and maximum values of $\{f_\Sigma(\theta)\}_{pdfa}$ are also shown for the slider crank based compressors. It is known that the phase angles of a slider crank based compressor are utilized to minimize the shaking forces and moments. In Figure 4.23, however, for comparison purposes, it is assumed that each optimal phase angle is equal to $\frac{360}{n}$ for the optimal slider crank based compressor. Hence, in the optimal slider crank based compressors shown in Figure 4.23, the shaking forces and moments can not be balanced by using the phase angles.

The problem of minimizing $\{f_{\Sigma}(\theta)\}_{pdfa}$, where $f(\theta)$ is $\tau(\theta)$, for the cases of n = 1, 2, 3, 4, 5 and 6 has also been solved; and the results are presented in Figure 4.24. The assumptions used to obtain this figure and the notation employed is similar to the ones that have been utilized to generate Figure 4.23.

In order to see the effects of the phase angles on the maximum of $\tau(\theta)$, τ_{max} , let the percent torque ratio, PTR, be defined via the equation

$$PTR = \frac{\tau_{max}}{\tau_{avg}} * 100 \tag{4.128}$$

For a compressor which utilizes n MinFaS-TaR mechanisms, PTR is a function of the (n-1) design variables α_1,α_2, …. ,α_{n-1}. Hence, for a compressor which utilizes n MinFaS-TaR mechanisms, one can obtain the minimum and maximum values of PTR by using α_1,α_2, …. ,α_{n-1} as the design variables. The results are shown in Figure 4.25. The assumptions used to obtain this figure and the notation employed is similar to the ones that have been utilized to generate Figure 4.23.

At this stage, it is also convenient to define the percent power ratio, PPR, via the equation

$$PPR = \frac{\mathrm{Pow}_{max}}{\mathrm{Pow}_{avg}} * 100 \tag{4.129}$$

where Pow designates required motor power. Note that when the motor speed, ω is constant (which is the case in the simulations), PPR and PTR will be identical. Hence, the graph given in Figure 4.25, also yields the minimum and maximum values of PPR for multi-cylinder slider crank based compressors and for compressors which utilize n MinFaS-TaR mechanisms.

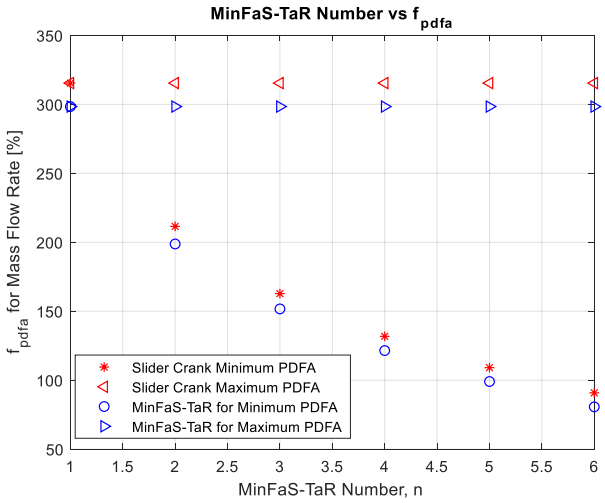

Figure 4.23. Minimum and Maximum Values of $\{f_{\Sigma}(\theta)\}_{pdfa}$, where $f(\theta)$ is $\dot{m}_o(\theta)$, for Multi-Cylinder Slider Crank Based Compressors and for Compressors Which Utilize Multiple MinFaS-TaR Mechanisms

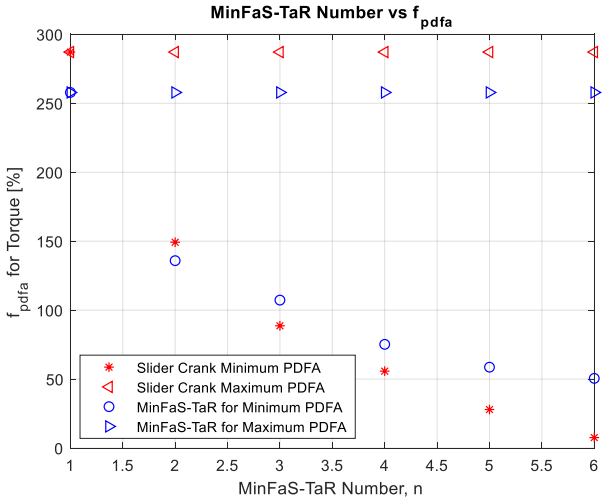

Figure 4.24. Minimum and Maximum Values of $\{f_{\Sigma}(\theta)\}_{pdfa}$, where $f(\theta)$ is $\tau(\theta)$, for Multi-Cylinder Slider Crank Based Compressors and for Compressors Which Utilize Multiple MinFaS-TaR Mechanisms

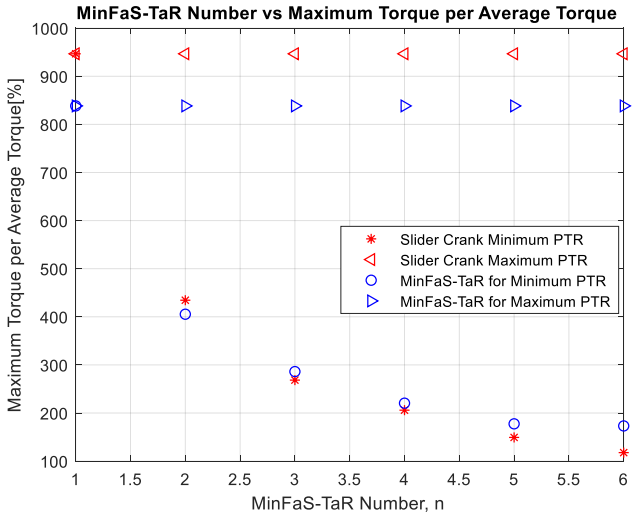

Figure 4.25 Minimum and Maximum Values of PTR for Multi-Cylinder Slider Crank Based Compressors and for Compressors Which Utilize Multiple MinFaS-TaR Mechanisms

4.4 Design of MinFaS-TaR Based Reciprocating Compressor

The slider crank mechanism that is utilized in a conventional reciprocating compressor converts a rotational motion into a translational motion (or, vice versa). The MinFaS-TaR mechanism may also be used to convert a rotational motion into a translational motion. The MinFaS-TaR mechanism has two important advantages over the slider crank mechanism.

(i) In the MinFaS-TaR mechanism, the translational and rotational motions can be related to each other in any desired manner. Clearly, this is not possible in the slider crank mechanism.

(ii) When gravitational acceleration is neglected, the reaction forces and moments associated with the joints that connect the MinFaS-TaR mechanism to the ground will always be zero (regardless of the motion of the mechanism and regardless of the loading on the mechanism). Clearly, this is not the case in the slider crank mechanism.

In this study, the first advantage has been exploited to determine the optimum piston motion that optimizes the performance of the compressor. A figure of MinFaS-TaR mechanism is shown in Figure 4.26.

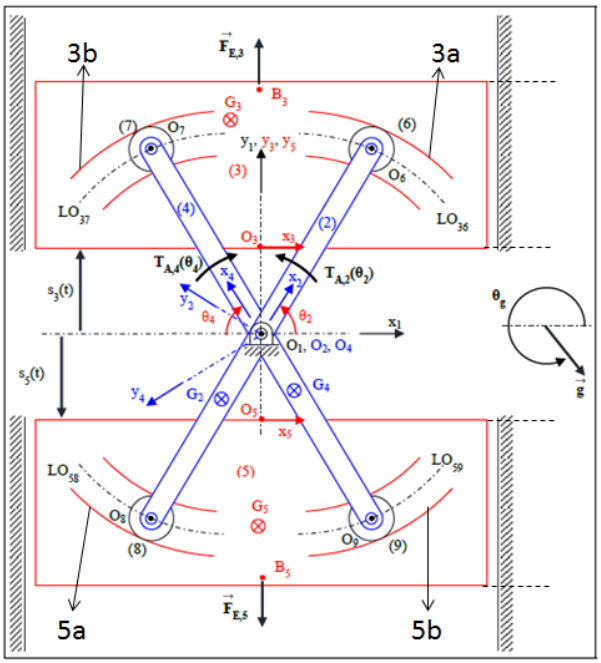

Figure 4.26. The MinFaS-TaR Mechanism [3]

In this section, the procedure for determining the shapes of the slots (designated by 3a, 3b, 5a and 5b in Figure 4.26) which yield an optimum piston motion that is obtained in chapter 4 will be given. Furthermore, a preliminary design of the MinFaS-TaR based reciprocating compressor will be presented.

4.4.1 Slot Profile Determination of the MinFas-TaR Based Compressor

In the MinFaS-TaR mechanism, the translational and rotational motions can be related to each other in any desired manner. This can be achieved by designing the shapes of the slots 3a, 3b, 5a and 5b and the kinematic dimensions properly. It should be noted that, it is sufficient to determine the profile of only one slot, since the remaining slot shapes are simply obtained by way of symmetry. Hence, only the determination of the shape of slot 3a will be considered in this section

By replacing $s_3(t)$ in Figure 4.26 with [$-x_p(\theta)$] (according to the notation that is employed, $s_3 = -x_p$), the x and y coordinates (with respect to the $O_3x_3y_3$ frame fixed to body 3) of a point on the slot profile ,i.e., x_{3a} and y_{3a} , may be obtained via the equations

$$x_{3a} = b_2\cos(\theta_2) \tag{4.130}$$

$$y_{3a} = b_2\sin(\theta_2) + x_p(\theta_2) \tag{4.131}$$

where $b_2 = \overline{O_1O_6}$ is the length of link 2 and θ_2 is the angular position of link 2 (see Figure 4.26). Once b_2 and $x_p(\theta_2)$ are decided upon, equations (4.130) and (4.131) will yield the parametric equations of slot 3a (with respect to the $O_3x_3y_3$ frame fixed to body 3). It should be noted that there will be a piston rigidly connected to link 3, the dimensions of which do not affect the shape of the slot profile. Figure 4.27, for instance, shows the profile obtained for slot 3a for b_2 = 0.2 [m] and for the optimum $x_p(\theta_2)$ obtained for Case-1 for minimization of objective-1 (see Table 4.9).

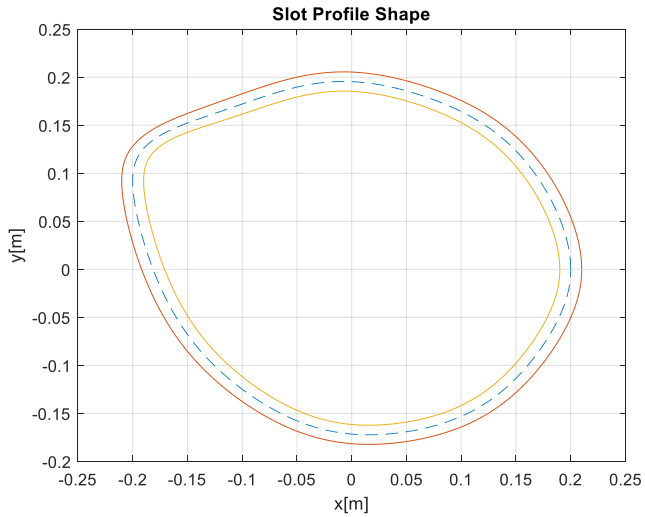

Figure 4.27. Slot Profile of Slot 3a Based on Optimum Piston Motion for Case-1 for Minimization of Objective-1(b_2 = 0.2 [m])

4.4.2 The MinFaS-TaR Based Reciprocating Compressor

In order to avoid any possibility of collision between links 3 and 5, links 3 and 5 consist of two parts, which are labelled as 3a, 3b, 5a and 5b. These parts are named in accordance with the labelling of the slot profiles as seen in Figure 4.26. The details of the connections between the links are described below.

- 3a and 3b are rigidly connected.
- 5a and 5b are rigidly connected.
- 3a and 5a are connected to the same crank (link-2).
- 3b and 5b are connected to the same crank (link-4).

A preliminary design for a MinFaS-TaR based reciprocating compressor is shown in Figure 4.28. The connection between link 3a and the corresponding cylinder is shown in Figure 4.29. In these figures, the outlet and the inlet valves are red and blue, respectively.

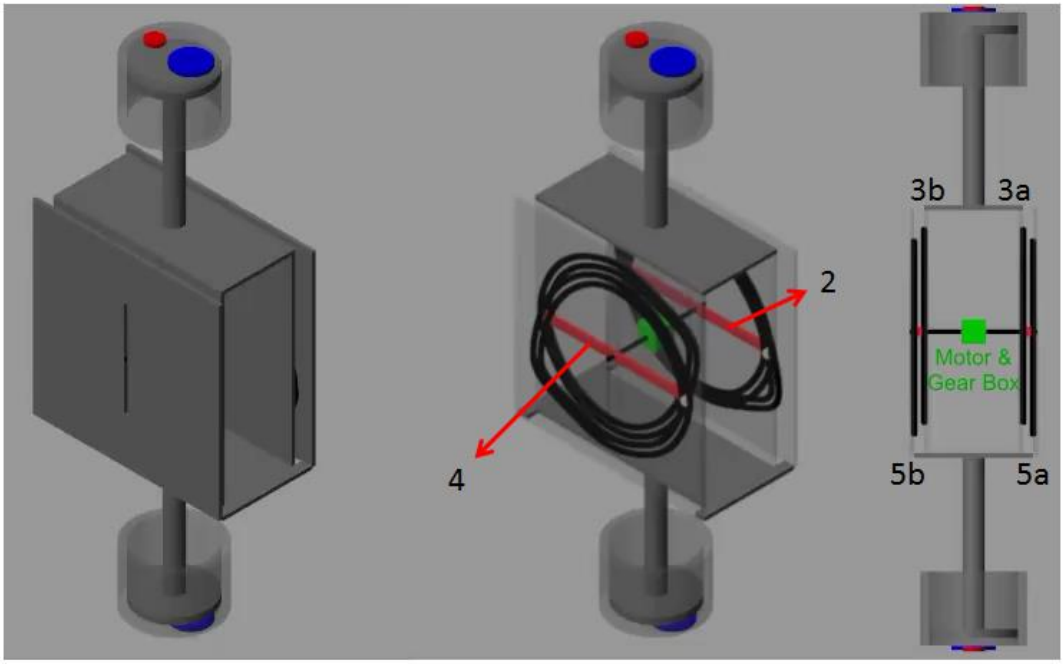

Figure 4.28. Preliminary Design of a MinFaS-TaR Based Reciprocating Compressor

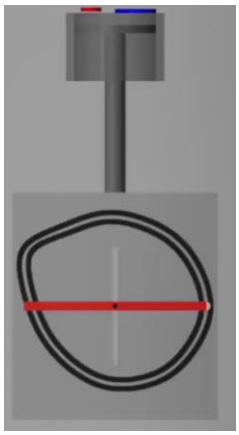

Figure 4.29. 3D Assembly of Link 3a and the Corresponding Cylinder

In order to visululize the mechanisim motion, some snapshots from the simulation are presented in Figure 4.30. Furthermore, some snapshots from the simulation for only the assembly of link 3a and the corresponding cylinder is shown in Figure 4.31. On the other hand, in Figure 4.31, while mechanism is moving, the corresponding chamber pressure is given in the right-lower corner and the corresponding chamber temperature is given in the right-upper corner.

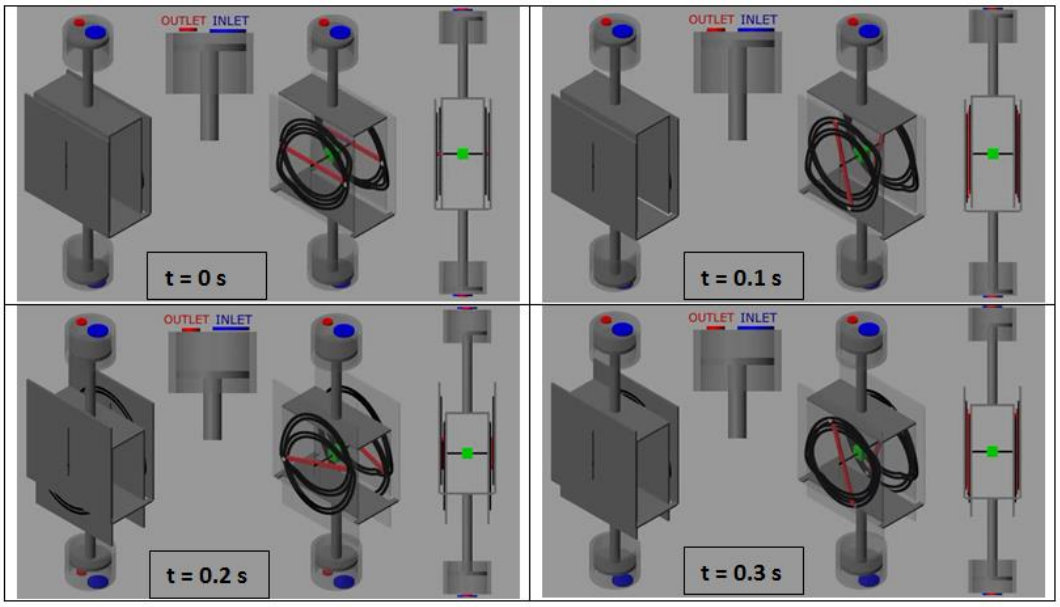

Figure 4.30. Snapshots of the Visual Simulation of the MinFaS-TaR based Compressor

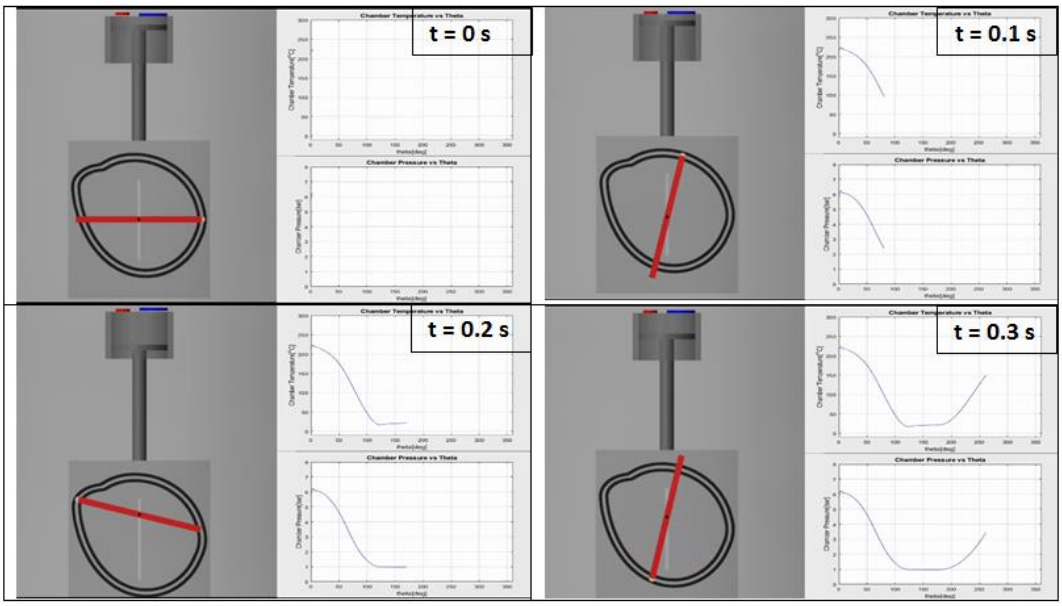

Figure 4.31. Snapshots of the Visual Simulation of the Assembly of Link 3a and the Corresponding Cylinder

CHAPTER 5

DISCUSSIONS AND CONCLUSION

The slider crank mechanism that is utilized in a conventional reciprocating compressor converts a rotational motion into a translational motion (or, vice versa). The MinFaS-TaR mechanism may also be used to convert a rotational motion into a translational motion. The MinFaS-TaR mechanism has two important advantages over the slider crank mechanism.

(i) In the MinFaS-TaR mechanism, the translational and rotational motions can be related to each other in any desired manner. Clearly, this is not possible in the slider crank mechanism.

(ii) When gravitational acceleration is neglected, the reaction forces and moments associated with the joints that connect the MinFaS-TaR mechanism to the ground will always be zero (regardless of the motion of the mechanism and regardless of the loading on the mechanism). Clearly, this is not the case in the slider crank mechanism. Hence, by nature, there are no vibrations transmitted to the chassis of the MinFaS-TaR mechanism. Furthermore, the frictional losses associated with the MinFaS-TaR mechanism and the wear associated with the bearings that are used to connect the MinFaS-TaR mechanism to the ground are minimum. It should be recalled that balancing of the shaking forces and moments takes into account, only, the inertia forces and moments in the mechanism. Hence, even in a slider crank mechanism that is balanced for the shaking forces and moments, the joint reactions (associated with the joints that connect the mechanism to the ground) due to the loading on the mechanism cannot be rendered to be zero for a nonzero loading.

Under the light of the above two advantages, it is clear that a reciprocating compressor utilizing a MinFaS-TaR mechanism will be much more advantageous than a reciprocating compressor utilizing a slider crank mechanism.

In this study, in order to benefit from the first advantage, the piston motion function $x_p(\theta)$ has been used as a design "function" to optimize the performance of the compressor. Here, x_p denotes the position of the piston of the compressor. θ, on the other hand, designates the angular position of the crank, or, cranks (in the case of a MinFaS-TaR based compressor) of the compressor. In addition to $x_p(\theta)$, the diameter of the cylinder, the diameters of the inlet and outlet valves and the motor speed (which is assumed to be constant) are selected as design parameters. Hence, the design parameter vector $\overrightarrow{DP}$, given by

$$\overrightarrow{DP} = [x_p(\theta); D_{cyl}; D_{vi}; D_{vo}; \omega] \tag{5.1}$$

may be used to optimize the performance of a MinFaS-TaR based compressor. Note that, $\overrightarrow{DP}$ is, rigorously, not a physical vector that has a magnitude and a direction. In this study, $\overrightarrow{DP}$ is used, loosely, to represent a list of design parameters that consists of a function and some scalar parameters. It should be noted that, in the case of a slider crank based compressor, $x_p(\theta)$ is constrained by the kinematics of the slider crank. Hence, it cannot be used as a design function to optimize the performance.

If $x_p(\theta)$ is selected to be the design function, it is difficult to predict the "shape" of the optimal design function. However, prediction of the optimal "shape" of the chamber pressure function, $P_c(\theta)$, where P_c denotes the chamber pressure, is quite intuitive. Hence, in most of the optimizations, $P_c(\theta)$ has been utilized as the design function. Here, it should be recalled that when the chamber pressure function, $P_c(\theta)$, is taken to be the design function, the corresponding piston motion function, $x_p(\theta)$ may be obtained via simulation (of the compression process).

The effect of the design function $x_p(\theta)$, solely, on the consumed energy may be observed from Figure 4.12 which shows the variation of W_{net}^{pm}, with respect to the design function $x_p(\theta)$, for various ω values. Using this figure, one obtains sav[50] = 2.70 , sav[100] = 3.05 , sav[200] = 3.81 , sav[300] = 1.59 sav[400] =7.00 , sav[500] = 0.33 sav[600] = 13.40, sav[700] = 17.29, sav[800] = 21.25 where $sav[\omega]$ designates the percent savings in W_{net}^{pm} [due to the changes in the design function $x_p(\theta)$] corresponding to a given ω value. The maximum saving occurs at ω = 800 rpm, yielding sav[800] = 21.25. Hence, by using the optimal $x_p(\theta)$, one can save % 21.25 of the consumed energy corresponding to the "worst" choice for $x_p(\theta)$. In other words, the compressor with the optimal $x_p(\theta)$ consumes % 78.75 of the energy consumed by the compressor corresponding to the "worst" $x_p(\theta)$. Hence, it is concluded that the piston motion function, $x_p(\theta)$, affects the consumed energy of the compressor extensively.

In order to assess the effects of various design parameters on the performance of a reciprocating compressor, 7 case studies (see Table 4.8 for the descriptions) have been considered in Chapter 4. By using the developed algorithms, optimal MinFaS-TaR based compressors have been obtained for each of these case studies. Next, the results of these optimizations will be discussed case by case. Whenever possible, the performances of the optimal MinFaS-TaR based compressors will also be compared to that of the slider crank based compressors.

Case-1: The results of the optimizations for the objective functions obj_1, obj_2 and obj_3 have been given in Table 4.9, Table 4.10 and Table 4.11, respectively. Here, it should be recalled that obj_1 , obj_2 and obj_3 denote the energy consumptions of a compressor defined by W_{net}^{pm}, W_{pos}^{pm} and W_{abs}^{pm}, respectively. Considering obj_1, Table 4.9 indicates that the MinFaS-TaR based compressor is %10 more efficient than the original slider crank based one. If SC_{mod} is taken into consideration, the savings due to the MinFaS-TaR based compressor can be considered to be quite

marginal. However, it should be noted that the capacity of SC_{mod} is %54 less than the MinFaS-TaR based compressor.

Considering the objective functions obj_2 and obj_3, the MinFaS-TaR based compressor is, again, more efficient than SC_{org}. The percent savings for obj_2 and obj_3 are %11.5 and %14.1, respectively. Here, it is important to note that in practice, regenerative motors are not employed, at least currently, in reciprocating compressors. Hence, the savings related to the energy consumptions given by obj_1 may be considered to be hypothetical. For practical considerations, obj_2 yields the most realistic energy consumption for reciprocating compressors.

The MinFaS-TaR based compressor is also more efficient than SC_{mod} (although the energy savings are not as striking as the ones obtained for SC_{org}). However, it should be noted that the capacity of SC_{mod} is dramatically less than the desired capacity.

Case-2 and Case-3: The results of the optimizations (for obj_1 , obj_2 and obj_3) for Case-2 and Case-3 have been presented in Table 4.12 and Table 4.13, respectively. These tables indicate that changes in the desired capacity do not affect the objective functions significantly. For these 2 cases, there are no slider crank based compressor results that are available for comparison.

Case-4, Case-5 and Case-6: These cases are related to multi-stage compressors.

For Case-4, the results of the optimizations for obj_1, obj_2 and obj_3 have been presented in Table 4.15, Table 4.16 and Table 4.17, respectively.

For Case-5, the results of the optimizations for obj_1, obj_2 and obj_3 have been presented in Table 4.18, Table 4.19 and Table 4.20, respectively

For Case-6, the results of the optimizations have been given in Table 4.14.

The results of Case-4 are similar to those of Case-1. However, as expected, the difference between the results of Case-4 and Case-5 is significant. The results

indicate, clearly, the advantage of using an intercooler. Furthermore, when the results of Case-6 is considered, one observes that compression of air from 1 bar to 36 bar in one stage should not be preferred due to the high energy consumption.

Case-7: This case study is related to compressors which utilize 2 or more slider crank or MinFaS-TaR mechanisms. While designing a MinFaS-TaR based compressor consisting of n MinFaS-TaR mechanisms, the (n-1) phase angles α_1 , α_2 , …. , α_{n-1} can be used as additional design variables [in addition to the ones given by the components of $\overrightarrow{DP}$ given by equation (5.1)]. These (n-1) phase angles may be used in an optimization where the objective is to make the mass flow rate, $\dot{m}_o(\theta)$, or the motor torque, $\tau(\theta)$, to be as uniform as possible. Although the (n-1) phase angles cannot be used to minimize obj_1 (since obj_1 is invariant with respect to the changes in the phase angles), they may be used to minimize the 2 objective functions obj_2 and obj_3 as well. It is known that the phase angles of a slider crank based compressor are utilized to minimize the shaking forces and moments. In Figure 4.23, Figure 4.24 and Figure 4.25, however, for comparison purposes, it is assumed that each optimal phase angle is equal to $\frac{360}{n}$ for the optimal slider crank based compressors. Hence, in the optimal slider crank based compressors shown in these figures, the shaking forces and moments cannot be balanced by using the phase angles.

Referring to Figure 4.23, as expected, the mass flow rate of the MinFaS-TaR based compressor becomes more uniform as the number of MinFaS-TaR mechanisms utilized increases. For instance, for a MinFaS-TaR based compressor which utilizes 6 MinFaS-TaR mechanisms, $\{f_\Sigma(\theta)\}_{pdfa}$ for the worst case divided by the $\{f_\Sigma(\theta)\}_{pdfa}$ for the best case is %372. Here, it should be recalled that the "smaller" $\{f_\Sigma(\theta)\}_{pdfa}$ is, the "smaller" will be the "deviation" of $f(\theta)$ from a constant (which is its average value). Referring to Figure 4.25, on the other hand, it is observed that the required maximum power of the driving motor decreases as the number of MinFaS-TaR mechanisms utilized increases. For instance, for a MinFaS-TaR based compressor which utilizes 6 MinFaS-TaR mechanisms, the

required maximum power of the driving motor for the best case is %21 of the required maximum power of the driving motor for the worst case.

There are some features which are shared by almost all cases. These common features are listed below.

- In general, if D_{cyl} is increased and/or ω is decreased, the energy consumption reduces.
- The inertias of the flywheels for the MinFaS-TaR based compressors are greater than the slider crank based compressor flywheel inertias. Here, it should be noted that the MinFaS-TaR mechanism may also be used as an energy storage device (instead of a flywheel), where the rate of energy storage, or energy discharge, can be controlled as desired. Hence, one can utilize an additional MinFaS-TaR mechanism which replaces the flywheel in a more efficient manner.
- The Fourier-8 type fit used for the periodicity of motion may lead to some inefficiencies. It appears that the discrete motion with cubic spline patching method is more practical. Although, the effect of the curve fit on energy consumption is not significant, the chamber pressure is quite sensitive to the motion profile as can be observed in Figure 4.14.
- When gravitational acceleration is neglected, the side forces on pistons that connect the MinFaS-TaR mechanism link-3 and link-5 will always be zero (regardless of the motion of the mechanism and regardless of the loading on the mechanism). Clearly, this is not the case in the slider crank mechanism.

Finally, some suggestions for future work are listed below.

- The optimization of the performance of a reciprocating compressor is time consuming and complicated due to the following reasons. (i) The problem is nonlinear (with nonlinear equality and inequality constraints). (ii) The number of design variables is large. (iii) The evaluation of the objective function takes a considerable amount of time (since it requires that the

compressor is simulated in order to obtain the steady state operating conditions). For instance, using a computer with i7-6820HQ CPU and 16.0 GB RAM, the optimization carried out for Case-1, requires 171 hours of elapsed time. Hence, due to the lack of a powerful work station(s), the number of design variables used in the optimizations have been limited. In the future, the number of design variables can be increased to include parameters such as, for instance, valve spring stiffnesses, independent inlet and outlet valve areas, etc. More importantly, the design functions $x_p(\theta)$ and $P_c(\theta)$ may be modelled in a more flexible manner by increasing the number of cam motion curves used in the models. In this manner, it will be possible to approach the global optima for the performance of the MinFaS-TaR based compressors which, certainly, will exceed the performances that have been obtained in this study (which utilizes only a limited number of design variables in the optimizations).

- In this study, the (n-1) phase angles α_1 , α_2 , …. , α_{n-1} have not been utilized to minimize the objective functions obj_2 and obj_3. In the future, the consumed energies defined by these 2 objective functions may be minimized by adding the (n-1) phase angles into the design parameters vector. Indeed, this will reduce the energy consumptions that have been obtained in this study.
- In this study, the n MinFaS-TaR mechanisms used in a multi MinFaS-TaR compressor have identical $x_p(\theta)$ design functions. In the future, when minimizing obj_2 or obj_3, each $x_p(\theta)$ design function, in each MinFaS-TaR mechanism, may be allowed to be different. Indeed, this will reduce the energy consumptions that have been obtained in this study.
- In this study, the compressor has been modelled using a 0D model. In the future, commercially available packages may be employed to use three dimensional computational fluid dynamics (CFD) models which will yield more accurate results for the thermo-fluid analysis of a reciprocating compressor.

- In this study, frictional effects and some of the inertial effects have been neglected. In the future, these effects may be included in the developed model.
- The methods developed to improve the performances of reciprocating compressors in this study can be extended to improve the performances of reciprocating pumps and/or internal combustion engines

REFERENCES

[1] R. Soylu, A Mechanical Torque Generator and Related Kinematic Chains. Turkish Patent Number : TR 2013 13065 B ; Japanese Patent Number : 6491223 ; USA Patent Number : US 10,683,916 B2.

[2] E. Söylemez, *Mechanisms 4th Ed*. Ankara: Middle East Technical University, 2009.

[3] H. Mencek, "Theoretical and Experimental Dynamic Performance Optimization of Planar Mechanisms Using Adjustment Systems and Mechanical Generators," Middle East Technical University, 2015.

[4] J. Hollingsworth, G. Phillippi, M. Hinchliff, C. Kulhanek, A. M. Rimpel, and F. Maywald, "Reciprocating Compressors," *Compression Mach. Oil Gas*, vol. 5, pp. 167–252, 2019.

[5] K. T. Ooi and T. T. Wan, "A Rotaprocating Compressor," in *International Compressor Engineering Conference*, 2000.

[6] K. T. Ooi and S. K. Ng, "Optimization Of A Rotaprocating Compressor," in *International Compressor Engineering Conference*, 2002.

[7] I. A. Sultan and A. Kalim, "Improving reciprocating compressor performance using a hybrid two-level optimisation approach," *Eng. Comput. (Swansea, Wales)*, 2011.

[8] J. H. Sol, "Description and Analysis of New Motion Conversion Mechanism for Heavy-Loaded Reciprocating Pumps," in *World Congress on Engineering*, 2014.

[9] P. Stouffs, M. Tazerout, and P. Wauters, "Thermodynamic analysis of reciprocating compressors," *Int. J. Therm. Sci*, vol. 40, pp. 52–66, 2001.

[10] J. Tuhovcak, J. Hejcik, and M. Jicha, "Modelling fluid flow in a reciprocating compressor," in *The European Physical Journal Conferences*, 2015.

[11] Z. Liu, Z. Lan, J. Guo, J. Zhang, Y. Xie, X. Cao, and Z. Duan, "A New Hybrid Reciprocating Compressor Model Coupled with Acoustic FEM Characterization and Gas Dynamics," *Appl. Sci*, vol. 9, no. 1179, 2019.

[12] M. Faezaneh-Gord, A. Niazmand, M. Deymidashtebayaz, "Optimizing Reciprocating Air Compressors Design Parameters Based On First Law Analysis," *U.P.B. Sci. Bull., Ser. D*, vol. 75, no. 4, pp. 13–26, 2013.

[13] M. Imran and M. Usman, “Mathematical modelling for positive displacement expanders,” *Posit. Displac. Mach.*, vol. 11, pp. 293–343, 2019.

[14] W.J.D. Annand, “Heat Transfer in the Cylinders of Reciprocating Internal Combustion Engines,” *Proc. Instn. Mech. Engnrs.*, vol. 177, pp. 973-996, 1963

[15] G. Woschni, “A Universally Applicable Equat for the Instantaneous Heat Transfer Coefficient in the Internal Combustion Engine,” *SAE Trans.*, vol. 76, no. 1968, pp. 3065–3083, 2019.

[16] R. Stone, *Introduction to Internal Combustion Engines*. 1992.

[17] R. P. Adair, E. B. Qvale, and J. T. Pearson, “Instantaneous Heat Transfer to the Cylinder Wall in Reciprocating Compressors,” in *International Compressor Engineering Conference School*, 1972.

[18] J. E. Shigley, *Mechanical Engineering Design 5th Ed*. McGraw-Hill 1989

[19] H. A. Rothbart and D. Eng, “Chapter 3 Modified Cam Curves,” in *CAM DESIGN HANDBOOK*, 2004, pp. 55–88.

[20] I. López-paniagua, J. Rodríguez-martín, J. J. Roncal-casano, S. Sánchez-orgaz, and J. J. Roncal-casano, “Step by Step Derivation of the Optimum Multistage Compression Ratio and an Application Case,” *Entropy*, pp. 1–13, 2020.

[21] K. Ueno, R. E. Bye, and K. S. Hunter, “Compressor Efficiency Definition,” 2003.

[22] S. T. Tümer, *ME418 Lecture Notes*, Middle East Technical University, 2017.

[23] J. J. Dicker, G. R. Pennock, J. E. Shigley, *Theory of Machines and Mechanisms 3rd Ed*. OXFORD UNIVERSITY PRESS, 2003.

APPENDICES

A. Appendix A

Results of the simulations for the conventional, slider crank based reciprocating compressor are presented below. The data corresponding to these simulations are given in Table 2.1.

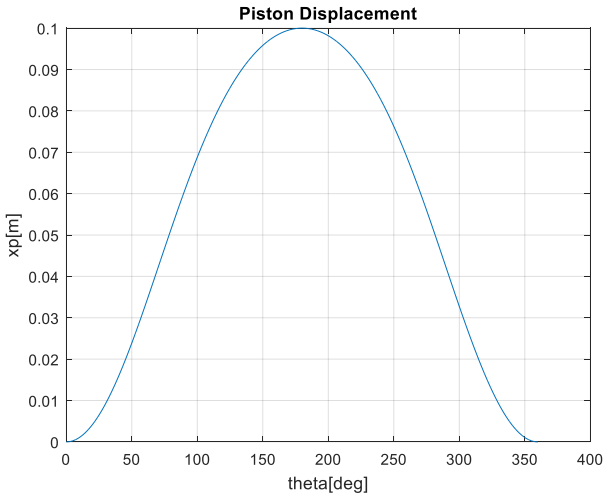

Figure A.1. Piston Displacement of the Conventional, Slider Crank Based Reciprocating Compressor

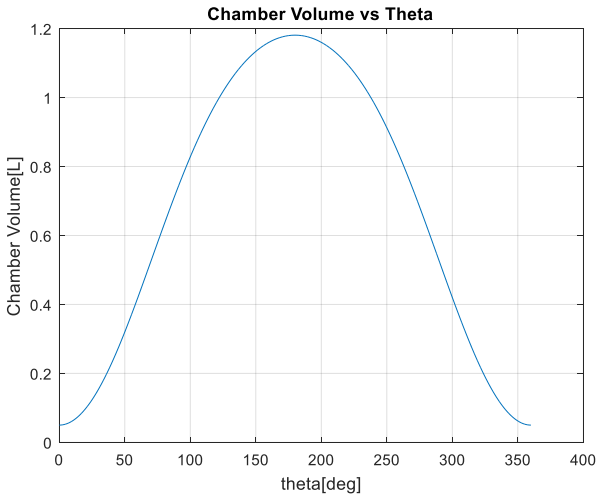

Figure A.2. Chamber Volume of the Conventional, Slider Crank Based Reciprocating Compressor

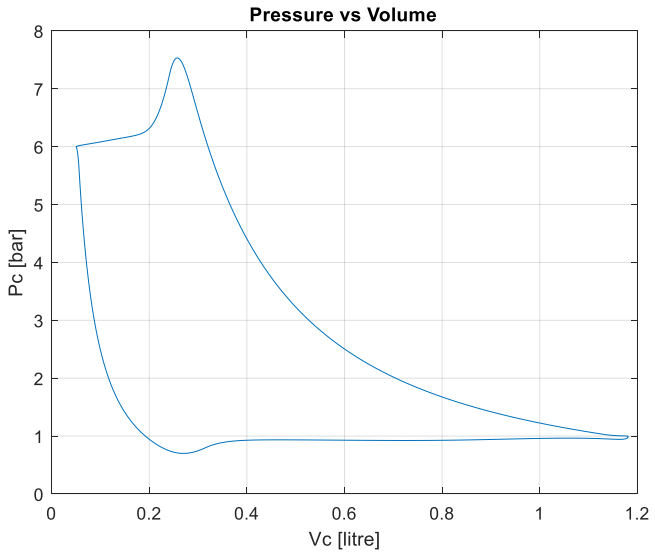

Figure A.3. PV Diagram of the Conventional, Slider Crank Based Reciprocating Compressor

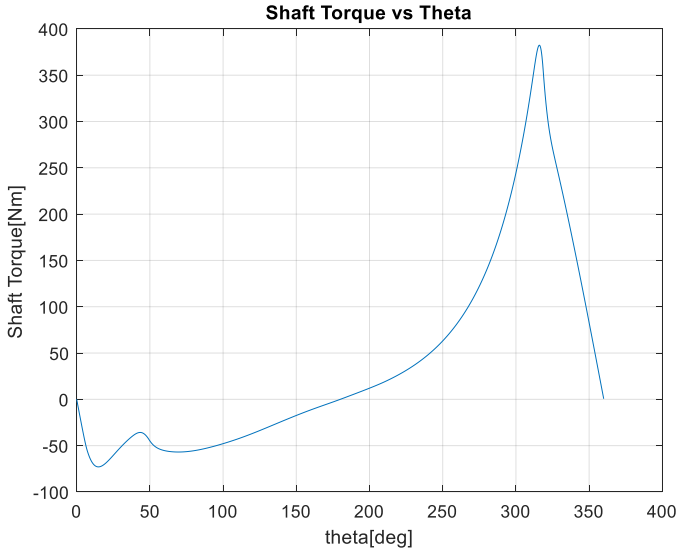

Figure A.4. Shaft Torque of the Conventional, Slider Crank Based Reciprocating Compressor

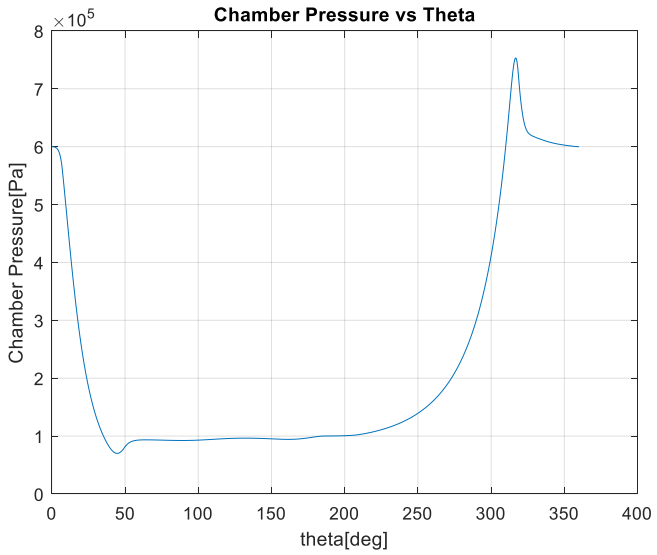

Figure A.5. Chamber Pressure of the Conventional, Slider Crank Based Reciprocating Compressor

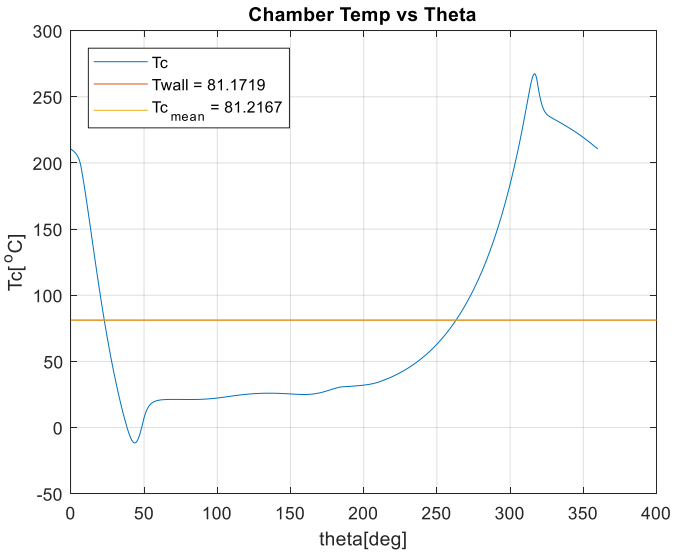

Figure A.6. Chamber Temperature of the Conventional, Slider Crank Based Reciprocating Compressor

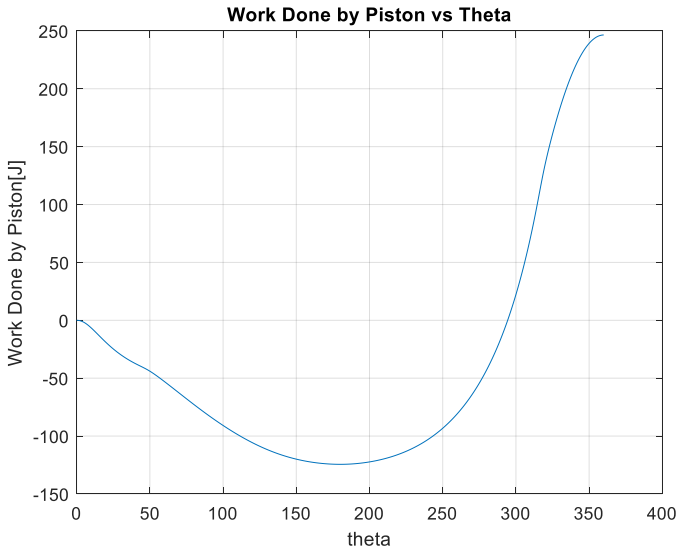

Figure A.7. Work Done for the Conventional, Slider Crank Based Reciprocating Compressor

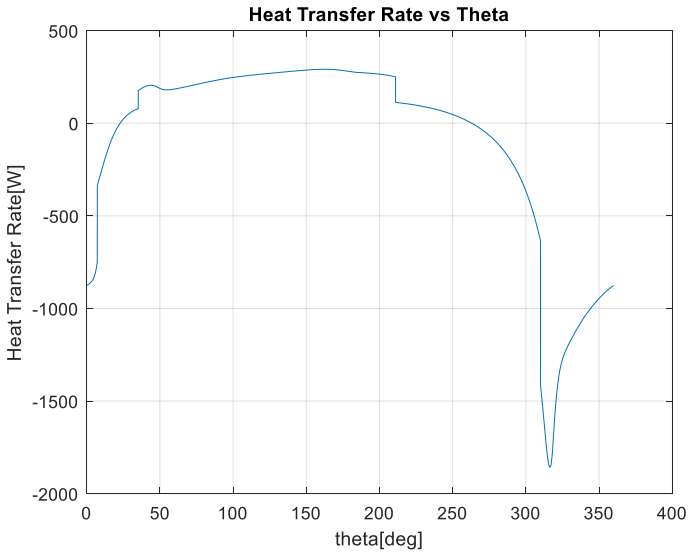

Figure A.8. Heat Transfer Rate of the Conventional, Slider Crank Based Reciprocating Compressor

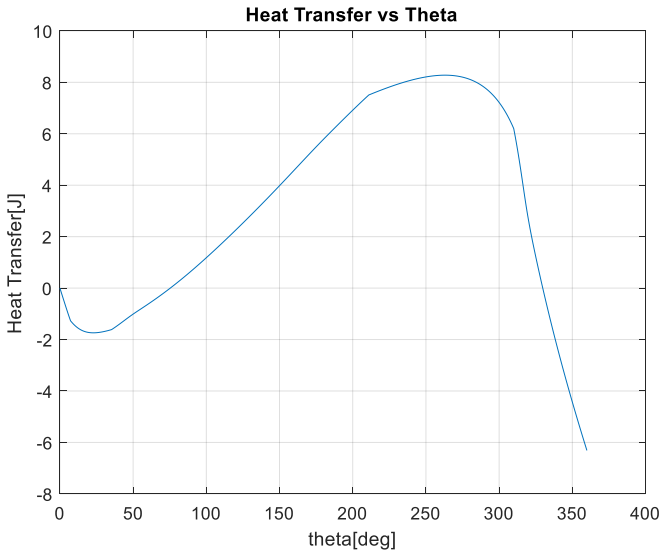

Figure A.9. Heat Transfer for the Conventional, Slider Crank Based Reciprocating Compressor

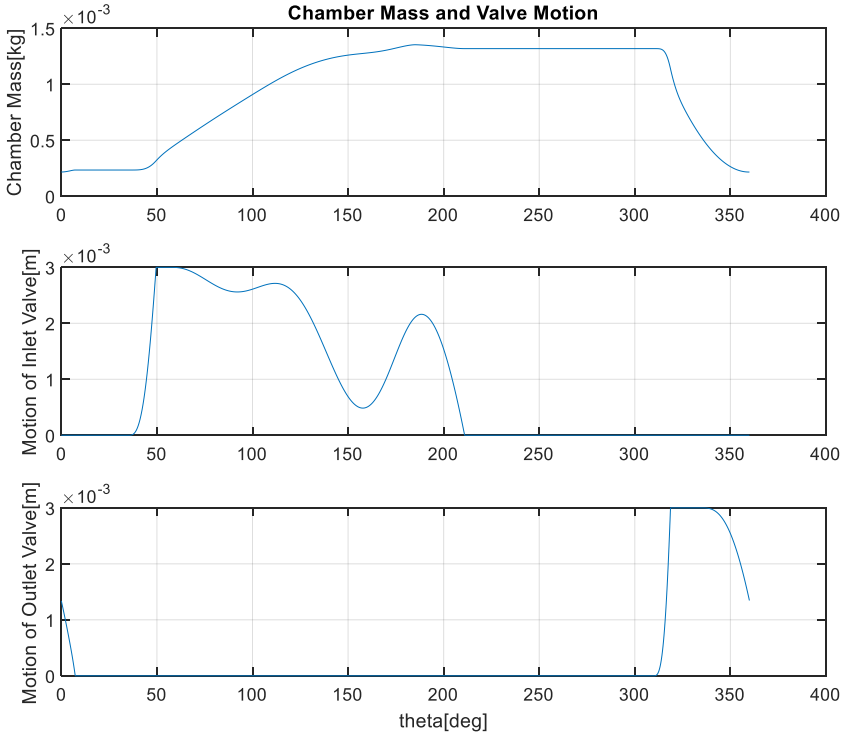

Figure A.10. Chamber Mass and Valve Motion of the Conventional, Slider Crank Based Reciprocating Compressor

B. Appendix B

In this Appendix, it is shown that neither τ_{rms} (defined by equation (A.1)), nor η_τ (defined by equation (3.43)) can predict ΔE. The proof is realized via two counter examples. The torque versus time plots of the two counter examples are given in Figure A.11 and Figure A.12.

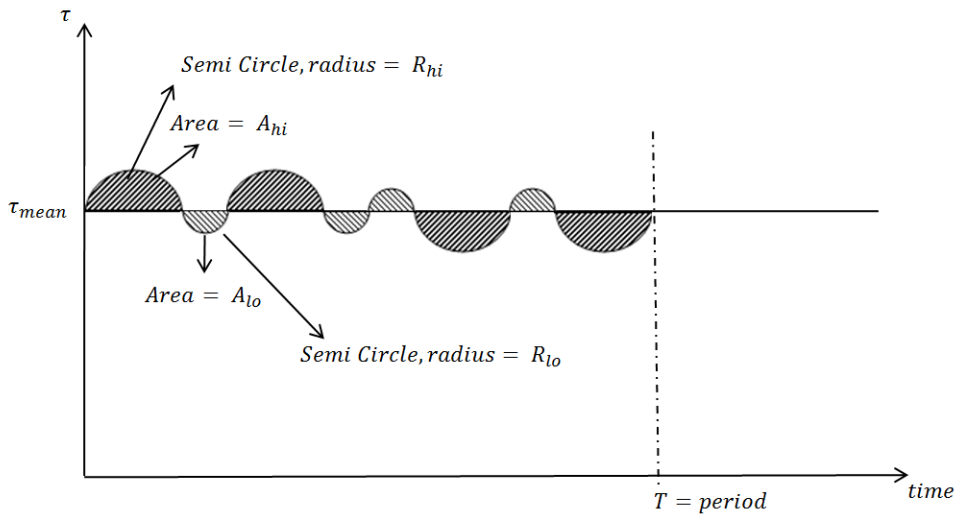

Figure A.11. Torque Versus Time Plot of the First Counter Example

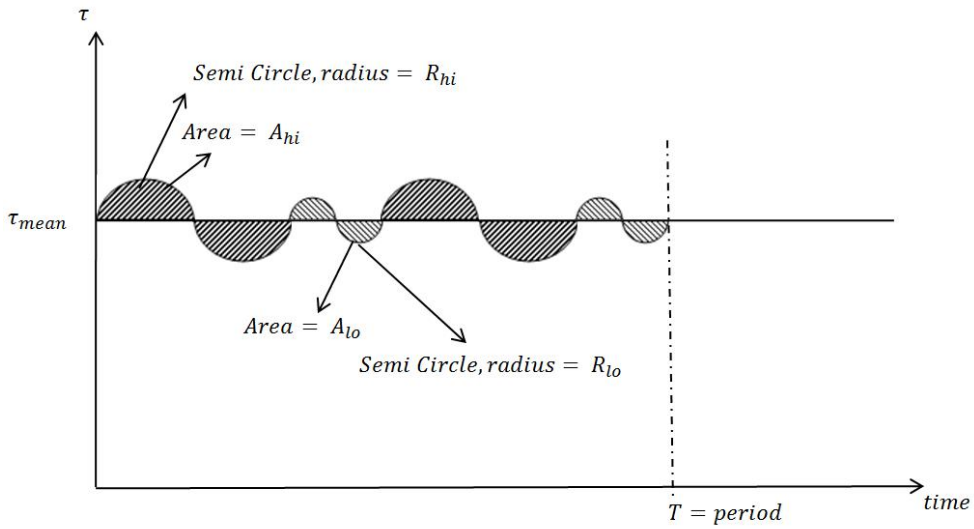

Figure A.12. Torque Versus Time Plot of the Second Counter Example

The root mean square of the torque, $\hat{\tau}_{rms}$, can be defined via the equation

$$\hat{\tau}_{rms} \triangleq \sqrt{\frac{\int_{\theta=0}^{\theta=T}(\tau(\theta)-\tau_{mean})^2 d\theta}{2T}} \tag{A.1}$$

For example, the root mean square of f(x) which is in the form of a semi-circle (see Figure A.13) can be determined as shown in equation (A.2).

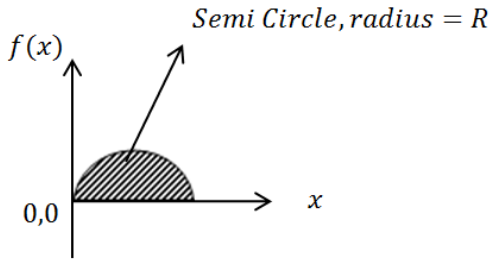

Figure A.13. A Semi Circle Graph

$$f_{rms} = \sqrt{\frac{\int_{x=0}^{x=2R}\left(f(x)\right)^2 dx}{2R}} = R\sqrt{\frac{2}{3}} \tag{A.2}$$

Using equation (A.2), $\hat{\tau}_{rms}$ values for the two counter examples can obtained as shown below.

$$(\hat{\tau}_{rms})_1 = 4\sqrt{\frac{2}{3}}(R_{hi}+R_{lo}) \tag{A.3}$$

$$(\hat{\tau}_{rms})_2 = 4\sqrt{\frac{2}{3}}(R_{hi}+R_{lo}) \tag{A.4}$$

As can be observed from the above two equations, $(\hat{\tau}_{rms})_1 = (\hat{\tau}_{rms})_2$.

The torque steadiness, η_τ, is defined via equation (3.43). Using this definition, one obtains η_τ for the first counter example, $(\eta_\tau)_1$, as follows.

$$(\eta_\tau)_1 = 1 - \frac{(\tau_{mean} + R_{hi}) - \tau_{mean}}{(\tau_{mean} + R_{hi}) + \tau_{mean}} = \frac{2\tau_{mean}}{R_{hi} + 2\tau_{mean}} \qquad \text{(A.5)}$$

Clearly, η_τ for the second counter example, $(\eta_\tau)_2$, is identical with $(\eta_\tau)_1$ [i.e., $(\eta_\tau)_2 = (\eta_\tau)_1$] since both τ_{mean} and τ_{max} values are identical for the 2 counter examples.

Next, ΔE values for the 2 counter examples, ΔE_1 and ΔE_2 , will be determined.

Energy Line Diagram for the First Counter Example:

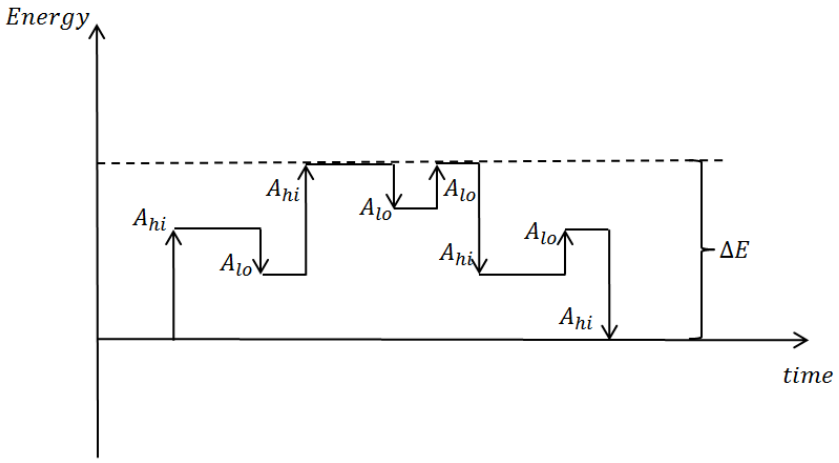

Figure A.14. Energy Line Diagram for the First Counter Example

From Figure A.14, it follows that

$$\Delta E_1 = 2A_{hi} - A_{lo} \qquad \text{(A.6)}$$

Energy Line Diagram for the First Counter Example:

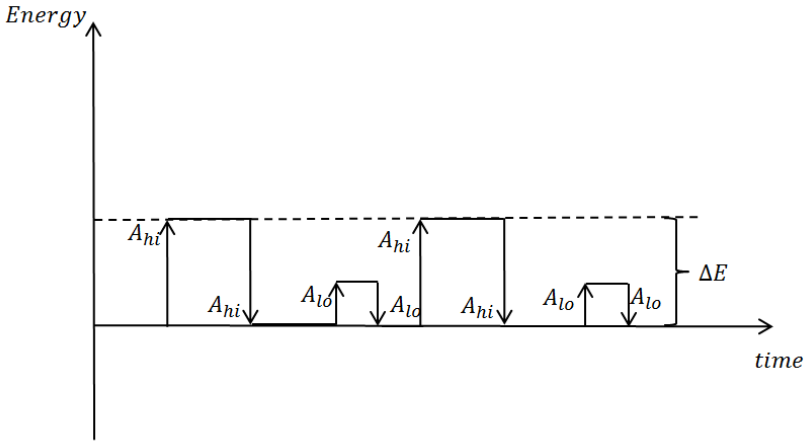

Figure A.15. Energy Line Diagram for the Second Counter Example

From Figure A.15, it follows that

$$\Delta E_2 = A_{hi} \tag{A.7}$$

From equations (A.6) and (A.7), one observes that $\Delta E_1 \neq \Delta E_2$. On the other hand, $(\tau_{rms})_1 = (\tau_{rms})_2$ and $(\eta_\tau)_1 = (\eta_\tau)_2$. Hence, it follows that neither τ_{rms}, nor η_τ can predict ΔE.

C. Appendix C

C.1. Case A1 for Cases M1-M6

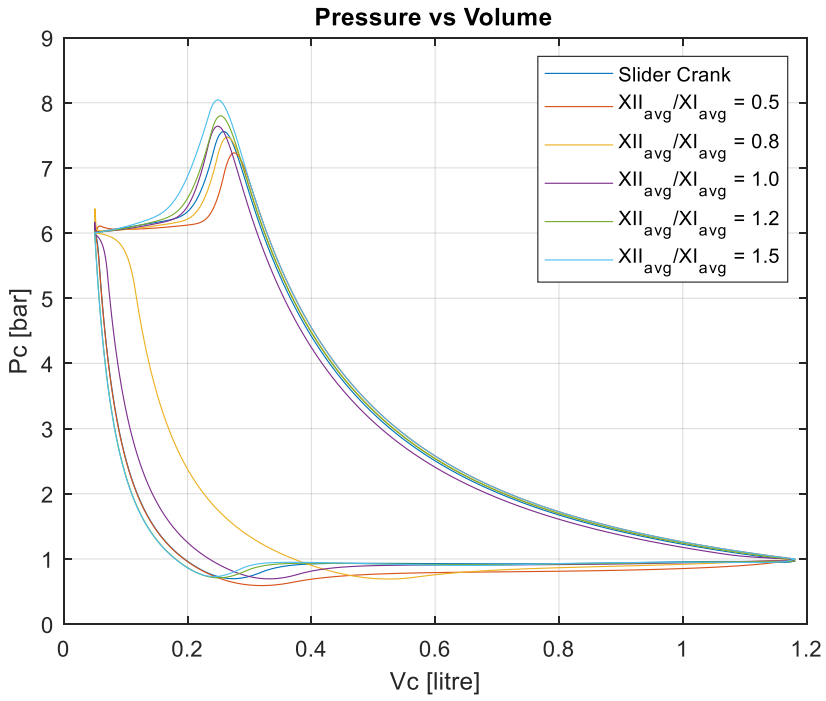

Figure A.16. PV Diagrams of Case A1 for Cases M1-M6

Table A.1 Performance Aspects of Case A1 for Cases M1-M6

Parameter	Unit	Value					
		M1	**M2**	**M3**	**M4**	**M5**	**M6**
W_{net}	[J]	246.41	260.11	216.73	246.59	254.29	259.61
W_{net}^{pm}	[kJ/kg]	221.18	230.94	228.24	220.51	221.12	223.34
η_{pm}^{iso}	[%]	68.12	65.24	66.01	68.33	68.14	67.46

Table A.1 (continued)

η_v	[%]	82.83	83.74	70.6	83.15	85.51	86.43
cap	[m^3/hr]	44.97	45.46	38.33	45.14	46.42	46.92
W_{pos}^{pm}	[kJ/kg]	333.4	330.27	388.2	329.21	326.94	328.36
W_{abs}^{pm}	[kJ/kg]	445.62	429.6	548.15	437.91	432.76	433.39
η_{pres}	[%]	61.65	62.16	60.78	62.29	61.46	59.97
I_f	kgm^2	1.54	1.37	1.55	1.54	1.61	1.69
ΔE in the Flywheel Design	[J]	269.96	241.14	272.2	269.85	282.74	296.59

C.2. Case A2 for Cases M1-M6

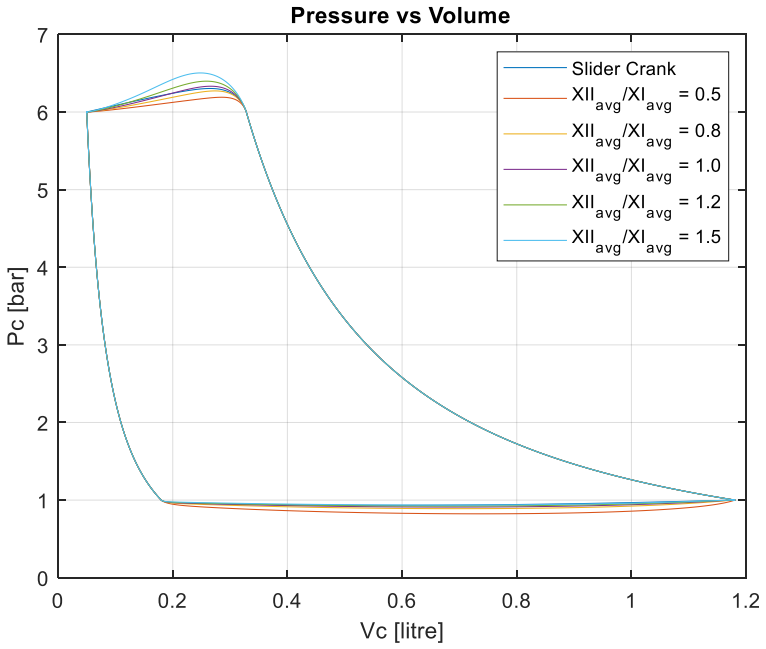

Figure A.17. PV Diagrams of Case A2 for Cases M1-M6

Table A.2 Performance Aspects of Case A2 for Cases M1-M6

Parameter	**Unit**	**Value**					
		M1	**M2**	**M3**	**M4**	**M5**	**M6**
$\boldsymbol{W_{net}}$	[J]	244.22	249.53	245.51	244.84	244.83	245.49
$\boldsymbol{W_{net}^{pm}}$	[kJ/kg]	207.98	217.54	210.82	209.31	208.73	208.77
$\boldsymbol{\eta_{pm}^{iso}}$	[%]	72.45	69.26	71.47	71.98	72.18	72.17
$\boldsymbol{\eta_v}$	[%]	87.31	85.29	86.59	86.97	87.21	87.43
$\boldsymbol{cap}$	[m^3/hr]	47.4	46.3	47.01	47.21	47.34	47.46
$\boldsymbol{W_{pos}^{pm}}$	[kJ/kg]	314.75	319.86	316.03	315.36	315.29	315.8
$\boldsymbol{W_{abs}^{pm}}$	[kJ/kg]	421.52	422.19	421.23	421.4	421.85	422.83
$\boldsymbol{\eta_{pres}}$	[%]	66.91	66.24	67.01	66.95	66.7	66.1
$\boldsymbol{I_f}$	kgm^2	1.53	1.37	1.49	1.54	1.59	1.65
ΔE in the Flywheel Design	[J]	268.47	240.39	260.62	270.83	279.44	290.28

C.3. Case A3 for Cases M1-M6

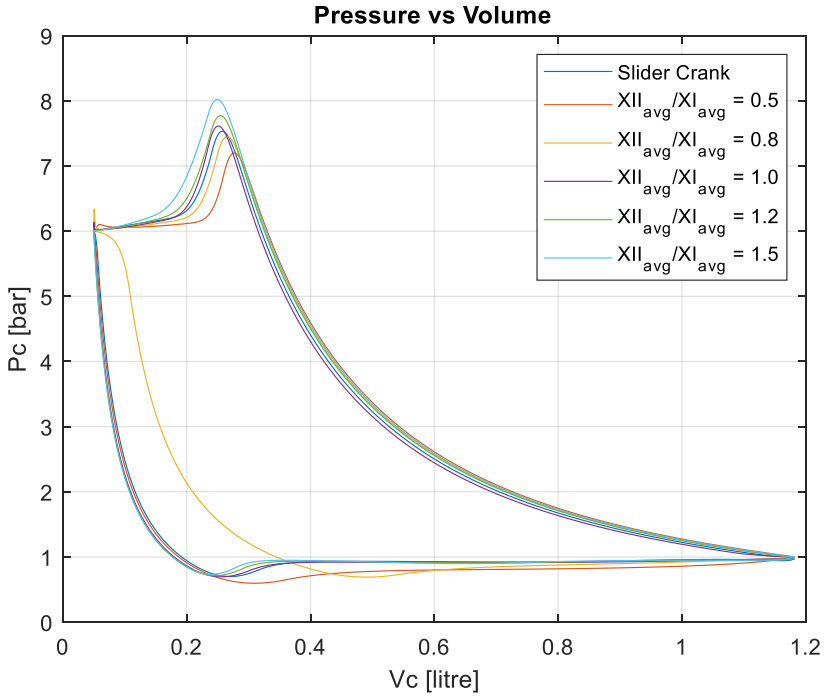

Figure A.18. PV Diagrams of Case A3 for Cases M1-M6

Table A.3 Performance Aspects of Case A3 for Cases M1-M6

Parameter	**Unit**	**Value**					
		M1	**M2**	**M3**	**M4**	**M5**	**M6**
W_{net}	[J]	246.49	262.1	233.27	248.98	255.48	260.35
W_{net}^{pm}	[kJ/kg]	227.18	238.37	233.04	227.06	226.91	228.32
η_{pm}^{iso}	[%]	66.32	63.21	64.65	66.36	66.4	65.99
η_v	[%]	80.68	81.75	74.43	81.53	83.71	84.79
cap	[m^3/hr]	43.8	44.38	40.4	44.26	45.45	46.03

Table A.3 (continued)

W_{pos}^{pm}	[kJ/kg]	341.85	340.16	369.96	337.41	334.52	334.94
W_{abs}^{pm}	[kJ/kg]	456.53	441.95	506.87	447.77	442.12	441.56
η_{pres}	[%]	60.13	59.65	59.36	60.7	60.05	58.74
I_f	kgm^2	1.54	1.38	1.53	1.54	1.61	1.69
ΔE in the Flywheel Design	[J]	269.44	242.2	267.65	270.81	282.98	296.6

C.4. Case A4 for Cases M1-M6

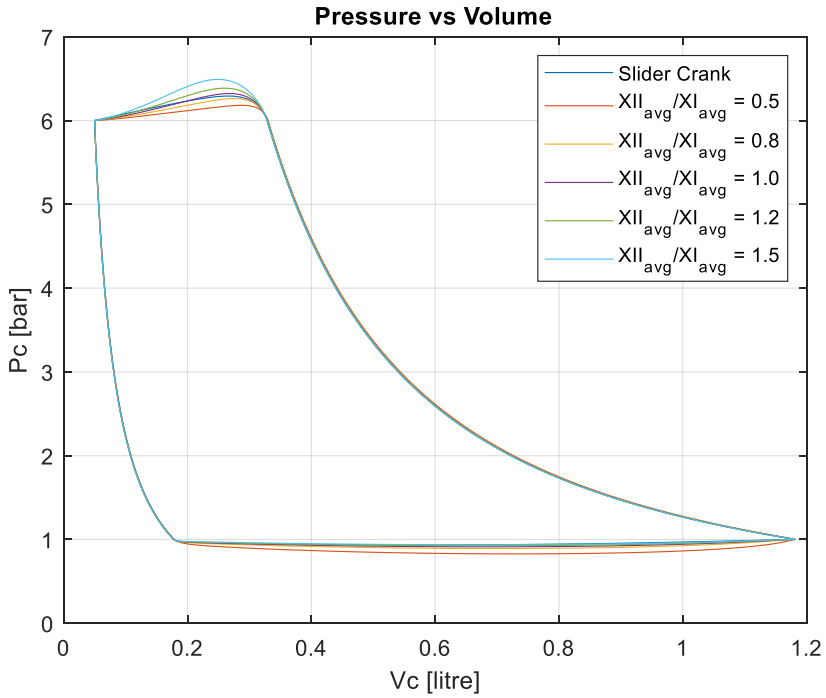

Figure A.19. PV Diagrams of Case A4 for Cases M1-M6

Table A.4 Performance Aspects of Case A4 for Cases M1-M6

Parameter	**Unit**	**Value**					
		M1	**M2**	**M3**	**M4**	**M5**	**M6**
$\boldsymbol{W_{net}}$	[J]	244.89	251.62	246.9	245.99	245.83	246.34
$\boldsymbol{W_{net}^{pm}}$	[kJ/kg]	212.68	224.41	216.45	214.46	213.52	213.16
$\boldsymbol{\eta_{pm}^{iso}}$	[%]	70.84	67.14	69.61	70.26	70.56	70.68
$\boldsymbol{\eta_{v}}$	[%]	85.61	83.37	84.81	85.29	85.6	85.92
$\boldsymbol{cap}$	[m^3/hr]	46.48	45.26	46.04	46.3	46.47	46.65
$\boldsymbol{W_{pos}^{pm}}$	[kJ/kg]	321.4	329.1	323.64	322.29	321.71	321.64
$\boldsymbol{W_{abs}^{pm}}$	[kJ/kg]	430.12	433.78	430.83	430.12	429.9	430.12
$\boldsymbol{\eta_{pres}}$	[%]	65.45	63.73	65.11	65.31	65.25	64.86
$\boldsymbol{I_f}$	kgm^2	1.53	1.38	1.49	1.55	1.59	1.65
$\boldsymbol{\Delta E}$ **in the Flywheel Design**	[J]	268.67	241.48	261.18	271.2	279.68	290.37

C.5. Case A5 for M1-M6

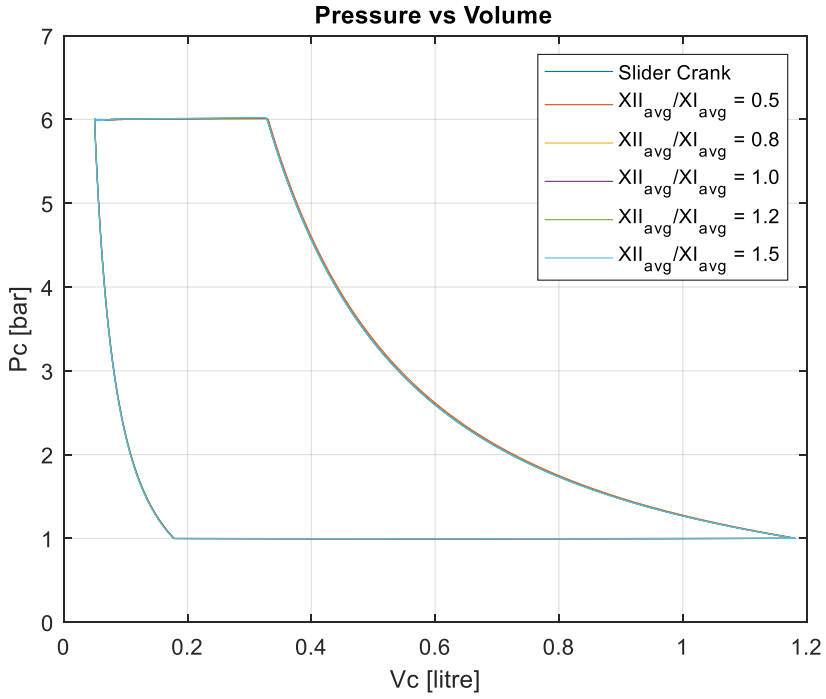

Figure A.20. PV Diagrams of Case A5 for Cases M1-M6

Table A.5 Performance Aspects of Case A5 for Cases M1-M6

Parameter	**Unit**	**Value**					
		M1	**M2**	**M3**	**M4**	**M5**	**M6**
$\boldsymbol{W_{net}}$	[J]	235.74	237.74	236.6	236.27	236.1	235.96
$\boldsymbol{W_{net}^{pm}}$	[kJ/kg]	201.98	204.53	203.03	202.48	202.1	201.72
$\boldsymbol{\eta_{pm}^{iso}}$	[%]	74.6	73.67	74.21	74.41	74.55	74.69
$\boldsymbol{\eta_v}$	[%]	86.78	86.43	86.65	86.76	86.86	86.98
$\boldsymbol{cap}$	[m^3/hr]	47.11	46.92	47.04	47.1	47.15	47.22

Table A.5 (continued)

W_{pos}^{pm}	[kJ/kg]	313.04	315.64	314.01	313.35	312.84	312.3
W_{abs}^{pm}	[kJ/kg]	424.1	426.76	424.99	424.21	423.57	422.89
η_{pres}	[%]	69.59	68.6	69.24	69.47	69.61	69.76
I_f	kgm^2	1.52	1.4	1.49	1.54	1.58	1.64
ΔE in the Flywheel Design	[J]	267.12	245.13	261.74	270.48	277.85	287.01

D. Appendix D

In this Appendix, derivation of the 6-5-6-5 piston motion curve, that is used to define the piston motion profile in Section 4.1.1, is presented.

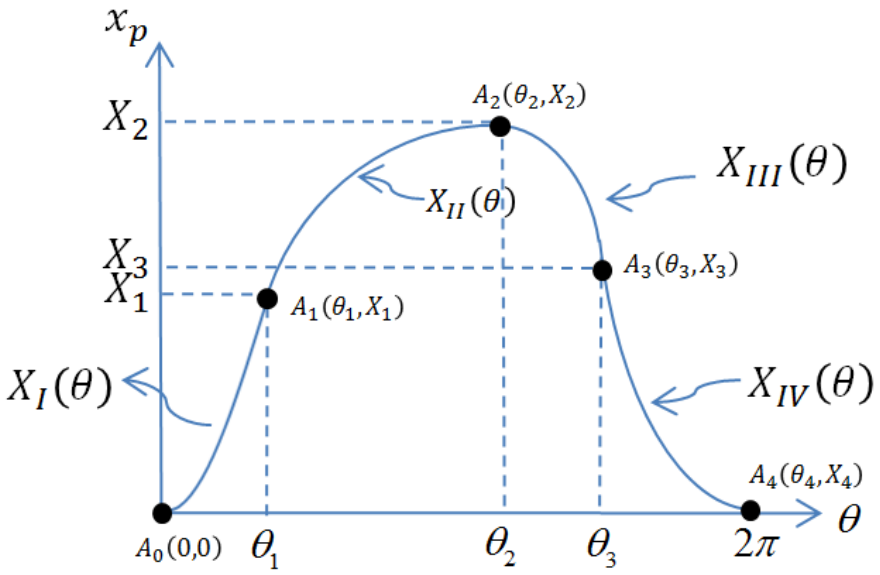

Figure A.21. 6-5-6-5 Polynomial

The coordinates of the points A_0, A_1, A_2, A_3 and A_4 in the $\theta - x_p$ plane (see Figure A.21) are listed below.

$$A_0 \rightarrow (0,0)$$

$$A_1 \rightarrow (\theta_1, X_1)$$

$$A_2 \rightarrow (\theta_2, X_2)$$

$$A_3 \rightarrow (\theta_3, X_3)$$

$$A_4 \rightarrow (2\pi, 0)$$

Note that all of the 5 points defined above are known, since it is assumed that the 6 parameters $\theta_1, X_1, \theta_2, X_2, \theta_3$ and X_3 are specified. The curve $x_p(\theta)$ (which passes through each of the 5 points A_0, A_1, A_2, A_3 and A_4) is defined by the 4

polynomial functions $X_I(\theta), X_{II}(\theta), X_{III}(\theta)$ and $X_{IV}(\theta)$ of degrees 6, 5, 6 and 6, respectively. i.e.,

$$x_p(\theta) = \begin{cases} X_I(\theta) & when \quad 0 \le \theta \le \theta_1 \\ X_{II}(\theta) & when \quad \theta_1 \le \theta \le \theta_2 \\ X_{III}(\theta) & when \quad \theta_2 \le \theta \le \theta_3 \\ X_{IV}(\theta) & when \quad \theta_3 \le \theta \le 2\pi \end{cases} \tag{A.8}$$

where

$$X_I(\theta) = a_{I0} + a_{I1}\theta + a_{I2}\theta^2 + a_{I3}\theta^3 + a_{I4}\theta^4 + a_{I5}\theta^5 + a_{I6}\theta^6 \tag{A.9}$$

$$X_{II}(\theta) = a_{II0} + a_{II1}\theta + a_{II2}\theta^2 + a_{II3}\theta^3 + a_{II4}\theta^4 + a_{II5}\theta^5 \tag{A.10}$$

$$X_{III}(\theta) = a_{III0} + a_{III1}\theta + a_{III2}\theta^2 + a_{III3}\theta^3 + a_{III4}\theta^4 + a_{III5}\theta^5 + a_{III6}\theta^6 \tag{A.11}$$

$$X_{IV}(\theta) = a_{IV0} + a_{IV1}\theta + a_{IV2}\theta^2 + a_{IV3}\theta^3 + a_{IV4}\theta^4 + a_{IV5}\theta^5 \tag{A.12}$$

In equations (A.9) - (A.12), $a_{I0}, a_{I1}, \dots, a_{I6}$ denote the unknown coefficients in $X_I(\theta)$; $a_{II0}, a_{II1}, \dots, a_{II5}$ denote the unknown coefficients in $X_{II}(\theta)$; $a_{III0}, a_{III1}, \dots, a_{III6}$ denote the unknown coefficients in $X_{III}(\theta)$ and $a_{IV0}, a_{IV1}, \dots, a_{IV5}$ denote the unknown coefficients in $X_{IV}(\theta)$. Hence, we have (7+6+7+6) = 26 unknown coefficients associated with the 4 polynomials $X_I(\theta), X_{II}(\theta), X_{III}(\theta)$ and $X_{IV}(\theta)$. Let, now,

$$X' = \frac{dx_p}{d\theta} \tag{A.13}$$

$$X'' = \frac{d^2x_p}{d\theta} \tag{A.14}$$

$$X''' = \frac{d^3 x_p}{d\theta} \tag{A.15}$$

where primes denote derivatives with respect to θ. The 4 polynomials $X_I(\theta), X_{II}(\theta), X_{III}(\theta)$ and $X_{IV}(\theta)$ should satisfy the following 26 continuity conditions at points A_0, A_1, A_2, A_3 and A_4.

At point A_0 :

$$X_I(0) = 0 \tag{A.16}$$

$$X_I'(0) = 0 \tag{A.17}$$

$$X_I''(0) = 0 \tag{A.18}$$

$$X_I'''(0) = 0 \tag{A.19}$$

At point A_1 :

$$X_I(\theta_1) = X_1 \tag{A.20}$$

$$X_{II}(\theta_1) = X_1 \tag{A.21}$$

$$X_I'(\theta_1) = X_{II}'(\theta_1) \tag{A.22}$$

$$X_I''(\theta_1) = X_{II}''(\theta_1) \tag{A.23}$$

$$X_I'''(\theta_1) = X_{II}'''(\theta_1) \tag{A.24}$$

At point A_2

$$X_{II}(\theta_2) = X_2 \tag{A.25}$$

$$X'_{II}(\theta_2) = 0 \tag{A.26}$$

$$X''_{II}(\theta_2) = 0 \tag{A.27}$$

$$X'''_{II}(\theta_2) = 0 \tag{A.28}$$

$$X_{III}(\theta_2) = X_2 \tag{A.29}$$

$$X'_{III}(\theta_2) = 0 \tag{A.30}$$

$$X''_{III}(\theta_2) = 0 \tag{A.31}$$

$$X'''_{III}(\theta_2) = 0 \tag{A.32}$$

At point A_3

$$X_{III}(\theta_3) = X_3 \tag{A.33}$$

$$X_{IV}(\theta_3) = X_3 \tag{A.34}$$

$$X'_{III}(\theta_3) = X'_{IV}(\theta_3) \tag{A.35}$$

$$X''_{III}(\theta_3) = X''_{IV}(\theta_3) \tag{A.36}$$

$$X'''_{III}(\theta_3) = X'''_{IV}(\theta_3) \tag{A.37}$$

At point A_4

$$X_{IV}(2\pi) = 0 \tag{A.38}$$

$$X'_{IV}(2\pi) = 0 \tag{A.39}$$

$$X''_{IV}(2\pi) = 0 \tag{A.40}$$

$$X'''_{IV}(2\pi) = 0 \tag{A.41}$$

Equations (A.16) - (A.41) are 26 linear equations in the 26 unknown coefficients (i.e., $a_{I0}, a_{I1}, \dots, a_{I6}$; $a_{II0}, a_{II1}, \dots, a_{II5}$; $a_{III0}, a_{III1}, \dots, a_{III6}$; $a_{IV0}, a_{IV1}, \dots, a_{IV5}$) associated with the four polynomials. Solving this linear equation system, one obtains the 26 unknown coefficients which yield the piston motion curve $x_p(\theta)$ via equation (A.8).

E. Appendix E

In this study, c_p , c_v and γ denote heat capacity at constant pressure, heat capacity at constant volume and isentropic expansion factor for an ideal gas, respectively. In the simulations, c_p , c_v and γ are taken to be constant at the inlet temperature. In order to assess the effect of this assumption, the compressor simulation has been run for the MinFaS-TaR based and slider crank based compressors for 2 different cases. In the first case, c_p, c_v and γ are taken to be constant at $T_i = 293K$. In the second case, c_p, c_v and γ are taken to be constant at $(T_c)_{max} = 540$. The simulations are performed for Case-1 in Table 4.9. The results are shown in Table A.6 and Table A.7. In order to compare the results for the two cases, a parameter, SA (saving), has been defined via the equation

$$SA = \frac{obj_{Slider\ Crank} - obj_{\text{MinFaS-TaR}}}{obj_{Slider\ Crank}} * 100 \qquad \text{(A.42)}$$

where obj_{SC} is the objective function determined for the slider crank based reciprocating compressor and obj_{MTR} is the objective function determined for the MinFaS-TaR based reciprocating compressor.

Table A.6 Case 1 (c_p, c_v and γ are constant at Their Respective Values at $T_i = 293K$)

	Unit	**MinFaS-TaR Based**	**Slider Crank Based**	**SA [%]**
$\boldsymbol{obj_1}$ **(** $\boldsymbol{W_{net}^{pm}}$ **)**	[kJ/kg]	204.41	227.29	10.1
$\boldsymbol{obj_2}$ **(** $\boldsymbol{W_{pos}^{pm}}$ **)**	[kJ/kg]	302.66	342.03	11.5
$\boldsymbol{obj_3}$ **(** $\boldsymbol{W_{abs}^{pm}}$ **)**	[kJ/kg]	392.69	456.77	14.1

Table A.7 Case 2 (c_p, c_v and γ are constant at Their Respective Values at $(T_c)_{max} = 540K$)

	Unit	**MinFaS-TaR Based**	**Slider Crank Based**	**SA [%]**
$\boldsymbol{obj_1}$ **(** $\boldsymbol{W_{net}^{pm}}$ **)**	[kJ/kg]	202.85	224.84	9.7
$\boldsymbol{obj_2}$ **(** $\boldsymbol{W_{pos}^{pm}}$ **)**	[kJ/kg]	300.42	340.34	11.7
$\boldsymbol{obj_3}$ **(** $\boldsymbol{W_{abs}^{pm}}$ **)**	[kJ/kg]	391.63	455.84	14.0

It can be observed from the 2 tables above, the parameter SA for the two cases are approximately the same. Hence, it can be concluded that the assumption of taking the c_p , c_v and γ values to be constant at their respective values at the inlet temperature is quite valid.

F. Appendix F

In this Appendix, the optimum piston motion curves are presented.

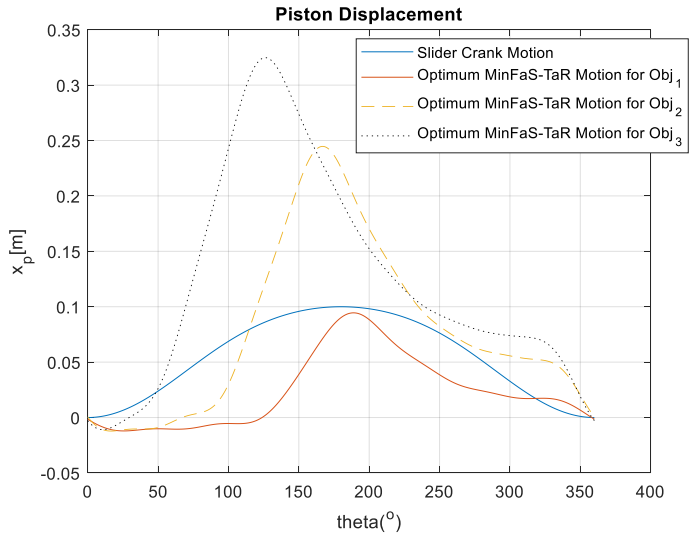

Figure A.22. The Piston Displacements of the Optimum MinFaS-TaR based Compressor and the Slider Crank Based Compressors for Case-1

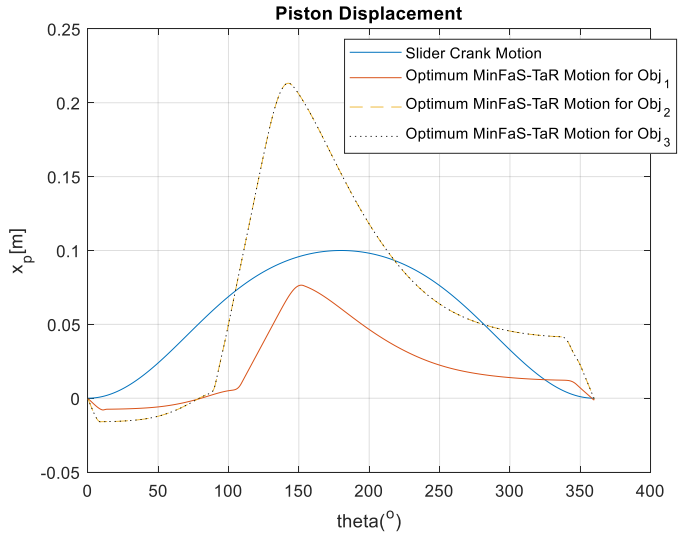

Figure A.23. The Piston Displacements of the Optimum MinFaS-TaR based Compressor and the Slider Crank Based Compressors for Case-2

Note that, in Figure A.23, the optimum piston motion for obj_2 and obj_3 are nearly overlapped.

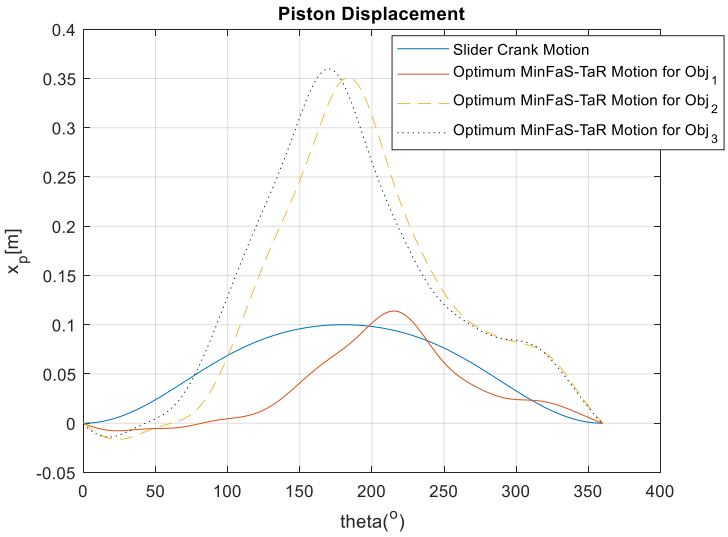

Figure A.24. The Piston Displacements of the Optimum MinFaS-TaR based Compressor and the Slider Crank Based Compressors for Case-3

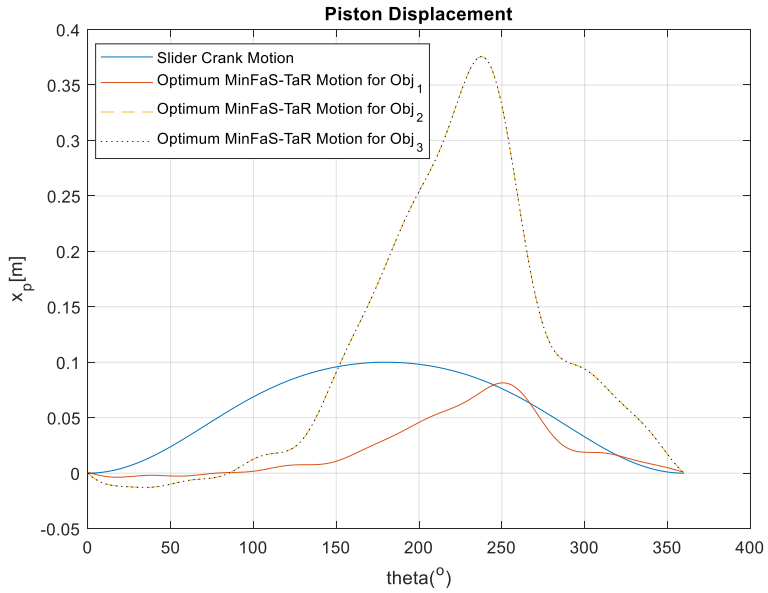

Figure A.25. The Piston Displacements of the Optimum MinFaS-TaR based Compressor and the Slider Crank Based Compressors for Second Stage of Two-Stage Compressor for Case-4

Note that, in Figure A.25, the optimum piston motion for obj_2 and obj_3 are nearly overlapped.

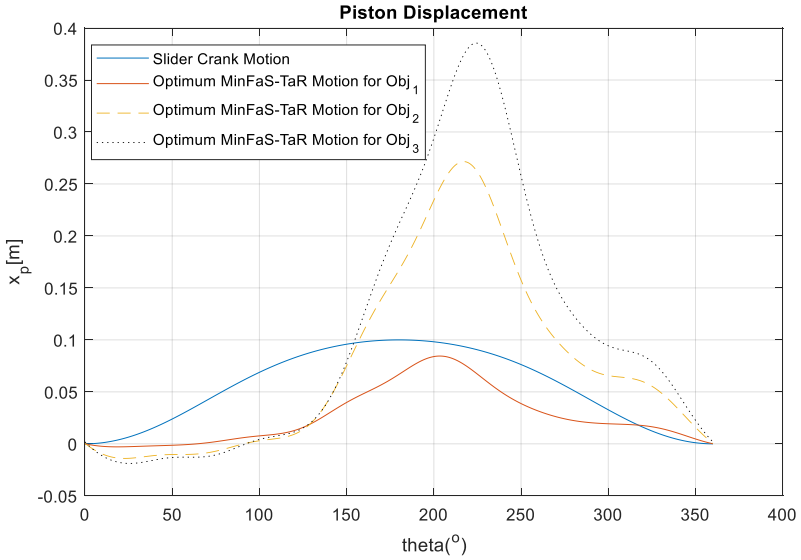

Figure A.26. The Piston Displacements of the Optimum MinFaS-TaR based Compressor and the Slider Crank Based Compressors for Second Stage of Two-Stage Compressor for Case-5

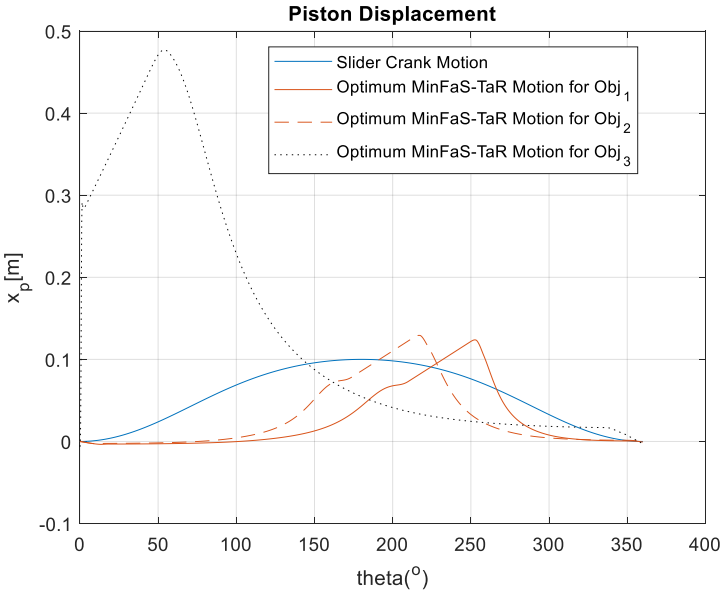

Figure A.27. The Piston Displacements of the Optimum MinFaS-TaR based Compressor and the Slider Crank Based Compressors for Case-6

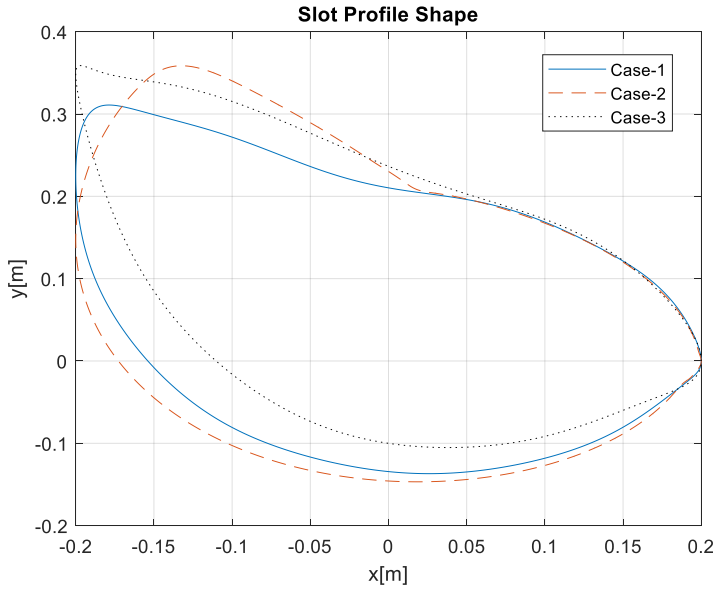

Figure A.28. Slot Profile of Slot 3a Based on Optimum Piston Motion for Case-1, 2 and 3 for Minimization of Objective-2 (b_2 = 0.2 [m])

Note that, b_2 is taken to be 0.25 [m] for Case-4, 5 and 6, since the slot profile has intersections if b_2 is taken 0.2 [m].

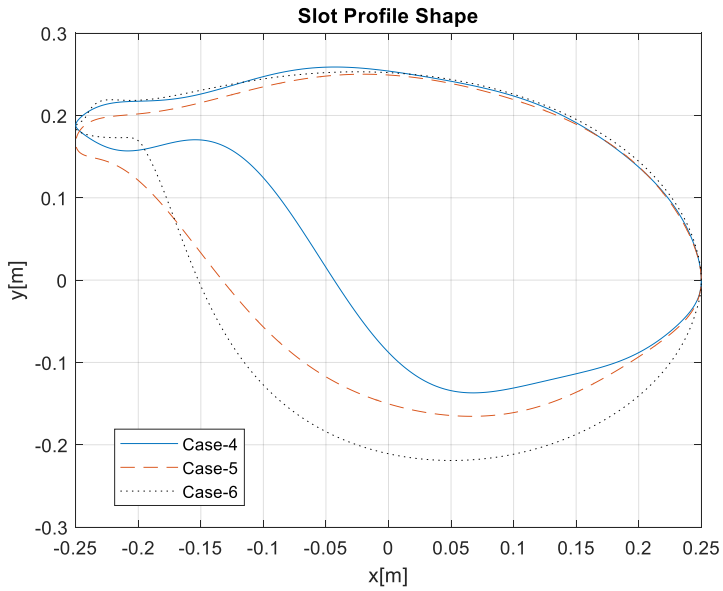

Figure A.29. Slot Profile of Slot 3a Based on Optimum Piston Motion for Case-4, 5 and 6 for Minimization of Objective-2 (b_2 = 0.25 [m])